OTEC condenser heat exchanger analysis

Modelling and model validation of the performance of an ammonia-water OTEC condenser heat exchanger using advanced condenser models

F.C. Geschiere

TU Delft

OTEC condenser heat exchanger analysis

Modelling and model validation of the performance of an ammonia-water OTEC condenser heat exchanger using advanced condenser models

by

F.C. Geschiere

to obtain the degree of Master of Science
at the Delft University of Technology,
to be defended publicly on Monday March 19, 2018, 2018 at 15:00.

Student number:	4095146	
Project duration:	April 15, 2017 - March 19, 2018	
Thesis committee:	Prof. Dr. Ir. T.J.H. Vlugt,	TU Delft
	Assoc. Prof. Dr. Ir. C.A. Infante Ferreira,	TU Delft, supervisor
	Assoc. Prof. Dr. Ir. H. Polinder,	TU Delft
	Ir. J. Kirkenier,	Bluerise, supervisor

This thesis is confidential and cannot be made public until March 19, 2023.

TU Delft

Summary

The increasing demand in renewable energy motivates the search for new renewable energy sources. The ocean is a vast energy source of both thermal and kinetic energy, however methods to harness this energy haven't reached maturity yet. Ocean Thermal Energy Conversion (OTEC), a method to harness the thermal energy of the ocean, could change this. In order to get to this stage of maturity, experimental and numerical research on the OTEC power cycle was done by Goudriaan [12] and Kuikhoven [23]. However, the numerical model developed showed inaccuracy for the condenser and lacked physical insight into the processes of heat transfer. The condenser and consequently, the cold water pipe, are a significant part of the investment costs of an OTEC plant. Therefore, the goal in this research was to increase the accuracy of the performance calculations of the condenser and to gain more knowledge on the physical phenomena in the condenser heat exchanger.

Two different methods were tested in order to improve the condenser model. In the first part a heat transfer correlation is fitted to the experimental data. A literature study was done on two phase heat transfer correlations to investigate what phenomena occur in two phase condensation flow. Relevant dimensionless quantities were chosen accordingly. The quantities used are the conventional Reynolds and Prandtl number. The mass transfer that occurs through absorption was represented by the Schmidt number.

The resulting correlation fit was tested on accuracy using the experimental data obtained by Goudriaan [12] and Kuikhoven [23]. To be able to compare the results of this research with their research, the in-depth validation was done for the same working fluid mass flow of 0.010 kg/s that was used by Goudriaan [12] and Kuikhoven [23]. The Schmidt number showed a positive effect on the accuracy.

The correlation was extrapolated for other working fluid mass flows as well. It was found that the correlation fit is a useful tool for the working fluid mass flows that have a large amount of experimental data available (the cases 0.007, 0.010 and 0.013 kg/s) but isn't as accurate for working fluid mass flow with a small amount of experimental data available (0.005 kg/s).

In the second part of the report a detailed condenser model was developed using the method of Fernández-Seara et al. [10]. This model was used to provide more physical insight into the two phase mixture behaviour in a condensation process. The model is also capable of predicting the required pressure on the working fluid side to provide full condensation.

Literature research was done on different aspects of the condensation process in a plate heat exchanger. Film thickness correlations were tested. Different heat transfer correlations developed for plate heat exchangers were investigated. Flow pattern theory and flow pattern maps were used to predict the flow behaviour. The method of Fernández-Seara et al. [10] was used to predict mass transfer through the vapor-liquid interface in the working fluid. A pressure iteration loop was added to predict the condenser pressure on the working fluid side.

The initial results were slightly off compared to the experimental measurements. The reason for the inaccuracy is expected to be the neglection of surface tension effects on the wettability of the working fluid. Dry surface voids are expected to occur in the liquid film with decreasing concentration. A correction factor based on surface tension was added to include this effect. The 0.010 kg/s case was validated in detail and showed decent accuracy. At 0.007 kg/s working fluid mass flow deviations were slightly more significant but the trends of the characteristic variables were similar to the experimental data. The mass transfer iteration loop showed inaccuracies and instabilities at the working fluid mass flows of 0.005 and 0.013 kg/s.

The model showed that for the range tested the condenser performs better with increasing concentration of ammonia. The non-linear behaviour of the mass diffusivity decreases the mass transfer coefficients at decreasing concentrations. The surface tension correction factor also adds to the decrease in performance, however, if the mass flux of the working fluid would be higher, this correction factor might not be valid because the dry surface voids might not occur any more. The overall heat transfer coefficient increases towards the outlet of the condenser.

Acknowledgements

First of all, I would like to thank my supervisor Carlos Infante Ferreira for his excellent supervision. Whenever I was struggling with a problem you would make time for me to discuss it. Your commitment and attention to detail supported me a lot during the process. Secondly, I would like to thank Joost Kirkenier for giving me the opportunity to do this research at Bluerise. Times got really busy during my thesis but your supervision was always very helpful.

Furthermore, I would like to thank everyone else at Bluerise, I really enjoyed my time here. The balance of work and table tennis in the old office will be missed, but I believe the atmosphere will become even better in the new office. I would like to thank Robin Goudriaan and Liona Kuikhoven for their previous research done and for taking the time to explain to me what the key aspects of their model were. I would like to thank Elias Dahlgren for gathering the experimental data I used for validation and Vilborg Guðjónsdóttir for reviewing my work.

I would also like to thank all my friends at the TU that made the whole process of writing a thesis more bearable with cups of coffee and lunch breaks. I want to thank my family, for always supporting me during my studies and my thesis. And finally, a special thanks to my girlfriend, Geertje, for being there for me throughout the process.

F.C. Geschiere
Delft, February 2018

Contents

Nomenclature

Acronyms

wm	Warm medium
MAE	Mean Absolute Error
NMAE	Normalised Mean Absolute Error
OTEC	Ocean Thermal Energy Conversion
OTWP	Ocean Thermal Water Production
SWAC	SeaWater Air Conditioning

Subscripts

a	Ammonia
b	Bulk
bot	Bottom iteration boundary
$buoy$	Buoyancy induced
c	Diffusion by condensation
cm	Cooling medium
$cond$	Condenser
$corr$	Corrected
dif	Difference
eff	Effective
eq	Equivalent
eq	Equivalent
$evap$	Evaporator
exp	Experimental
f	Film
fg	Latent
$flat$	Flat plate
g	Gravity induced
i	Interface
in	Inlet
inn	Inner
j	Element in vector

-

l	Liquid
mod	Model
$norm$	Value used to normalise results
ou	Outer
out	Outlet
pr	Projected
s	Sensible
sat	Saturation
top	Top iteration boundary
v	Vapor
w	Water
$wall$	Wall
wet	Wetted
wf	Working fluid

Dimensionless quantitie s		**Units**
Bd	Bond number	-
Bo	Boiling number	-
Ca	Capillary number	-
Co	Convection number	-
Fr	Froude number	-
Ga	Galileo number	-
Ja	Jakob number	-
K_f	Film number (inverse of Kapitza number)	-
Ka	Kapitza number (inverse of Film number)	-
Le	Lewis number	-
Nu	Nusselt number	-
Pr	Prandtl number	-
Ra	Rayleigh number	-
Re	Reynolds number	-
Sc	Schmidt number	-
Sh	Sherwood number	-
St_m	Stanton number	-
We	Weber number	-
X	Lockhart-Martinelli parameter	-

Greek Symbols

α	Heat transfer coefficient	W/m^2K
β	Chevron angle	°
δ	Thickness	m
ϵ	Heat transfer correction factor	-
Γ	Mass flow rate of condensate film per unit width	kg/(ms)
κ	Mass transfer coefficient	$mol/(m^2s)$
Λ	Corrugation wave length	m
λ	Thermal conductivity	W/(mK)
μ	Dynamic viscosity	$kg/(ms^2)$
ν	Kinematic viscosity	kg/(sm)
ϕ	Surface enhancement factor	-
Ψ	Thermal expansion coefficient	-
ψ	Thermal expansion coefficient	1/K
ρ	Density	kg/m^3
σ	Surface tension	N/m
ξ	Friction factor	-

Roman Symbols

A	Area	m^2
a	Amplitude of sinusoidal corrugation pattern	m
b	Mean channel spacing	m
c	Concentration	-
c_p	Heat capacity	J/K
D	Mass diffusivity	m^2/s
d_h	Hydraulic diameter	m
F	Force	N
$Fact$	Correction factor	-
g	Gravitational constant	$m^3/(kgs^2)$
$\dot{G}$	Mass flux	$kg/(m^2s)$
Ge	Geometry parameter	-
h	Enthalpy	J/kg
j	Molar flux	mol/sm^2
L	Height heat exchanger channel	m
M	Molar mass	kg/mol

$\dot{m}$	Mass flow	kg/s
n	Number of vector elements used	-
P	Wetted perimeter	m
p	Pressure	Pa
p^*	Pressure correction factor	-
p_c	Critical pressure	Pa
q	Vapor quality	
$\dot{Q}$	Heat transfer	W
$\dot{q}$	Heat flux	W/m^2
R	Gas-to-liquid volume ratio	-
T	Temperature	K
U	Overall heat transfer coefficient	W/(m^{2}K)
u	Velocity	m/s
W	Width heat exchanger	m
x	Horizontal coordinate in heat exchanger channel	m
y	Vertical coordinate in heat exchanger channel	m
z	Ratio of the ammonia molar flux and the total molar flux	-

1 Introduction

An ever-increasing demand of renewable energy requires the market to look beyond the more matured forms of renewable energy like solar, wind and hydro energy. Ocean energy is a form of renewable energy that has a huge potential but is still virtually unused [4]. However, more researches, feasibility studies and initiatives are started every day. Especially on islands where land mass is limited but the ocean's energy is in abundance the resource is an interesting possibility. These islands are in general dependent on imported oil and are more vulnerable to climate change [30]. Ocean Thermal Energy Conversion (OTEC) is a method to harness this energy and convert it to electricity.

1.1. OTEC cycle

The ocean surface water is warmed up by the sun's radiation and thus acts like an energy storage of solar energy. This effect is especially large in the tropical regions where the solar radiation is most powerful. Consequently, the difference in temperature between the surface water and the cold deep sea water creates a thermal energy potential. This energy potential can be extracted by an Ocean Thermal Energy Conversion cycle. This operates with the principle of an organic rankine cycle or an advanced mixture cycle, as shown in figures 1.1a and 1.1b, respectively. The organic rankine cycle in figure 1.1a has two heat exchangers, an evaporator and a condenser. The heat required in the evaporator is provided by the warm ocean surface water and the cooling required in the condenser is provided by the cold deep sea water. The vaporised fluid powers a turbine which produces electricity. When using a non-azeotropic mixture as the working fluid the cycle changes slightly to the advanced cycle shown in figure 1.1b. The working fluid will not evaporate completely, thus in order to not damage the turbine, the liquid part has to be separated from the vapor part. The vapor then powers the turbine and the liquid is used to preheat the working fluid in a recuperator, which then flows to the evaporator.

1.1.1. Working fluid

In the tropics the maximum temperature of the warm sea water is usually around 25-30 °C. For the cycle to be functional the working fluid medium saturation temperature should be below this temperature. Therefore commonly used working fluids are pure ammonia and highly concentrated ammonia diluted with water. Using a non-azeotropic mixture instead of a pure fluid has the benefit of a varying saturation temperature. The difference is shown in the T-Q diagrams in figures 1.2a and 1.2b. This occurs because of the different saturation temperatures of both fluids. The fluid with the lower saturation temperature will change phase first when heat is transferred to or extracted from the mixture. This causes the liquid concentration to change. Consequently, the saturation temperature of the fluid changes. This effect can be beneficial for the efficiency of the heat exchangers. The area between the cold and warm temperatures in a T-Q diagram represents the exergy losses. Therefore, if the phase change line of the working fluid has an angle induced by the mixture properties, the exergy losses can be decreased, as can be seen in figure 1.2b.

1.2. Bluerise BV

Bluerise is a Delft based company specialised in ocean energy applications. Currently research is conducted in the fields of OTEC, SeaWater Air Conditioning (SWAC) and Ocean Thermal Water Production (OTWP). In

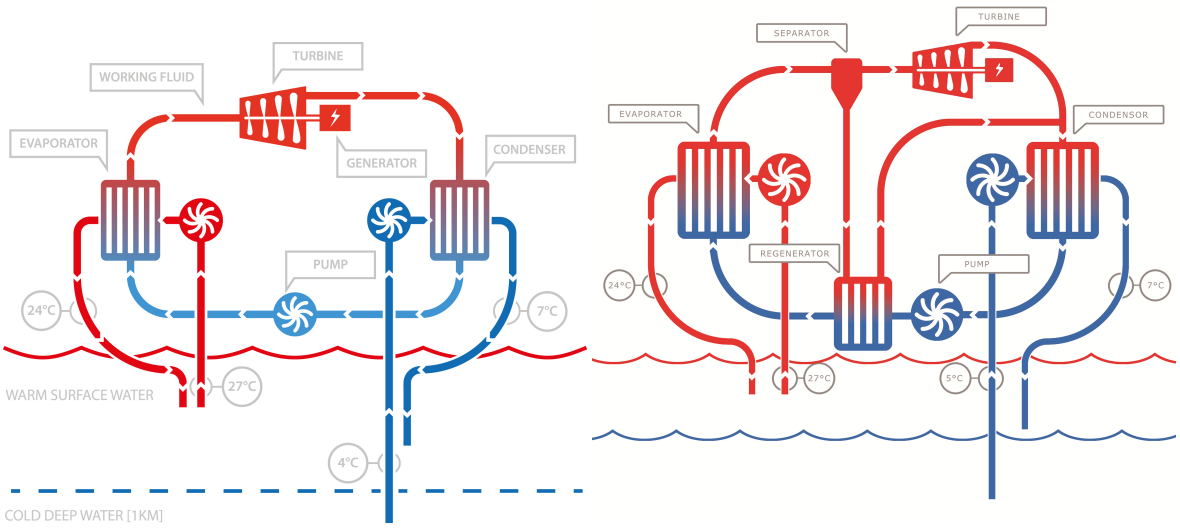

(a) (b)

Figure 1.1: (a) OTEC organic rankine cycle for pure working fluids (b) OTEC advanced cycle for working fluid mixtures.

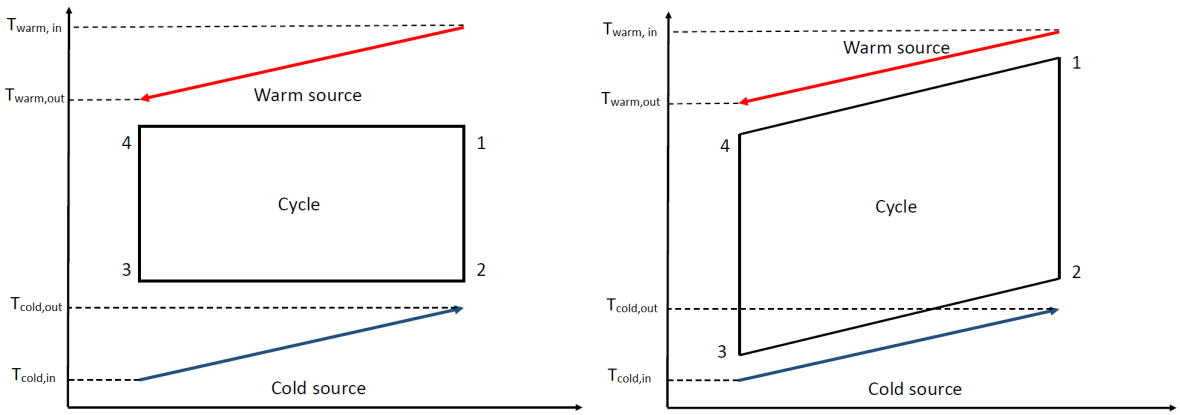

(a) (b)

Figure 1.2: Thermodynamic cycle of OTEC. (a) T-Q diagram for a pure working fluid (b) T-Q diagram for a mixture working fluid. [12]

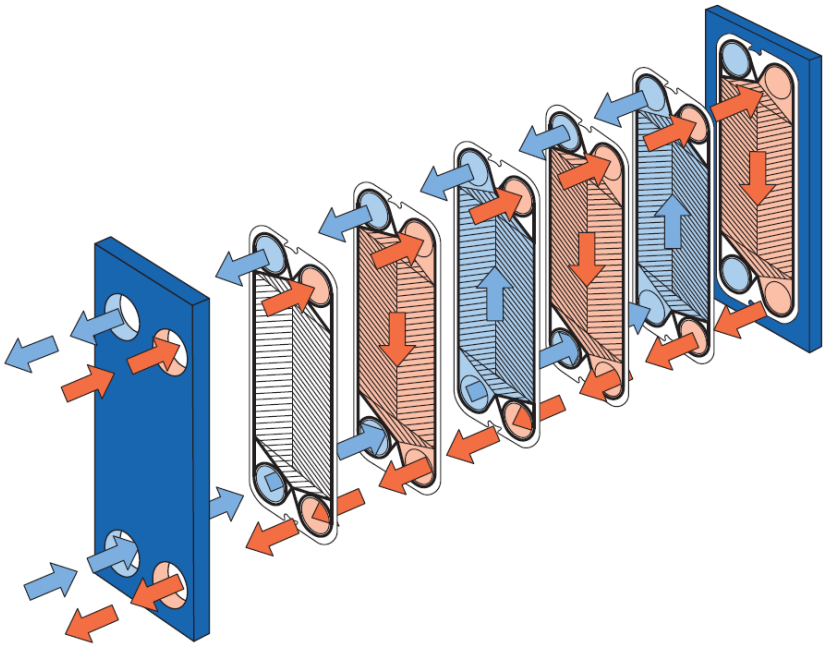

Figure 1.3: Exploded view of heat exchanger, adopted from Kirkenier [22]

.

an ecopark these different technologies can be combined using one common source; the ocean.
The research is done in close collaboration with Delft University of Technology. An experimental setup of a 100 W OTEC cycle was built in the department of Process and Energy and later an experimental OTWP setup was added to the research facility. To test the ecopark on a larger scale, locations in the tropics are selected to build the first economically feasible pilot plant, incorporating both OTEC and OTWP technology. Projects are set up on several locations in the tropics, the first pilot projects in Jamaica and Curaçao are close to realisation.

1.3. OTEC experimental setup

The OTEC experimental setup of 100 W built by Delft University of Technology and Bluerise BV is an advanced OTEC cycle (figure 1.1b) operated with ammonia water as the working fluid. The warm and cold seawater streams are represented by tap water reservoirs that are kept at a constant temperature of approximately 27.5 $°C$ and 5 $°C$, respectively.

For this research the condenser heat exchanger is especially interesting. The heat exchanger used in the experimental setup is a brazed plate heat exchanger. The exploded view in figure 1.3 shows the working principle of a plate heat exchanger. Warm and cold fluid flows exchange heat through the plates in between the flows. The flows are counter current. More detailed definitions and dimensions of the heat exchanger can be found in Appendix A. Sensors are placed to monitor the processes in the cycle. The working fluid state is measured with temperature and pressure sensors that are placed in the working fluid vapor flow at the outlet of the turbine, in the liquid flow coming from the recuperator and in the liquid flow at the outlet of the condenser. The working fluid liquid mass flow is measured at the inlet of the condenser. The total working fluid mass flow is measured at the outlet of the cold medium in the recuperator. The cooling medium state is measured by pressure and temperature sensors at the inlet and the outlet of the condenser heat exchanger. The cooling medium mass flow is measured at the inlet.

1.3.1. Sensor accuracy

The experimental data has a finite accuracy. In order to validate the model the accuracy of the experiments has to be taken into account first. The important sensors for the condenser and their accuracy are shown in table 1.1 [43]. The temperature, pressure and mass flow all have an important influence on the total heat transfer. The temperature sensor accuracy is relatively high and will therefore not be of great influence. The inlet and outlet mass flow sensor are very accurate (0.375%). The pressure sensors are most inaccurate with

Table 1.1: Accuracy of relevant sensors (Veijer [43])

	Wika A-10 (0-10 barg)	Bronkhorst CORI-FLOW M15	AE Sensors DF140TM	Pt-100 RTD
Purpose	Pressure (in- and outlet)	Mass flow working fluid in- and outlet	Mass flow water	Temperature (in- and outlet)
Sensor accuracy	±0.41 bar	±0.00003 kg/s	±0.0127 l/s	$\pm(0.03°C + 0.0005T(°C))$
ADC accuracy	±0.10 bar	-	±0.0059 l/s	-
Combined accuracy	±0.51 bar	±0.00003 kg/s	±0.0186 l/s	$\pm(0.03°C + 0.0005T(°C))$
Reference value	9.5 barg	0.008 kg/s	0.448 l/s	30 $°C$
Accuracy percentage	5.37%	0.375%	4.15%	0.15%

5.37% inaccuracy. The cold water flow is with 4.15% accuracy also not very accurate, however, as was stated by Veijer [43], this has an insignificant effect on the heat transfer.

1.4. Condenser modelling

The OTEC cycle as used in the experimental setup is a two phase mixture cycle on the working fluid side. The mixture is ammonia-water with a high concentration of ammonia. This makes modelling the heat transferred more complex. To be able to predict this heat transfer, two phase flow and mixture effects are to be taken into account. For describing the heat transfer in a heat exchanger different methods can be used.

The most common one is developing empirical relations through curve fitting. A dataset with experimental data is used to fit certain dimensionless quantities to get an accurate heat transfer correlation. The range of the dataset and the dimensionless quantities determine in what regime these correlations can be used. For single phase flows the correlations developed are valid for a broad range of flow conditions. For two phase flows most correlations are valid for narrow ranges or for specific conditions and geometries. It is thus of importance to analyse different empirical relations and develop new relations where the existing relations don't apply. The method which uses two phase correlations is an efficient, inexpensive and accurate way to predict heat transfer. The correlations however, are only valid for the range in which they are developed. The pressure in this method can also not accurately be determined by the condenser model, as will be explained later in this report.

Another more detailed way to describe two phase mixture heat transfer is a method based on mass transfer developed by Fernández-Seara et al. [10]. Fernández-Seara et al. [10] applied it to a vertical tubular absorber. The method involves dividing the two phase fluid into two single phase fluids; the liquid mixture and the vapor mixture. The single phase fluids are described with single phase correlations. The interaction between the two phases is separately modelled by the method. Chapter 6 describes this method. By describing the phases separately, more insight can be gained into the processes in the heat exchanger. This makes it easier to identify and describe the phenomena. Several studies report the use of the method for different applications. Nuijten [29] developed a model for the condenser of the OTEC cycle using an ammonia-water mixture as the working fluid in a plate heat exchanger. Aarts [1] developed a plate heat exchanger model for a compression-resorption heat pump with higher temperatures. Shi [35] developed a model for the absorption of ammonia-water and $CO_2 - NH_3 - H_2O$ mixture in mini-channels, Rijpkema [33] and Nefs [28] also worked on a model for minichannel heat exchangers but only using ammonia-water as a working fluid.

1.5. Problem statement

A model was developed for the complete experimental setup of the OTEC cycle by Goudriaan [12] and Kuikhoven [23]. The heat exchangers were modelled using two phase heat transfer correlations developed specifically for plate heat exchangers. The goal of the study was to determine whether a pure working fluid of ammonia or an ammonia-water mixture would give the best performance of the OTEC cycle. The results, as can be found in Chapter 3, matched the experimental data, for the recuperator and for the evaporator. The condenser results however, were significantly off, especially for the temperature. For the full scale OTEC plant the cold water piping for the condenser will be one of the most costly parts. To properly predict the flow and thus the pipe diameter, it is important to simulate the performance of the condenser accurately.

Another limitation of the model was the pressure in the system. When the working fluid is not completely condensed the pressure will rise in the condenser to be able to reach full condensation. This mechanism

will be later explained in the report. The pressure in the condenser is therefore an important parameter when determining the performance of the system. Therefore, the condenser pressure should be calculated in the condenser. In the model developed previously this pressure was iterated in the cycle, but not in the condenser.

It was found that using a mixture as the working fluid decreases performance. It was expected that this is due to unfavourable mixture effects occurring. However, as the model was designed, the physical processes occurring during phase change in both heat exchangers were described by two phase heat transfer correlations that only incorporate the Reynolds and the Prandtl number and therefore could not incorporate mixture effects. This method also gives only marginal insight in the physical processes of the system. Therefore, it is complicated to assess what the dominant processes are that cause a decrease in performance at lower concentrations.

This model was also limited in a practical way by computational time. A calculation of one data point took on average over an hour to complete. The model contained a significant amount of iteration loops. Since the loops were simple calculations it calculates in a workable time frame, however, making the model more complex could greatly increase the computational time of the calculations.

1.6. Research objective and approach

The objective of this research is to develop a model for the condenser in the OTEC cycle that provides detailed information of the phenomena occurring inside the heat exchanger. The research consists of two different parts with subobjectives. The first part focuses on providing an accurate heat transfer coefficient to improve the condenser calculations in the OTEC model developed by Goudriaan [12] and Kuikhoven [23]. The subobjectives are as follows:

- Determine what dominant phenomena could occur and select dimensionless quantities that represent these phenomena.
- Extrapolate the research of Goudriaan [12] and Kuikhoven [23] by validating the condenser model for other working fluid mass flows.
- Fit a heat transfer correlation that predicts the heat transfer of the condenser accurately.

The second part focusses on the whole condenser process by developing a detailed model using the method developed by Fernández-Seara et al. [10]. The subobjectives are as follows:

- Predict the pressure on the working fluid side of the condenser.
- Determine what processes are dominant in the condenser heat exchanger.
- Find the specific processes that cause a decrease in performance when ammonia-water is used as the working fluid instead of pure ammonia.
- Predict the states of the different fluids throughout the heat exchanger.

1.7. Thesis outline

Part I describes the method of fitting a heat transfer correlation to the experimental data gathered with the OTEC experimental setup that can be implemented in the work of Goudriaan [12] and Kuikhoven [23]. Chapter 2 provides a theoretical background for fitting data in a correlation with a review of relevant dimensionless quantities. In Chapter 3 the work done by Goudriaan [12] and Kuikhoven [23] is analysed, the choice of dimensionless quantities is explained and the fitting procedure and validation are shown. In Chapter 4 the resulting correlation fit is compared to other correlation fits and the results are shown for other mass flows. Chapter 4 ends with conclusions and recommendations.

In Part II the OTEC condenser model developed using the method of Fernández-Seara et al. [10] and Aarts [1] is described. Chapter 5 provides a theoretical background including thermodynamic, flow and mass transfer theories. The method of Fernández-Seara et al. [10] and Aarts [1] is also explained here. In Chapter 6 the working principle and the model choices are described. The chapter ends with the validation. In Chapter 7 the results of the model are analysed. The chapter ends with conclusions and recommendations.

I

Heat transfer coefficient curve fit method

2

Theoretical background

Heat transfer in two phase flows is a complex phenomenon to describe. The flow inside a heat exchanger should be described as well as the heat transfer behaviour of the fluids. For many non-ideal situations the analytical solutions are therefore not available. For the OTEC cycle the same problem is present. The heat exchanger is a plate heat exchanger, which incorporates complex two phase flow and the working fluid is a mixture.

Curve fitting a heat transfer correlation is a method to predict this complex heat transfer inside the heat exchanger while not fully describing its physical processes, a more bottom-up approach. Many researchers in the heat transfer field develop correlations for the heat transfer coefficient that are valid for certain flow conditions and geometries through experimental research and data fits. Dimensionless quantities that describe characteristic parts of the flow are fitted to experimental data. The fits are often valid for specific geometries and specific flow regime ranges. The same method is applied to the OTEC cycle in this chapter.

2.1. Dimensionless Quantities

With the use of dimensionless numbers heat transfer correlations can be fitted to certain situations and conditions using experimental data. A least-squares method can be used to investigate what factors are most relevant. This method provides a solution which is accurate and computationally inexpensive but only valid for a certain range of conditions. For this method to be accurate it is important to determine the dominant forces and properties that influence the heat transfer so that a representative set of dimensionless quantities can be chosen. Literature was studied to provide an extensive overview of the relevant dimensionless numbers.

2.1.1. Single phase flow

Heat transfer in a single phase flow is less complex than in a two phase flow. Therefore, when developing heat transfer correlations the ranges in which they are valid are relatively large and only the Prandtl number and the Reynolds number are necessary to properly describe most flows. In literature heat transfer correlations were developed for single-phase flow plate heat exchangers. As mentioned in the review of Gudjonsdottir [13] the heat transfer correlations found in literature can be described by:

$$Nu = aRe^{b}Pr^{c}, \tag{2.1}$$

coefficients a, b and c are coefficient that can be fitted to certain experimental data. Validity regimes are bounded only by Reynolds numbers. This means that in liquid flow the dominant phenomena that influence the heat transfer coefficients are flow characteristics and fluid properties. However, as Goudriaan [12] and Kuikhoven [23] stated for single-phase flow there are several relations for the same regime. The curves show slope differences, but the trends remain similar.

2.1.2. Two phase flow

For two phase flow it is challenging to find fixed dimensionless quantities that, when fitted, can describe any form of two phase heat transfer. Many different quantities have been developed, investigated and used

in literature. Most of the researches include both the Prandtl and Reynolds number but other quantities were added for various different situations. To judge the relevance of all the dimensionless quantities for the situation of the OTEC cycle it is important to identify all phenomena that occur in a two phase mixture flow that could influence the heat transfer coefficient. An overview of the dimensionless quantities that were found in literature is stated below. They are categorised by the phenomena that they describe.

2.1.3. Flow characteristics

The flow characteristics are present in every heat transfer correlation in the form of the widely used Reynolds number:

$$Re = \frac{\rho u d_h}{\mu}. \tag{2.2}$$

The physical interpretation is the ratio of inertial force over viscous force. It is used to define the degree of turbulence in a flow. In two phase mixture flows the Reynolds number takes different forms. Yan et al. [46] propose a Reynolds equivalent number which describes both phases with the vapor fraction and a mass flux:

$$Re_{eq} = \frac{\dot{G}_{eq} d_h}{\mu_l}, \tag{2.3}$$

$$\dot{G}_{eq} = \dot{G} \cdot \rho_{eq}, \tag{2.4}$$

where ρ_{eq} is defined as:

$$\rho_{eq} = \left[(1-q) + q \left(\frac{\rho_l}{\rho_v} \right)^{\frac{1}{2}} \right]. \tag{2.5}$$

Han et al. [15] take a similar approach using the same Reynolds equivalent number as Yan et al. [46]. Amalfi et al. [2] define two regimes where in one of the regimes the Nusselt number is not a function of the Reynolds number and in the other regime it is affected by Re_v and Re_l, the Reynolds numbers of the vapor and liquid, respectively.

2.1.4. Mass transfer

Mass transfer occurs in mixtures and two phase fluids. During condensation or evaporation the ammonia-water two phase mixture of OTEC has both. Water and ammonia exchange mass through diffusion and the ammonia vapor and liquid also transfer mass through diffusion. This mass transfer also includes heat transfer. There is little research done regarding the influence of this phenomenon on the heat transfer coefficient. In plate heat exchanger literature this effect isn't taken directly into account in the heat transfer correlation even though research conducted by Nuijten [29], Aarts [1] and Fernández-Seara et al. [10] suggested that it is of importance. To add this property in a correlation a dimensionless quantity could be added. From mentioned literature the following quantities are relevant for mass transfer:

$$Sc = \frac{\mu}{\rho D}. \tag{2.6}$$

The physical interpretation of the Schmidt number is the ratio of momentum diffusivity (viscosity) over mass diffusivity. It is also called the mass transfer equivalent of Prandtl's number, since it only contains fluid properties [27].

$$Sh = \frac{\kappa d_h}{D}. \tag{2.7}$$

The physical interpretation of the Sherwood number is the ratio of convective mass transfer over the rate of diffusive mass transport. Sherwood number is the mass transfer equivalent of the Nusselt number. Sherwood number can also be written as a function of the Reynolds number and the Schmidt number $Sh = f(Re, Sc)$. Lewis number can also be used:

$$Le = \frac{\lambda}{\rho D c_p}. \tag{2.8}$$

Its physical interpretation is the ratio of thermal diffusivity over mass diffusivity. The Lewis number is important in determining the relationship between mass and heat transfer coefficients [27]. It can also be rewritten as $Le = Sc/Pr$. Another interesting quantity is the Stanton mass number ($\mathrm{St_m}$):

$$St_m = \frac{Sh}{ReSc} = \frac{\kappa}{u}. \tag{2.9}$$

The physical interpretation of the Stanton mass number is the ratio of the mass transfer coefficient and the velocity of the flow.

2.1.5. Scale

When working on small scale surface tension can be a dominant force, so much so that it can also be of influence on the heat transfer coefficient. The surface tension can influence the flow pattern and wettability of the wall-fluid contact. On sufficiently small scale the surface tension can influence the flow velocity through capillary forces. The following dimensionless quantities are relevant for describing surface tension effects:

$$We = \frac{\rho u^2 d_h}{\sigma}, \tag{2.10}$$

the physical interpretation of the Weber number is the relative importance of the fluid's inertia compared to its surface tension.

$$Bd = \frac{d_h^2 g(\rho_l u - \rho_v u)}{\sigma_l}, \tag{2.11}$$

the physical interpretation of the Bond number is the ratio of gravitational forces over surface tension forces.

$$Ca = \frac{u_l \mu_l}{\sigma_l}, \tag{2.12}$$

the physical interpretation of the capillary number is the ratio of viscous force over surface tension.

Amalfi et al. [2] showed that for evaporative flows these quantities can be of interest in some plate heat exchangers. A distinction was made between the macro- and microscale. To determine whether a heat exchanger works in a certain regime the Bond number was used for analysing the flow. When working in the microscale the Weber number was added to the correlation. When working in the macroscale the Bond number was added to the correlation. Amalfi et al. [2] didn't include other dimensionless numbers in the microscale equation and no other papers report taking surface tension into account for the heat transfer coefficient.

2.1.6. Phase change

Several non-linear effects are introduced by the phase change of the working fluid. Vapor and liquid interaction occurs and a liquid film can develop in a non-uniform way. Since the process is complex a large variety of dimensionless quantities is found in literature representing these effects. Since the difference between condensation and evaporation is significant a distinction is made.

Condensation

Guo and Anand [14] described condensation in a rectangular channel. A stratified wavy film was observed in this configuration. Dimensionless numbers were introduced to represent this in the correlation. Firstly, the Galileo number:

$$Ga = \frac{\rho_l(\rho_l - \rho_v) g d_h^3}{(\mu_l)^2}, \tag{2.13}$$

Guo and Anand [14], Winkelmann [45] and Yara et al. [47] used the Galileo number for condensing flows. The Galileo number's physical interpretation is the ratio of gravitational force over viscous force. It is expected that for stratified wavy film the liquid wants to fall down because of gravity but is resisted by viscous forces. A two phase multiplier was also mentioned called the Lockhart-Martinelli parameter:

$$X = \left(\frac{1-q}{q}\right)^{0.9} \left(\frac{\rho_v}{\rho_l}\right)^{0.5} \left(\frac{\mu_l}{\mu_v}\right)^{0.1}. \tag{2.14}$$

However, in Palmer et al. [31] it was found that the Lockhart-Martinelli parameter has very little effect on the Nusselt number. The Jakob number was also mentioned in Kedzierski and Kim [20] and Palmer et al. [31] for condensation processes:

$$Ja = \frac{c_{p,l}(T_{sat} - T_{wall})}{h_{fg}}, \tag{2.15}$$

which is defined as the ratio of sensible heat to latent heat. A higher temperature difference between the condensing refrigerant and the wall results in a lower heat transfer coefficient. Froude and Convection number are used for higher mass fluxes.

Evaporation

The Lockhart-Martinelli Paramater and Jacob's number were also mentioned in literature (Palmer et al. [31] and Hsieh et al. [18]) on evaporative flows. In Han et al. [15] and Amalfi et al. [2] a boiling equivalent number was used:

$$Bo_{eq} = \frac{\dot{q}}{\dot{G}_{eq} h_{fg}}. \tag{2.16}$$

The physical interpretation of the boiling number is the mass of vapor generated per unit area of heat transfer surface over mass flow rate per unit flow cross-sectional area. Davidson [8] argued that it represents the stirring effect of the bubbles upon the flow. Longo et al. [26] used the Boiling number to divide the heat transfer coefficient in regimes where nucleate boiling or convective boiling is dominant:

$$Bo \cdot X > 0.15 * 10^{-3} \ \ (nucleate\ boiling), \tag{2.17}$$

$$Bo \cdot X < 0.15 * 10^{-3} \ \ (convective\ boiling). \tag{2.18}$$

The convection number was included in correlations developed by Sterner and Sunden [38] and Palmer et al. [31] for convective flows:

$$Co = \left(\frac{1-q}{q}\right)^{0.8} \left(\frac{\rho_v}{\rho_l}\right)^{0.5}, \tag{2.19}$$

it includes the gas density, liquid density and vapor fraction. It was not reported where the factors 0.8 and 0.5 come from. It has some similarity with the Lockhart-Martinelli parameter. In the relation for the mixture R32/R152a Palmer et al. [31] reported a very small effect of the Froude number with a significance of 0.088:

$$Fr = \frac{\dot{G}^2}{\rho^2 g d_h}. \tag{2.20}$$

Its physical interpretation is defined as the ratio of the flow inertia to the external field. In configurations that operate in another regime (mainly higher mass flux) it is seen that Froude plays a more significant role in the heat transfer.

2.1.7. Fluid properties

The fluid properties are present in every heat transfer correlation in the form of the widely used Prandtl number:

$$Pr = \frac{\mu c_p}{\lambda} \tag{2.21}$$

The physical interpretation of the Prandtl number is the ratio between momentum diffusivity and thermal conductivity.

2.1.8. Correction factors

Since most correlations cannot be fitted exactly by only using dimensionless numbers, correction factors are used that slightly alter the trend of a certain correlation. These factors are also dimensionless quantities however, they don't represent a certain physical phenomenon. It usually involves just one characteristic dimensionalised parameter.

A widely used correction factor is related to the geometry. Different ways to incorporate this parameter into correlations were found in literature. Most commonly geometry parameters are included in the correlation. Han et al. [15] used the chevron angle and the hydraulic diameter in a dimensionless geometry parameter as follows:

$$Ge = 2.81 \left(\frac{b}{d_h}\right)^{-0.041} (\beta)^{-2.83} \tag{2.22}$$

and gets a heat transfer coefficient that agrees within 25% in the range of $\beta = 20° - 45°$. Longo et al. [26] used a different geometry parameter for both condensation and evaporation. A term called the surface enhancement factor describing the ratio between the actual and the projected area of the plates. It is defined as follows:

$$\phi = \frac{A_{pr}}{A}. \tag{2.23}$$

Variations of these correction factors were also found. Longo et al. [26] also used a dimensionless correction factor for the pressure which is defined as follows:

$$p^* = p/p_c, \tag{2.24}$$

a mean absolute deviation of 20% for evaporation and 16% for condensation within the range of 28°-70° chevron angle was obtained. Kim [21] used a correction factor that is based on flow pattern behaviour. A wetted area parameter was used. It is supposed to include the effect of maldistributed liquid film on the heat transfer correlation and defined as follows for water slightly diluted with octanol:

$$\frac{A_{wet}}{A} = 0.052Re^{0.58}. \tag{2.25}$$

2.1.9. Summary

In table 2.1 a summary of all the dimensionless numbers can be found describing all the numbers and their reference document. What can be seen from the table is that almost all correlations include a Reynolds number and a Prandtl number, which is expected. Most correlations include some form of two phase modification, most in the form of a Reynolds equivalent number. Some however choose different dimensionless quantities to describe the phase change, but there is no real agreement among papers in that region. Mass transfer seems to be mostly neglected in literature as well as flow patterns and mixture effects. Mixture effects however are partially taken into account by transport theorems to include the non-linearity.

Table 2.1: Summary of all dimensionless numbers found in literature on both two-phase and single-phase correlations

Relevant dimensionless numbers heat transfer						
			Dimensionless	Formula	Physical interpretation	Reference
Single-phase flow			Reynolds	$Re = \frac{\rho v d_h}{\mu}$	Inertial forces over viscous forces	-
			Prandtl	$Pr = \frac{c_p \mu}{\lambda}$	Viscous diffusion rate over thermal diffusion	-
Two-phase flow						
	Mass transfer		Schmidt	$Sc = \frac{\mu}{\rho D}$	Momentum diffusivity over mass diffusivity	Mills [27]
			Sherwood	$Sh = \frac{\kappa d_h}{D}$	Convective mass transfer over the rate of diffusive mass transport	Mills [27]
			Lewis	$Le = \frac{\lambda}{D}$	Thermal diffusivity over mass diffusivity	Mills [27]
			$\text{Stanton}_{\text{mass}}$	$St_m = \frac{Sh}{ReSc} = \frac{\kappa}{u}$	Mass transferred liquid over the mass capacity of the liquid	Mills [27]
	Flow characteristics					
			Reynolds equivalent	$Re_{eq} = \frac{G_{eq} d_h}{\mu_l}$	Reynolds with two-phase influence	Yan et al. [46], Thonon and Bontemps [41]
	Scale		Weber	$We = \frac{\rho (u)^2 d_h}{\sigma}$	Inertial forces over surface tension forces	Amalfi et al. [2]
			Bond	$Bd = \frac{d_h^2 g(\rho_l u - \rho_v u)}{\sigma_l}$	Gravitational forces over surface tension forces	Amalfi et al. [2]
			Capillary	$Ca = \frac{u_l \mu_l}{\sigma_l}$	Viscous forces over surface tension forces	Nuijten [29]
	Phase change					
		Condensation	Galileo	$Ga = \frac{\rho_l (\rho_l - \rho_v) g d_h^3}{(\mu_l)^2}$	Gravitational over viscous forces	Guo and Anand [14], Winkelmann [45], Yara et al. [47]
			Jacob	$Ja = \frac{c_{p,l}(T_{sat} - T_{wall})}{h_{fg}}$	Heat transfer over latent heat	Palmer et al. [31], Hsieh et al. [18]
		Evaporation	Martinelli parameter	$X = \left(\frac{1-q}{q}\right)^{0.9} \left(\frac{\rho_v}{\rho_l}\right)^{0.5} \left(\frac{\mu_l}{\mu_v}\right)^{0.1}$	Influence of vapor fraction	Palmer et al. [31], Longo et al. [26]
			Boiling equivalent	$Bo_{eq} = \frac{\dot{q}}{G_{eq} h_{fg}}$	Mass of vapor generated per unit are of heat transfer surface over mass flow rate per unit flow cross-sectional area	Longo et al. [26], Davidson [8], Han et al. [15], Amalfi et al. [2]
			Convection	$Co = \left(\frac{1-q}{q}\right)^{0.8} \left(\frac{\rho_g}{\rho_l}\right)^{0.5}$	Influence of vapor fraction, similar to X	Sterner and Sunden [38], Palmer et al. [31]
			Froude	$Fr = \frac{G^2}{\rho^2 g d_h}$	Ratio of the flow inertia to the external field	Palmer et al. [31]
	Fluid properties		Prandtl	$Pr = \frac{\mu c_p}{K}$	Viscous diffusion rate over thermal diffusion rate	-
Correction factors						
	Geometry		Ge	$Ge = 2.81 \left(\frac{b}{d_h}\right)^{-0.041} (\beta)^{-2.83}$	The influence of the chevron angle on the heat transfer coefficient	Han et al. [15]
			Dimensionless pressure	$p^* = p/p_c$		Longo et al. [26]
			Wetted area correction	$\frac{A_{wet}}{A} = 0.052 Re^{0.58}$	Effect of maldistribution of the liquid film	Kim [21]

3

Methods

In 2016 a model was developed by Goudriaan [12] and Kuikhoven [23] to describe and predict the process of an OTEC power cycle using a mixture of ammonia and water. However, as will be mentioned later in this chapter, the heat transfer in the heat exchangers wasn't predicted accurately for some components. In this chapter the results of the different components are assessed and where needed a fit is developed for the heat transfer correlations that proved to be inaccurate using the method described in Chapter 2. Since commonly used dimensionless quantities turned out to be not sufficient for some components, new quantities were explored as well. The new heat transfer correlations are compared to experimental data for validation.

3.1. Analysis work done by Goudriaan [12] and Kuikhoven [23]

In order to improve the model, the work done by Goudriaan [12] and Kuikhoven [23] was studied to identify the most deviant results. In the report the model was validated for the range stated in table 3.1.

The most illustrative results are shown in the following sections. The plots containing the heat transfer are used as a measure of accuracy. The correlations are evaluated for the three different heat exchangers present in the OTEC experimental setup, the recuperator, condenser and evaporator. Kuikhoven [23] and Goudriaan [12] did extensive research on the correlations found in literature and they fitted their own correlation for the single-phase flow.

3.1.1. Recuperator

The recuperator has two single phase flows; the weak concentration ammonia water coming from the separator and the strong concentrated ammonia coming from the condensor. The same correlation is used for both the ammonia-water mixture flows in the heat exchanger. Goudriaan [12] and Kuikhoven [23] use a correlation developed by Donowski and Kandlikar [9]. Accurate results were obtained compared to the experimental result. In figure 3.1 the predicted heat transfer of the recuperator was compared to the measured heat transfer with different concentrations. The correlation developed by Donowski and Kandlikar [9] predicts the heat transferred properly and was used. As shown in figure 3.1 the deviations are reasonably small.

Table 3.1: Conditions research Kuikhoven [23] and Goudriaan [12]

Conditions	
$\dot{m}_{wf}$	0.010 [kg/s]
$\dot{m}_{wm}$	0.3 [kg/s]
$T_{wm,in}$	27°C
$\dot{m}_{cm}$	0.225 [kg/s]
$T_{cm,in}$	5 [°C]
c_a	90-100%

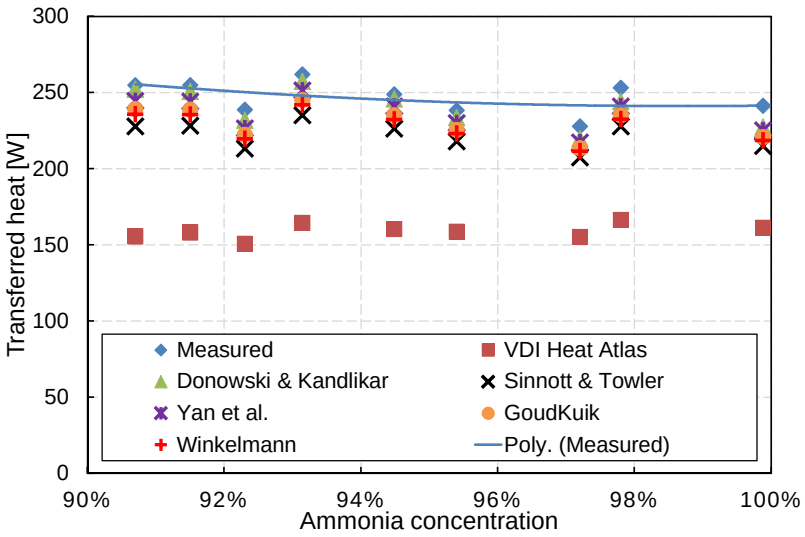

Figure 3.1: Heat transferred in the recuperator at different concentrations [12] [23]

3.1.2. Condenser

The condenser has a two phase absorption process on the working fluid side and a single phase liquid water flow on the cooling medium side. For the single phase water side a fit including a Reynolds and Prandtl number was sufficient to properly describe the heat transfer coefficient of the flow. Goudriaan [12] and Kuikhoven [23] developed and validated a new correlation to fit the single phase water flow. Since it was fitted to the heat exchanger it is assumed to be accurate. For the water side heat transfer correlations in both the evaporator and the condenser the fitted correlation was used.

For the working fluid side two phase correlations for condensation in plate heat exchangers were evaluated by Goudriaan [12] and Kuikhoven [23]. The heat transferred in the heat exchanger that was measured experimentally was plotted against the heat transferred predicted by different two phase flow heat transfer correlations. These results are shown in figure 3.2. As can be seen from figure 3.2 the performance of the condenser is overpredicted by the correlation developed by Yan et al. [46] and underpredicted by the other correlations tested. It is thus important to develop a new correlation fitted to the experimental data obtained.

3.1.3. Evaporation

For evaporation Goudriaan [12] and Kuikhoven [23] selected several correlations developed for the evaporation process in plate heat exchanger. The heat transfer measured in the experiments and the heat transferred predicted by the correlations was plotted. These results are shown in figure 3.3. It was concluded that the correlation developed by Ayub [3] for direct expansion gave the most accurate prediction of the system behaviour and as seen in the figure this is reasonably accurate.

3.1.4. Summary

Extensive research was done by Goudriaan [12] and Kuikhoven [23] on relevant heat transfer coefficients for the processes present in the different heat exchangers. In this section a brief assessment of their results was done. Conclusions were that the evaporator and the recuperator flows were properly described by the heat transfer correlations used in their model. The evaporator heat transfer was slightly off, but still with an acceptable accuracy. The recuperator was accurately predicted. The condenser heat transfer seemed to be predicted inaccurately. Therefore a new correlation must be developed. The water flow on the cooling medium side of the evaporator and the condenser was properly described by the fit they developed.

3.2. Dimensionless quantities

For development of the heat transfer coefficient of the condenser the dimensionless quantities that will be fitted have to be determined. The conventional way of developing a two phase heat transfer correlation is by

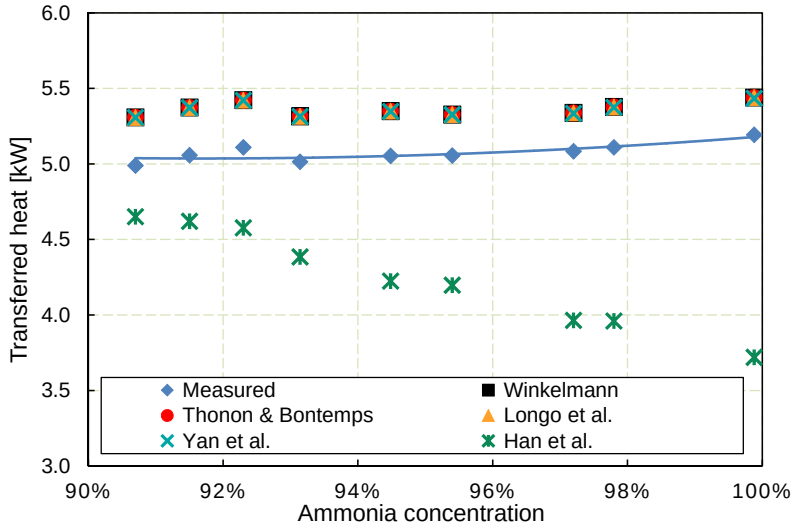

Figure 3.2: Heat transferred in the condenser at different concentrations [12] [23]

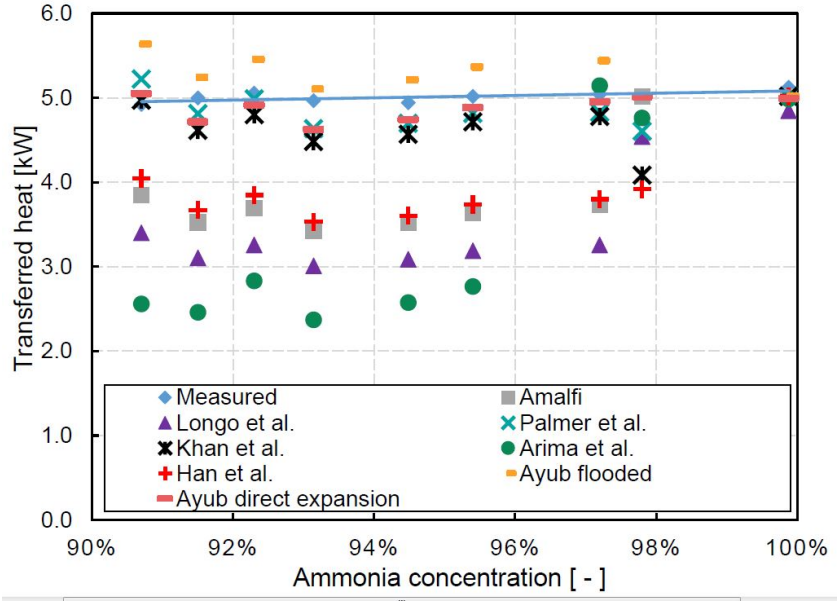

Figure 3.3: Heat transferred in the evaporator at different concentrations [12] [23].

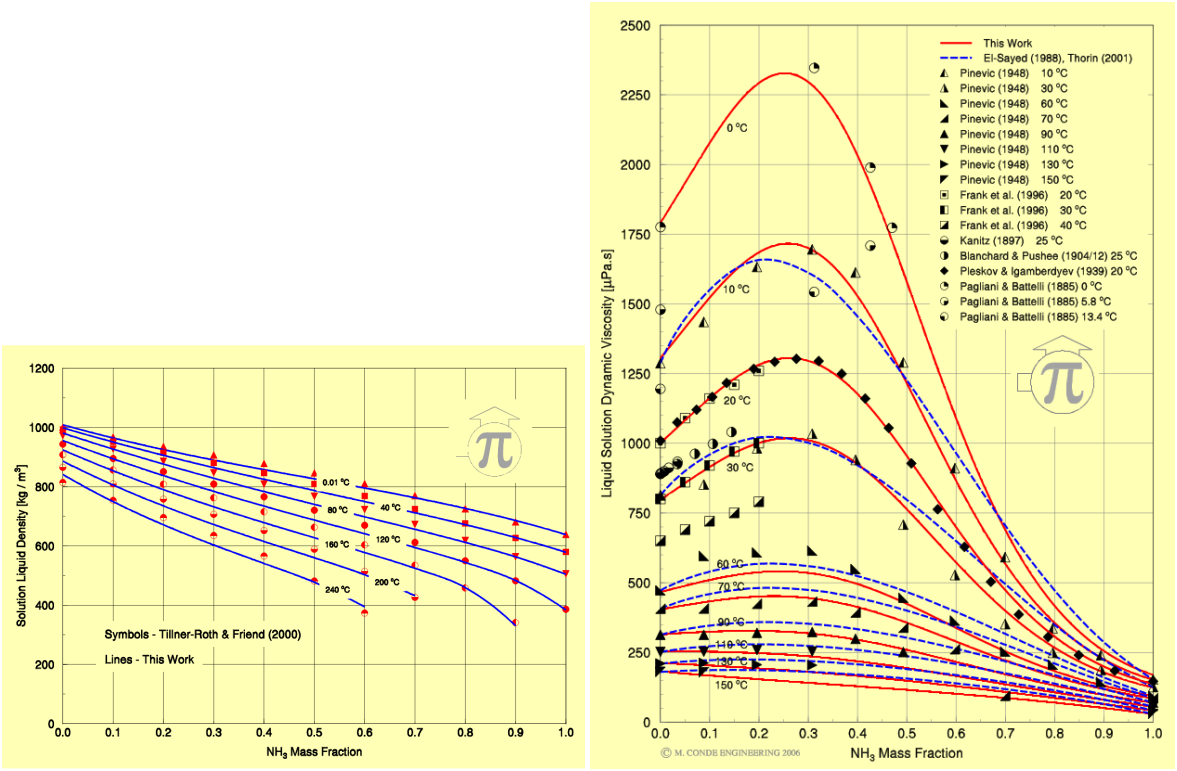

(a) (b)

Figure 3.4: (a) Density of an ammonia water solution (b) Dynamic viscosity of an ammonia water solution [7].

using the following format for the heat transfer:

$$Nu = aRe_{eq}^{b} Pr^{c}. \tag{3.1}$$

However, it is expected that flow characteristics (Reynolds) and fluid properties (Prandtl) are not sufficient to describe a complex absorption process. As stated in Fernández-Seara et al. [10] the absorption process is influenced by the mixture in a non-linear way. Table 2.1 shows the relevant dimensionless numbers. In order to know what dimensionless quantities are important it is interesting to see what the mixture properties of ammonia water are.

3.2.1. Physical properties of ammonia-water

From what is shown in figure 3.2 it can be expected that a dimensionless quantity has to be added that imposes a negative influence on the heat transfer with decreasing concentration. The physical properties of ammonia water are generated from databases developed by Conde [7]. The main physical properties used in heat transfer correlations are the ones used in the Reynolds and the Prandtl number. In the Reynolds number ρ and μ are present. The behaviour of both properties with changing concentration are shown in figures 3.4a/b, respectively. μ and ρ both increase at lower concentrations. In the Reynolds number the increase of the dynamic viscosity has a negative influence on the heat transfer and the increase of density has a positive influence on the heat transfer. Therefore it is expected that the Reynolds number won't be altered much by a change in concentration.

The Prandtl number consists of μ, c_p and λ and are shown in figures 3.4b and 3.5a/b, respectively. All of which are material properties. The specific heat decreases at lower concentrations, having a negative effect on heat transfer. The thermal conductivity increases slightly at lower concentrations, having a positive influence on the heat transfer. Therefore some influence of the concentration decrease is present in the Prandtl number. However, the influence is not sufficient to account for the decrease in performance of the condenser at lower concentrations. Therefore new material properties should be brought into the heat transfer correlation that are specifically relevant for changes in concentration. In table 2.1 it is seen that not any specific concentration related dimensionless quantities are used. Most quantities related to phase change that are added are

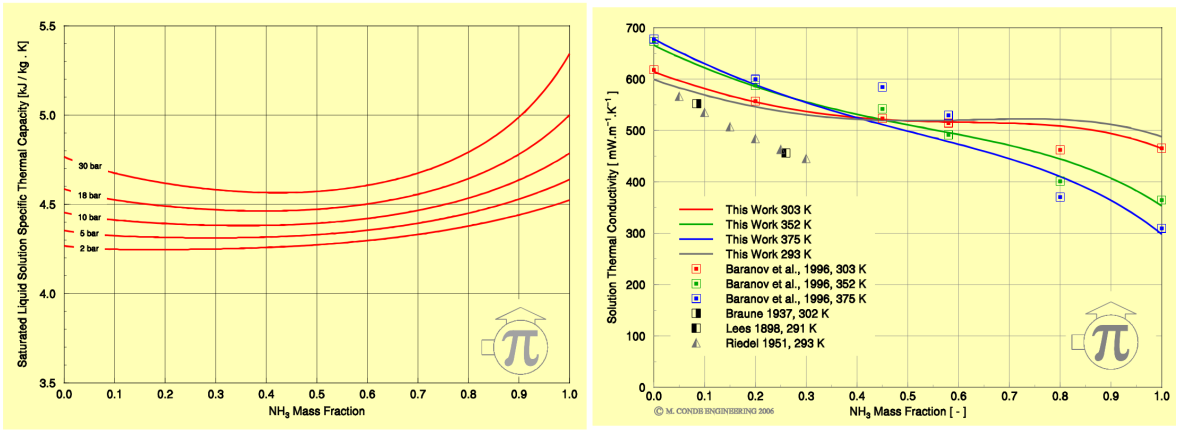

(a) (b)

Figure 3.5: (a) Specific heat at constant pressure for ammonia water (b) Thermal conductivity of ammonia water [7].

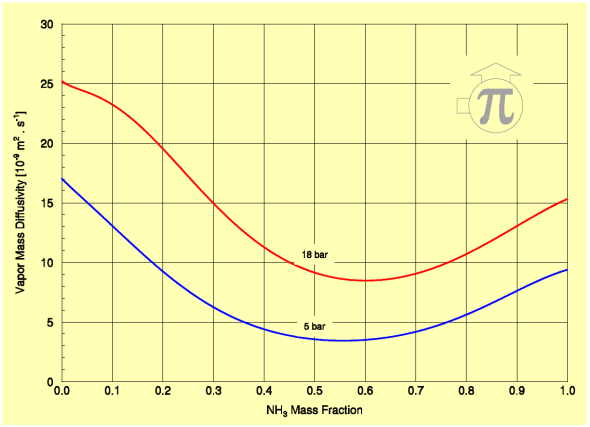

Figure 3.6: Mass diffusivity of ammonia water Conde [7].

either only related to the vapor fraction and density or are flow characteristics related. These quantities are not expected to be influenced significantly by mixture effects.

A more logical factor would be to include mass transfer. Through the vapor liquid interface mass is transferred from the vapor to the liquid. The mass transfer coefficient is proportionally influenced by the mass diffusivity D of the fluid. Therefore higher mass diffusivity results in a better heat transfer. What makes this property especially interesting is the fact that it has a very non-linear character when the concentration is changed. The mass diffusivity of water is higher than the mass diffusivity of ammonia. However, as seen in figure 3.6 the diffusivity goes down when adding a small percentage of water to pure ammonia. Therefore, at lower concentrations, the mass diffusivity has a negative influence on the heat transfer. In Fernández-Seara et al. [10] it is shown that mass transfer would have a significant effect on the heat transfer for a similar setup.

Another factor that could also play a role in the heat exchanger is surface tension. On very small scale the surface tension could be a dominant factor in the flow characteristics of the flow through capillary forces. On larger scale surface tension could play a role as well. Surface tension influences the wetting of a surface. When the surface tension increases the liquid wants to agglomerate and not spread out over the wall surface [21]. This could influence the heat transfer as well. However, there are no known dimensionless quantities that take into account the material properties of the surface tension. The quantities involving surface tension in table 2.1 are primarily focused on small scale applications.

3.2.2. Analysis

The main effect that needs to be incorporated in the heat transfer coefficient is the influence of the concentration of ammonia. From the previous section it can be concluded that with the present state of heat transfer correlations this is not sufficiently taken into account. If table 2.1 is regarded, the choice of dimensionless

Table 3.2: Cases tested for correlation fit, x indicates that the exponent was fitted for that particular case.

Exponent	Cases		
	1	2	3
a	x	x	x
b	x	x	x
c			x
d		x	x

quantities can be narrowed down with the following statements:

- Correction factors, numbers without physical meaning which should not be used in the first place.
- Geometry, the geometry stays the same for all experimental data obtained.
- Phase change, as mentioned in the section before, the phase change quantities take only vapor fraction and density into account but nothing concentration related.
- Scale, these dimensionless quantities are related to capillary forces over flow forces. Even though it is interesting that the surface tension is taken into account, the quantities are designed for small scale and the ratios are thus not as interesting as on large scale.

So that leaves mass transfer numbers. Schmidt and Sherwood are the ones most commonly used for mass transfer applications. Schmidt being the equivalent of Prandtl for mass transfer and Sherwood being the equivalent of Nusselt for mass transfer. Since the factor will be used to calculate the Nusselt number it makes more sense to use Schmidt number. Therefore the correlation that has to be fitted is the following:

$$Nu = aRe_{eq}^{b} Pr^{c} Sc^{d}. \tag{3.2}$$

To accurately analyse the influence of the dimensionless quantities different cases were tested and the results analysed. Three cases were designed where only a part of the quantities were fitted and others were fixed. Table 3.2 shows the different cases that were tested. The prefactor and the Reynolds number exponent were fitted in every case.

3.3. Curve fitting

In order to test the cases in table 3.2, the curves have to be fitted against the experimental data. The procedure is shown in this section.

3.3.1. Time dependency study

For the model to fit the curve to the dimensionless quantities it has to calculate all experimental data for one iteration of one dimensionless quantity. Since this is very time consuming a time dependency study was conducted to evaluate what experimental data points are computationally most expensive. In figure 3.7a the experimental data is plotted in a concentration vs mass flow diagram. The experimental data points are used for the inlet conditions of the model developed by Goudriaan [12] and Kuikhoven [23]. The time it takes to calculate the stream properties at the outlet of the condenser is shown in figure 3.7b. As can be seen the model becomes a lot slower at higher ammonia concentrations. This is due to the fact that calling thermodynamic properties from the database from Rattner and Garimella takes longer at higher concentrations. Since a study including all the data points takes too much computing time a selection of points was chosen to study which is shown in figure 3.8. Apart from the reduced computational time it is also interesting to see how well the experimental data fits to the points outside the region. If these show a reasonable accuracy the correlation fit can not only be used for interpolation but also for extrapolation.

3.3.2. Fitting procedure

The procedure of fitting the correlation is shown in fig 3.9. A simplified version of the condenser is shown in the figure. Goudriaan [12] and Kuikhoven [23] fitted the single phase correlation of water. Also the single phase mixture correlation was investigated and the correlation developed by Donowski and Kandlikar [9] was sufficiently accurate for the OTEC demo. Therefore, these two correlations are kept constant and are assumed

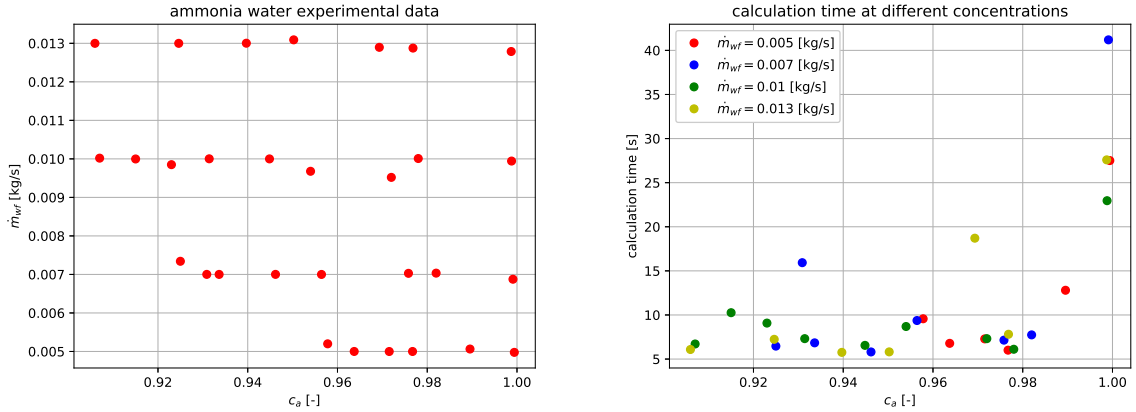

(a) (b)

Figure 3.7: Experimental data points measured in OTEC experimental setup; (a) mass flow vs concentration (b) calculation time for calculating the output of the model using experimental input data.

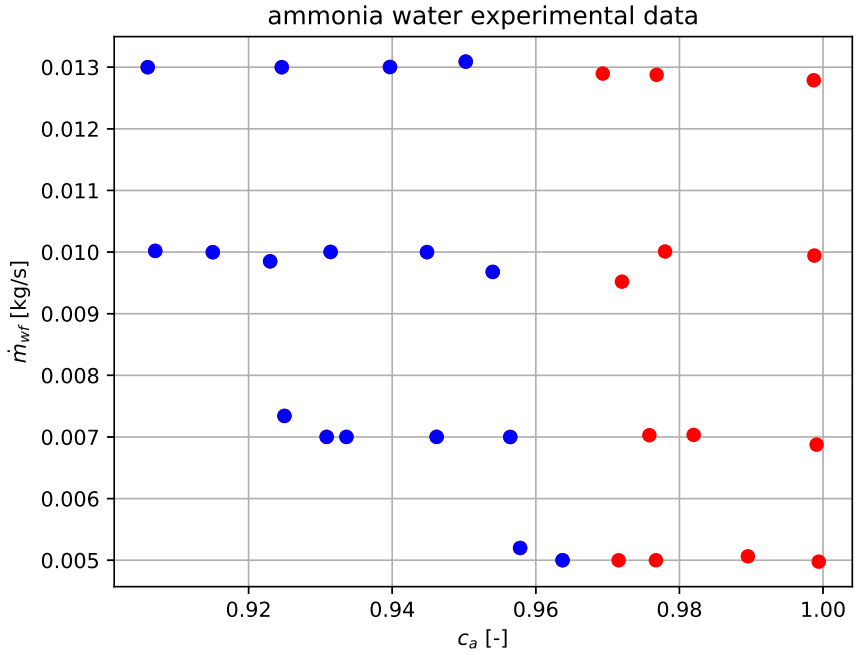

Figure 3.8: The blue dots are the experimental points used for fitting the correlation.

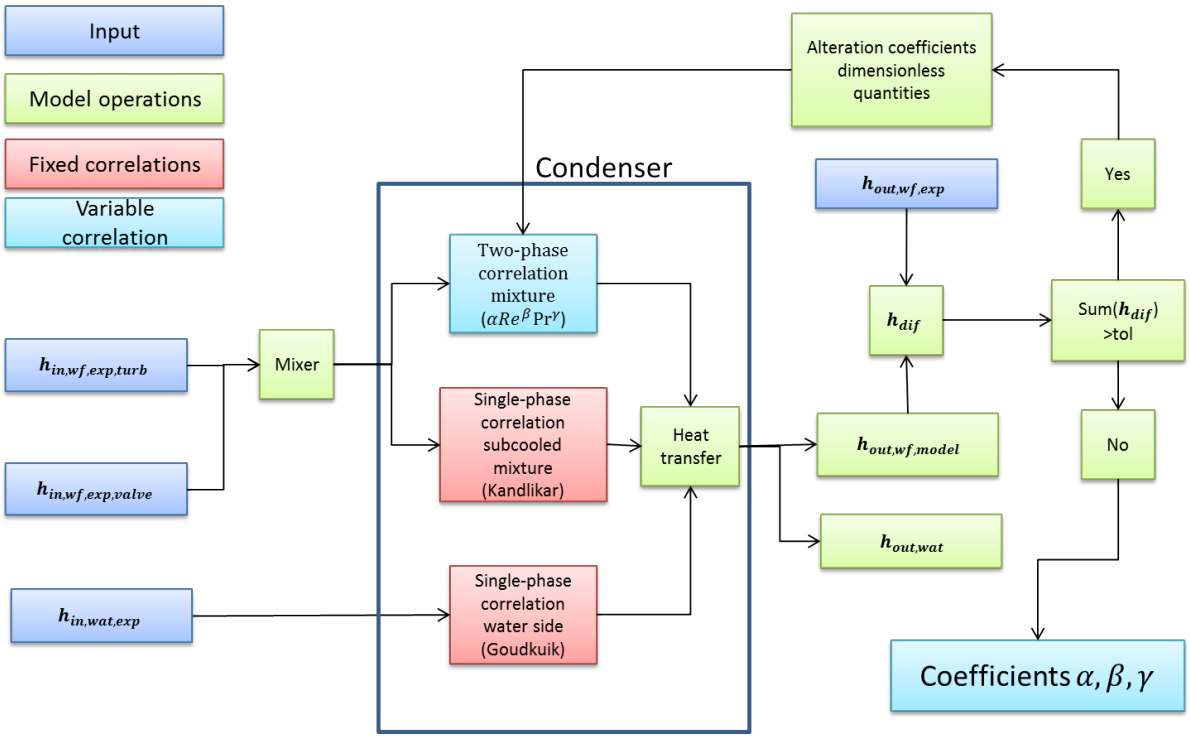

Figure 3.9: Procedure for fitting the two phase flow condenser correlation.

to be accurate. The inputs of the model are the experimental stream properties before the condenser. The condenser model calculates the enthalpy at the outlet of the system ($h_{out,wf,model}$). The enthalpy is compared to the experimental outlet enthalpy ($h_{out,wf,exp}$) and the difference is saved in a vector (h_{dif}), if the sum of this vector is bigger than the tolerance the coefficients of the dimensionless quantities are altered and the loop starts over.

3.4. Sensor accuracy

To properly assess the validity of the model the accuracy of the sensors has to be taken into account. From section 1.3.1 it can be seen that the pressure sensors are the least accurate. The pressure has a significant influence on the other characteristic parameters. However, changing the pressure in the condenser partly changes the process of the heat exchanger. Reducing the pressure would increase the vapor quality, however in reality the working fluid is assumed to always reach full condensation. Increasing the pressure would enhance the subcooled process and disproportionally decrease the working fluid temperature. Therefore deriving the accuracy of the dependent quantities was not done for this model.

3.5. Validation

The dataset was analysed and converged to the following solutions. The cases mentioned in table 3.2 were fitted and resulted in the following correlations:

$$Nu_1 = 1.22 Re_{eq}^{0.46} Pr^{0.33} Sc^{0}, \tag{3.3}$$

$$Nu_2 = 1.36 Re_{eq}^{0.64} Pr^{0.33} Sc^{-0.40}, \tag{3.4}$$

$$Nu_3 = 1.16 Re_{eq}^{0.48} Pr^{-0.50} Sc^{0.17}. \tag{3.5}$$

For comparison of the different solutions the condenser output enthalpy of the mixture was chosen as the characteristic parameter because of its direct relation to performance of the condenser and because it is not as sensitive to inaccuracy as the temperature. The enthalpy is plotted against the concentration for different mass flows in figures 3.10 to 3.12.

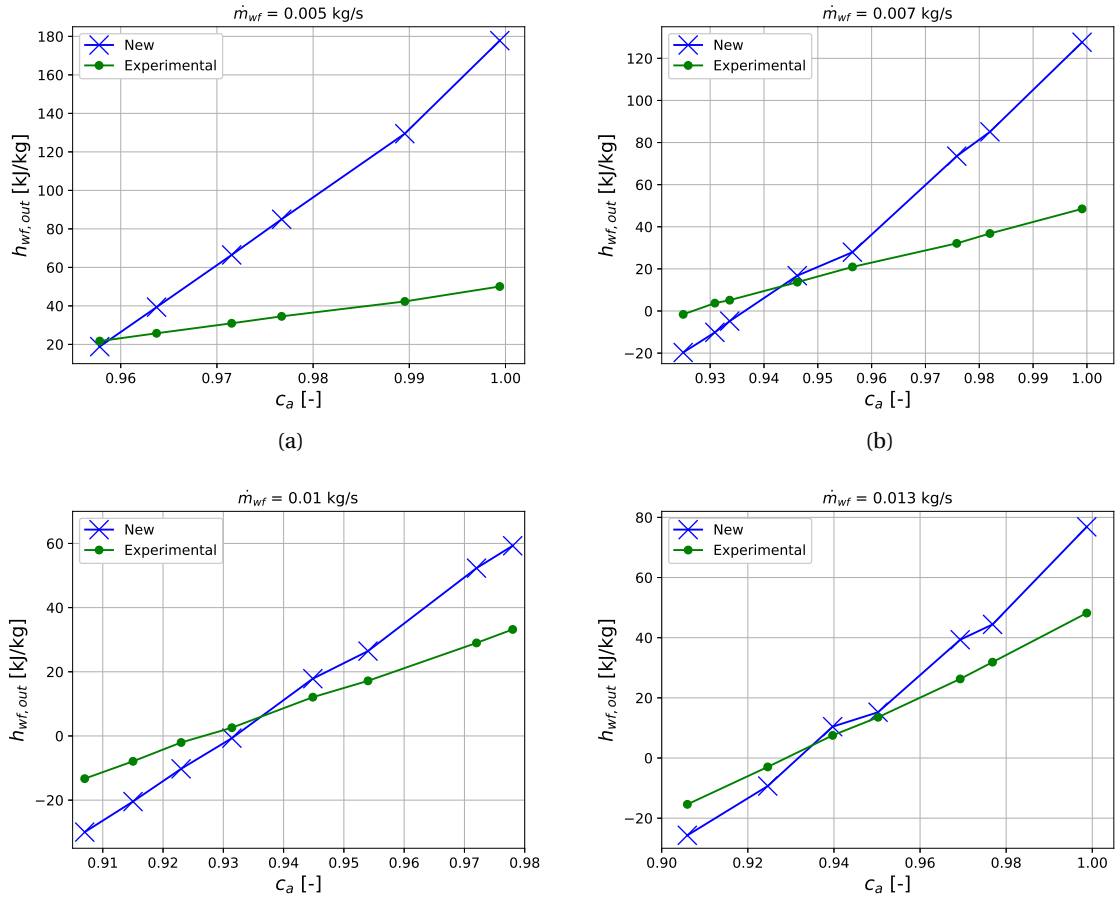

Figure 3.10: Case 1 mixture output enthalpy of the condenser working fluid at different concentrations for working mass flows (a) 0.005 kg/s (b) 0.007 kg/s (c) 0.010 kg/s (d) 0.013 kg/s.

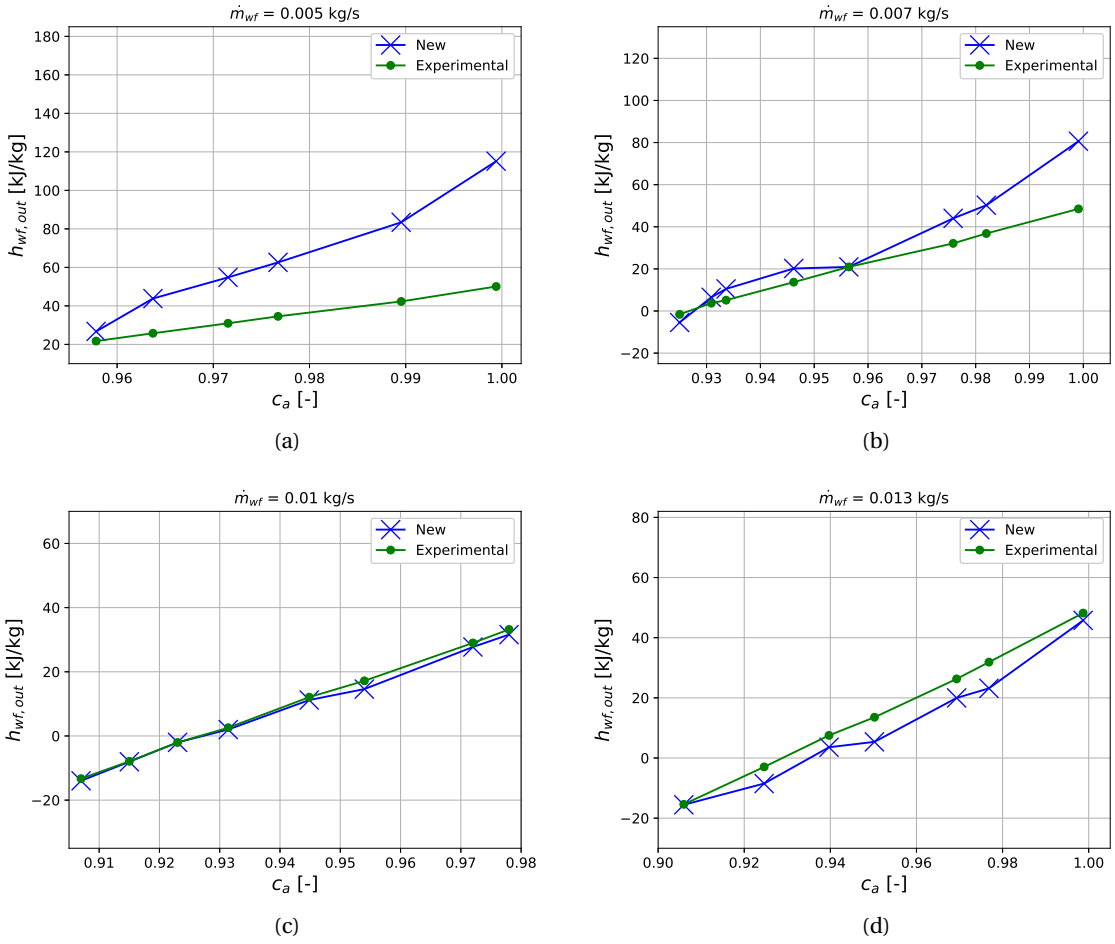

Figure 3.11: Case 2 mixture output enthalpy of the condenser working fluid at different concentrations for working mass flows (a) 0.005 kg/s (b) 0.007 kg/s (c) 0.010 kg/s (d) 0.013 kg/s.

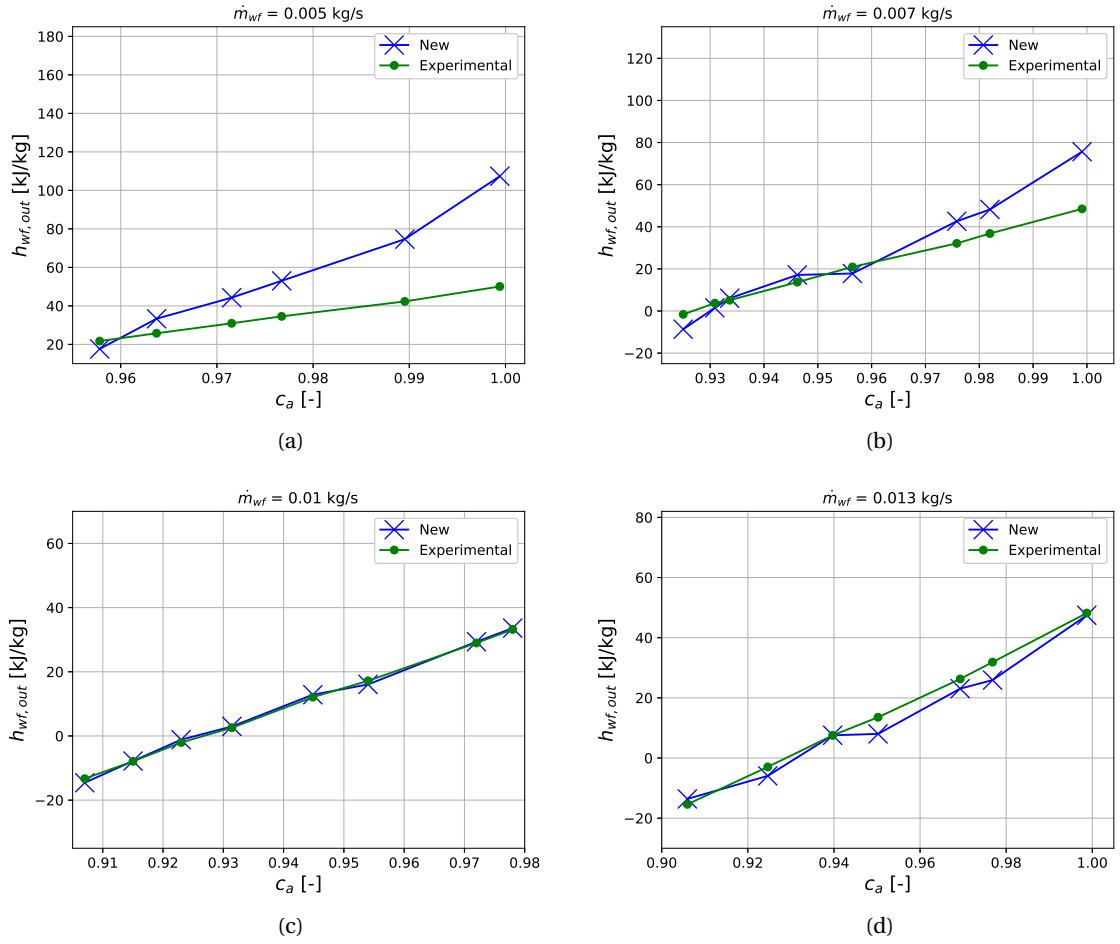

Figure 3.12: Case 3 mixture output enthalpy of the condenser working fluid at different concentrations for working mass flows (a) 0.005 kg/s (b) 0.007 kg/s (c) 0.010 kg/s (d) 0.013 kg/s.

Table 3.3: Mean Average Error and Normalized Mean Average Error of the outlet enthalpy of the model for the three different cases.

$c_a = 90-100\%$		
Cases	MAE [kJ/kg]	NMAE [-]
1	21.88	0.35
2	8.32	0.13
3	5.20	0.08

Table 3.4: Mean Average Error and Normalized Mean Average Error of the outlet enthalpy of the model for case three for different working fluid mass flows.

$c_a = 90-100\%$			
Case	$\dot{m}_{wf}$ [kg/s]	MAE [kJ/kg]	NMAE [-]
3	0.005	20.74	0.317
	0.007	5.13	0.078
	0.010	0.80	0.0122
	0.013	2.37	0.036
	Total	5.20	0.0795
	Total (excluding 0.005)	1.32	0.020

In table 3.3 the deviations of the outlet enthalpy of the experimental data and the model solutions are shown. The deviations are expressed in a Mean Absolute Error (MAE) and a Normalised Mean Absolute Error (NMAE), which are defined as follows:

$$MAE = \frac{\sum_{j=1}^{n} (h_{out,exp,j} - h_{out,mod,j})}{n} \qquad NMAE = \frac{\left(\frac{\sum_{j=1}^{n} (h_{out,exp,j} - h_{out,mod,j})}{n} \right)}{h_{norm}}. \tag{3.6}$$

Where n is defined as the amount of data points used in the calculation and h_{norm} is defined as the highest experimental value minus the lowest experimental value of the outlet enthalpy of the working fluid:

$$h_{norm} = max(h_{out,exp}) - min(h_{out,exp}). \tag{3.7}$$

From table 3.3 it can then be concluded that including the Schmidt number (case 2) in the equation improved the accuracy of the results. Also it seems that the equation slightly improved when varying the Prandtl number (case 3) which suggests that the Prandtl and the Schmidt number influence one another. It can also be seen that the more experimental points there are for a certain mass flow, the more accurate the fitted solution is. It can be expected that a more accurate solution can be found if more experimental data is gathered at different working fluid mass flows. To identify the magnitude of the error, table 3.4 shows the error per mass flow specifically. The 0.013 and 0.010 kg/s mass flow modelled data was accurate, the data for a working fluid mass flow of 0.007 kg/s was less accurate but can still be used in the model. As can be expected, at 0.005 kg/s working fluid mass flow the accuracy was lower. It is thus advised to not use the correlation for this mass flow. The accuracy of the fitted correlation was also validated using the characteristic parameters used in the studies by Goudriaan [12] and Kuikhoven [23]; working fluid outlet temperature, cooling medium outlet temperature, heat transferred by the cooling medium and heat transferred by the working fluid. The results are shown in table 3.5.

3.5.1. Discussion

The validated result can be used to generate new results for the condenser output values. The empirical correlation that was found to be most accurate is the following:

$$Nu = 1.16 Re_{eq}^{0.48} Pr_l^{-0.5} Sc_l^{0.17}. \tag{3.8}$$

Writing this out with the physical properties that it represents results in the following equation:

$$Nu = 1.16 \left(\frac{\rho_{eq} \dot{G} d_h}{\mu} \right)^{0.48} \left(\frac{\mu c_p}{\lambda} \right)^{-0.5} \left(\frac{\mu}{\rho_l D} \right)^{0.17} = 1.16 \rho_{eq}^{0.48} \rho_l^{-0.17} \dot{G}^{0.48} d_h^{0.48} \mu^{-0.81} c_p^{-0.5} \lambda^{0.5} D^{-0.17}. \tag{3.9}$$

Table 3.5: Deviations from the experimental and model values for relevant parameters for a working fluid mass flow of 0.010 kg/s.

	$T_{wf,out}$	$T_{cm,out}$	$\dot{Q}_{cm}$	$\dot{Q}_{wf}$
		c = 0.978		
Exp	10.57 °C	10.49 °C	5179.7 W	5101.3 W
Mod	10.66 °C	10.40 °C	5105.0 W	5105.0 W
Deviation	0.84%	-0.87%	-1.44%	0.07%
		c = 0.972		
Exp	10.61 °C	10.53 °C	5218.0 W	5068.1 W
Mod	10.68 °C	10.37 °C	5081.0 W	5081.0 W
Deviation	0.74%	-1.54%	-2.01%	0.25%
		c = 0.954		
Exp	10.89 °C	10.48 °C	5171.0 W	5049.4 W
Mod	10.64 °C	10.36 °C	5066.9 W	5066.9 W
Deviation	- 2.26%	-1.17%	-2.8 %	0.35%
		c = 0.9448		
Exp	11.23 °C	10.50 °C	5191.1 W	5045.2 W
Mod	11.39 °C	10.33 °C	5045.3 W	5045.3 W
Deviation	1.48%	-1.63%	-2.37%	0.00%
		c = 0.9314		
Exp	11.28 °C	10.43 °C	5131.9 W	5018.4 W
Mod	11.36 °C	10.30 °C	5010.2 W	5010.2 W
Deviation	0.72%	-1.34%	-2.37%	0.16%
		c = 0.923		
Exp	11.61 °C	10.53 °C	5224.8 W	5128.8 W
Mod	11.80 °C	10.39 °C	5101.2 W	5101.2 W
Deviation	1.64%	-1.30%	-2.37%	-0.54%
		c = 0.915		
Exp	11.59 °C	10.50 °C	5186.3 W	5080.46 W
Mod	11.60 °C	10.34 °C	5056.5 W	5056.5 W
Deviation	0.14%	-1.45%	-2.50%	-0.47%
		c = 0.907		
Exp	11.67 °C	10.46 °C	5153.8 W	5024.0 W
Mod	11.40 °C	10.29 °C	5002.1 W	5002.1 W
Deviation	-2.31%	-1.66%	-2.94%	-0.43%

This can be compared to a general two phase condenser heat transfer coefficient developed for plate heat exchangers found in literature. For comparison the heat transfer coefficient developed by Yan et al. [46] is used:

$$Nu = 4.118 Re_{eq}^{0.4} Pr_l^{0.33} = 4.118 \left(\frac{\dot{G} \rho_{eq} d_h}{\mu} \right)^{0.4} \left(\frac{\mu c_p}{\lambda} \right)^{0.33} = 4.118 \rho_{eq}^{0.4} \dot{G}^{0.4} d_h^{0.4} \mu^{-0.07} c_p^{0.33} \lambda^{-0.33}, \tag{3.10}$$

the values for ρ_{eq}, $\dot{G}$ and d_h are reasonably similar. However, μ shows a much smaller negative factor in the correlation developed by Yan et al. [46] and c_p and λ even show opposite effects to the heat transfer. Also a negative effect is found by the liquid density induced by the Schmidt number. A possible explanation could be that the film concentration profile is non-uniform and influences the heat transfer in a negative way. Adding new quantities could also influence the exponent of other quantities. For instance, the Schmidt number also contains the dynamic viscosity, thus influencing the factor of Prantdtl and Reynolds. An other explanation is that a local optimum was found which is technically not physical but happens to work for the experimental data points. Since there is only a limited amount of experimental data points it is possible that there are not enough data points to carefully estimate the influence of all quantities on heat transfer.

The solutions predicted for the output of the condenser showed good agreement with the experimental values that were measured. In table 3.5 it can be seen that for a working fluid mass flow of 0.010 kg/s, the working fluid outlet temperature stayed within 2.5% accuracy, the cooling medium outlet temperature stayed within 1.7% accuracy, the cooling medium heat transfer also stayed within 3% accuracy and the working fluid heat transfer stayed within 0.6% accuracy. Therefore it can be stated that for the range for which the correlation is developed the correlation showed a very good fit. As stated in section 3.4, the sensor accuracies were not taken into account.

4

Results and discussion

In this chapter it is discussed how the results shown in the previous chapter influence the characteristic parameters of the system. A comparison is made with the previous work done by Goudriaan [12] and Kuikhoven [23] for the working fluid mass flow of 0.010 kg/s. For the other working fluid mass flows the model results are compared to the experimental output to assess the overall validity of the correlation.

4.1. Comparison to previous studies

For comparison to previous studies the working fluid mass flow is taken fixed at 0.010 kg/s. This flow is selected because this is the mass flow in which most of the experimental data is gathered and because Goudriaan [12] and Kuikhoven [23] based their analysis on this dataset. The impact of the new correlation is evaluated in this section. Characteristic condenser performance parameters for the condenser are plotted against the results of other correlations used by Goudriaan [12] and Kuikhoven [23]. The heat transferred ($\dot{Q}_{cond}$), the overall heat transfer coefficient (U), the outlet temperature of the cooling medium ($T_{cm,out}$) and the working fluid outlet temperature ($T_{wf,out}$) are plotted in figures 4.1a/b/c/d. In figure 4.1b and c the results for $T_{cm,out}$ and U of other correlations are not shown because they weren't reported in the research of Goudriaan [12] and Kuikhoven [23]. For U only four values were given for the experimental data.

4.2. Other working fluid mass flows

There is also experimental data available that is measured for other working fluid mass flows. In order to judge the validity of the correlation it is important to compare the model data with this other mass flow data as well. Comparing the experimental data with the model calculations for these mass flows yields the results shown in figures 4.2 and 4.4. The working fluid heat transfer, the working fluid outlet temperature and the cooling medium outlet temperature are shown in the figures.

4.3. Discussion

For the 0.010 kg/s working fluid mass flow dataset, the following can be seen in figures 4.1a/b/c/d:

- The results show good agreement with the experimentally measured data.
- The other correlations that were found in literature for conventional plate heat exchanger flows are significantly different from the new correlation developed. This could mean that it is indeed necessary to add a quantity to the correlation that takes more fluid properties and mixture properties like the Schmidt number into account.
- The cooling medium outlet temperature and heat transfer are less accurate than the outlet temperature and heat transfer of the working fluid. This can be explained by the fact that the amount of heat transferred in the model is assumed to be ideal and therefore no losses to the environment are taken into account. This assumption leads to an inaccuracy in the heat transfer since it can be expected that there will be some heat losses. The model validation is based on the working fluid temperature and heat transfer, therefore the working fluid side is accurate with this assumption and the inaccuracy is on the water side.

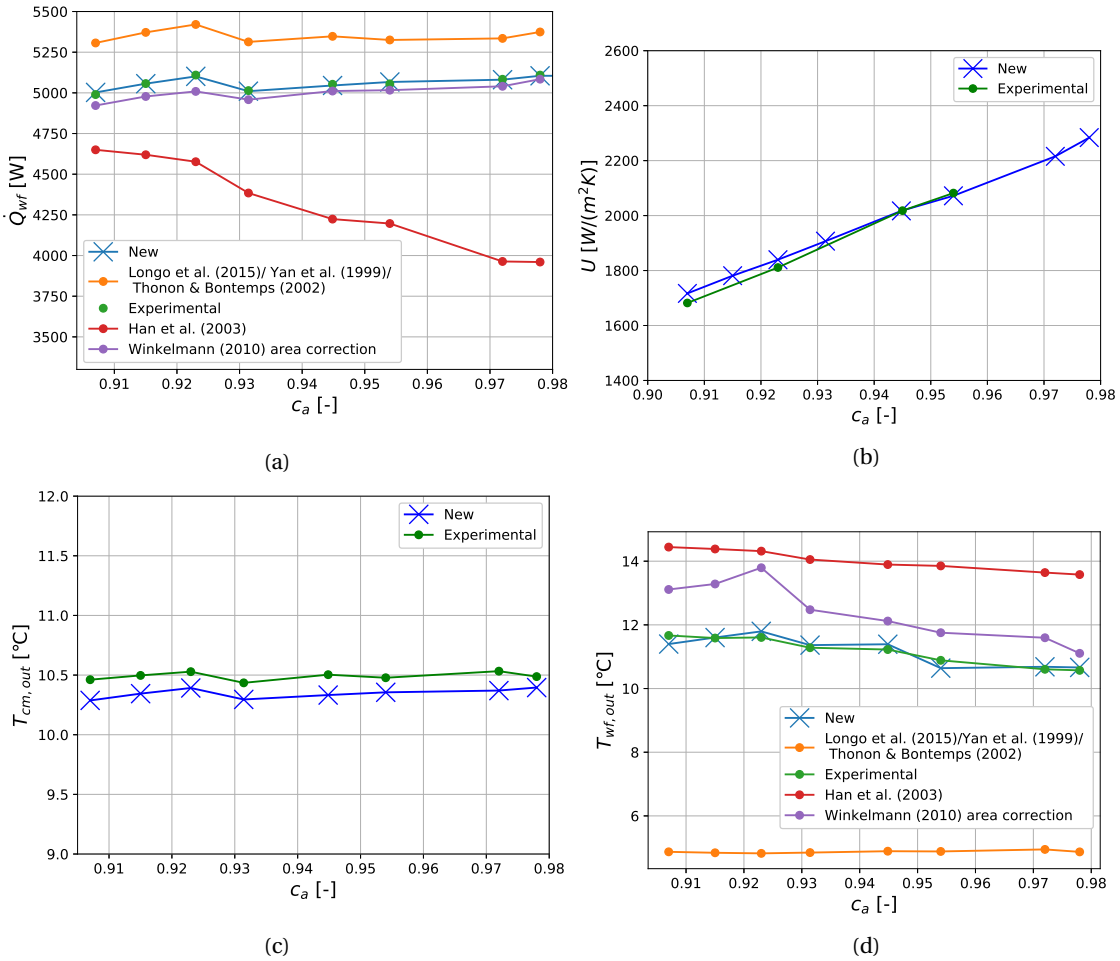

Figure 4.1: Condenser parameters compared to correlations mentioned in Goudriaan [12] en Kuikhoven [23] for $m_{wf} = 0.010 kg/s$; (a) the heat transferred from the working fluid side (b) the overall heat transfer coefficient (c) the outlet temperature of the cooling medium (d) the working fluid outlet temperature.

The result from using the same correlation for other working fluid mass flows can be found in figures 4.2 to 4.4. The results are reasonably accurate, but less accurate than for the 0.010 kg/s case. Especially the sensitive working fluid temperature gets more inaccurate with varying mass flows. This illustrates both the problem and power of this method for this case. The following observations elaborate that:

- The fitting method includes physical phenomena by adding dimensionless quantities to a correlation. In a two phase process however, complex phenomena are present, which may not be properly represented by the three dimensionless quantities used.

- The experimental values available for the condenser are limited, and thus the range in which the correlation was developed is limited. As can be seen by figures 4.2 to 4.4, the solution gets less accurate when operating outside of this range. For a better solution, more experimental data over a larger range are necessary.

- The method is an efficient way to get accurate results when the working range is limited.

4.4. Conclusion and recommendations

The objective of the first part of this study was to improve the model developed by Goudriaan [12] and Kuikhoven [23]. This was done by assessing the performance of the model as it is and improving the heat transfer coefficients where necessary. For better performance it was necessary to fit a new heat transfer correlation for the condenser of the model. This was done by identifying the relevant dimensionless quantities

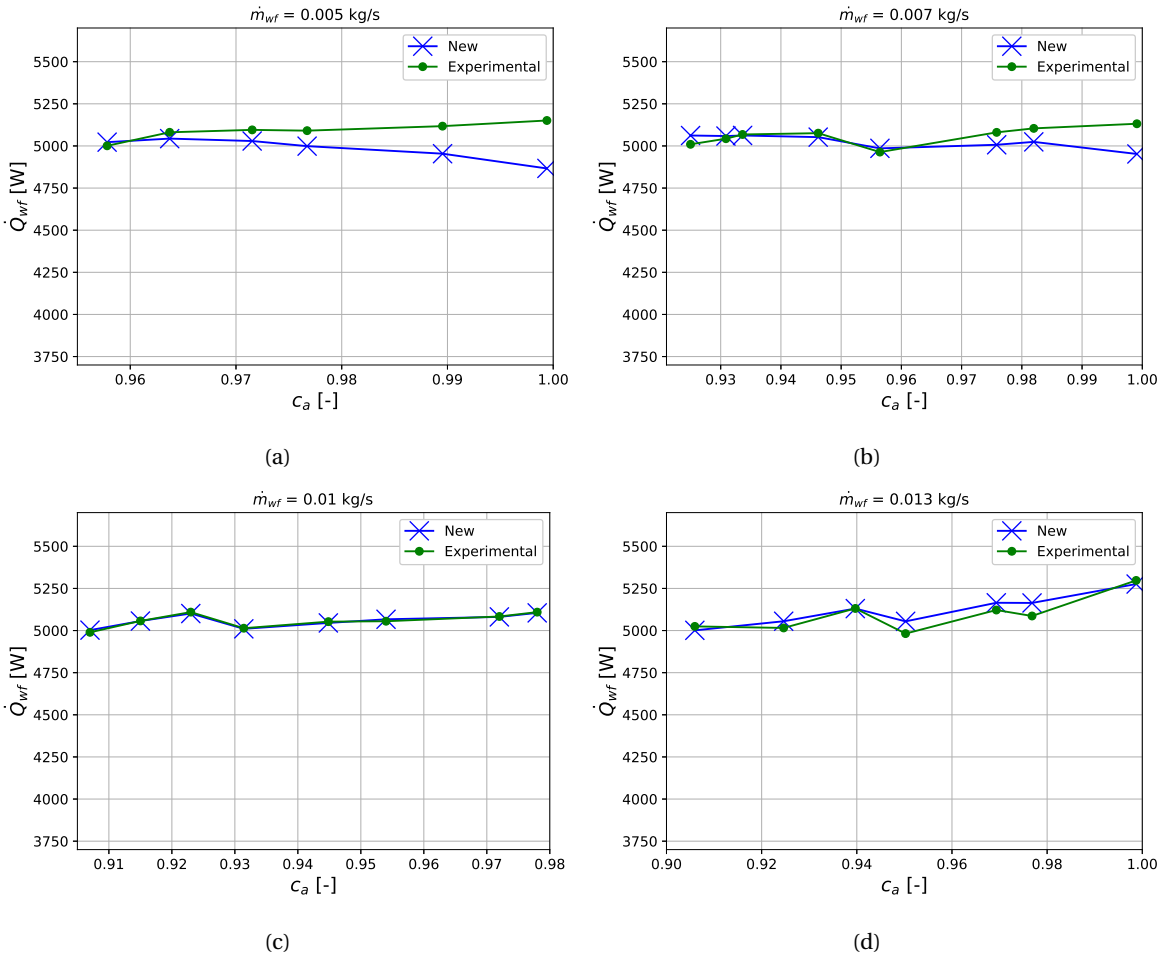

Figure 4.2: Heat transferred on the working fluid side compared to experimental data for different mass flows; (a) 0.005 kg/s (b) 0.007 kg/s (c) 0.010 kg/s (d) 0.013 kg/s.

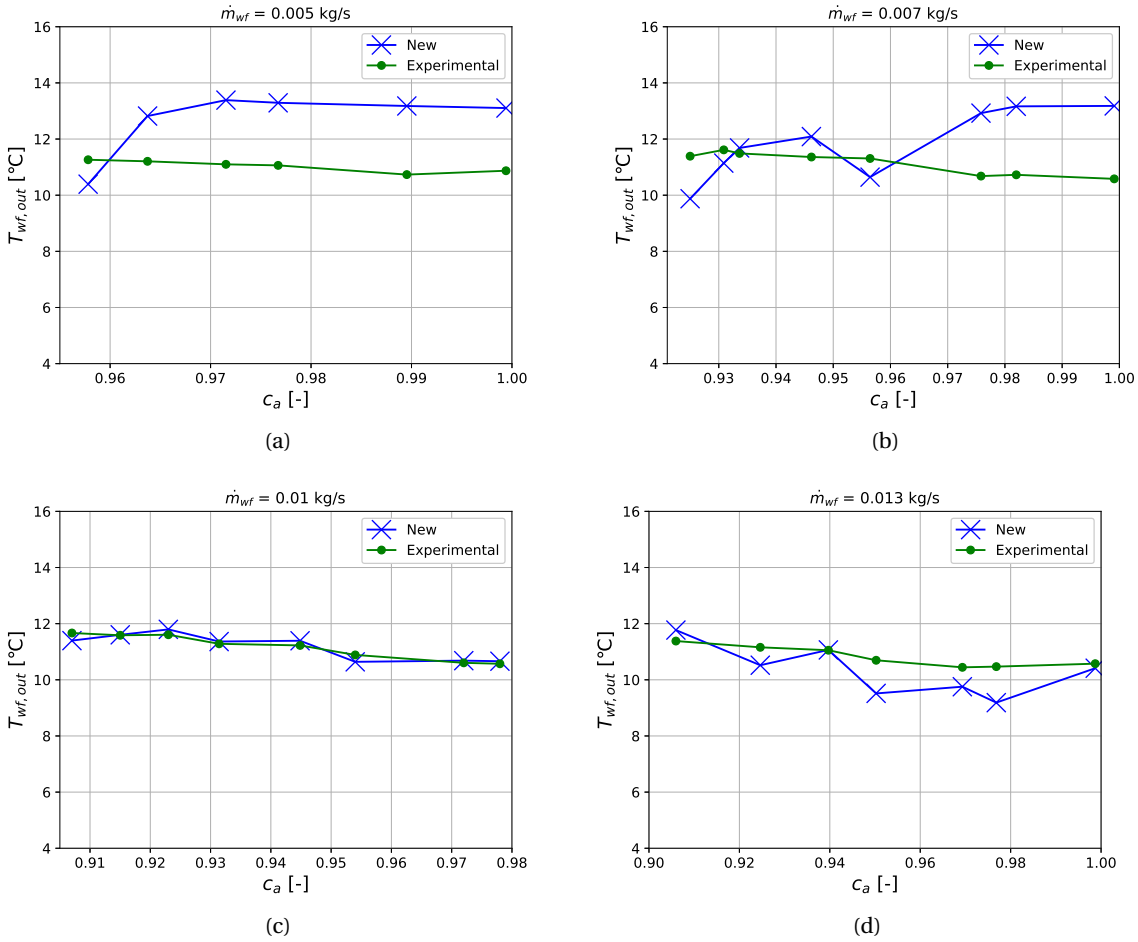

Figure 4.3: Working fluid outlet temperatures compared to experimental data for different mass flows; (a) 0.005 kg/s (b) 0.007 kg/s (c) 0.010 kg/s (d) 0.013 kg/s.

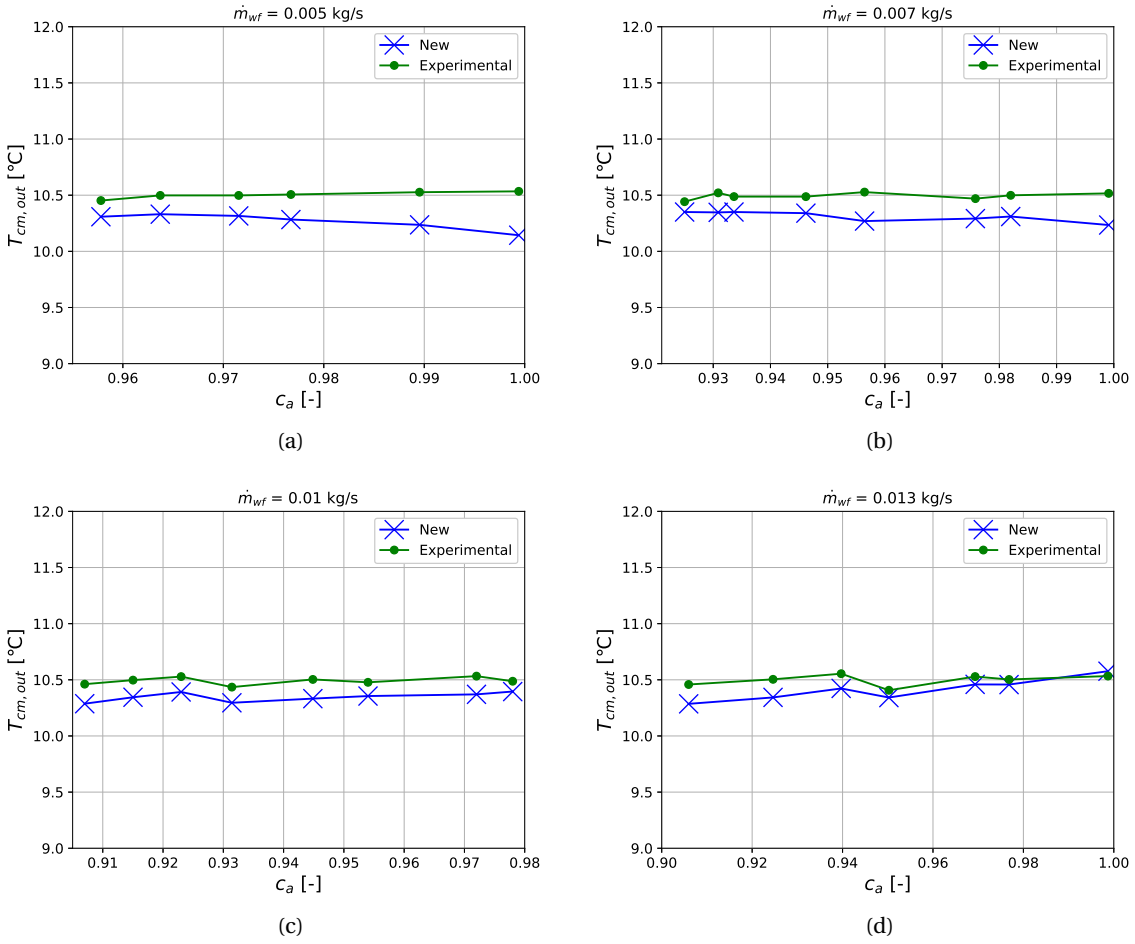

Figure 4.4: Cooling medium outlet temperatures compared to experimental data for different mass flows; (a) 0.005 kg/s (b) 0.007 kg/s (c) 0.010 kg/s (d) 0.013 kg/s.

and fitting the exponents to the experimental data. The curve fitting method proved to have both good aspects and less ideal aspects. The highlights in the results were the following:

- For the working fluid mass flow of 0.010 kg/s case the accuracy of the outlet values were as follows; the temperature of the working fluid stayed within 2.4% accuracy, the cooling medium temperature didn't exceed 1.7% accuracy, the cooling medium heat transfer was within 3% accuracy and the working fluid heat transfer stayed within 0.6% accuracy. The outlet enthalpy had an overall Mean Absolute Error of 0.8 kJ/kg and a Normalised Mean Absolute Error of 0.0122.
- Extrapolating for other mass flows lead to decent results as well. However, the deviations from the experimental values were more significant. For 0.005, 0.007 and 0.013 kg/s the MAE were 20.74, 5.13 and 2.37 kJ/kg, respectively, and the NMAE were 0.317, 0.078, 0.036, respectively.
- The resulting heat transfer coefficient showed a significantly different trend compared to previously developed heat transfer coefficients found in literature.

With these results the following observations and conclusion can be formulated:

- The new condenser correlation fitted in this research improves the results of the total cycle model developed by Goudriaan [12] and Kuikhoven [23].
- Curve fitting the two phase heat transfer coefficient of the working fluid is an accurate method within the region of the experimental data to which it is fitted.
- When using the correlation outside of the range of the experimental data used the model solutions are more off probably due to the lack of physical background of the curve fitting method. Therefore it is a useful method for predicting the performance of the condenser in the experimental OTEC setup, but it is an unreliable tool for predicting the performance of the condenser in a full scale OTEC plant.
- The behaviour and exponents of the dimensionless quantities are unexpected compared to available literature and physical background. The exponents of the specific heat and the thermal conduction were opposite of what is commonly developed for other correlations. The mass diffusivity is expected to have a positive impact on the heat transfer but the new correlation showed a negative relation. Therefore it is possible that a local optimum was found for the correlation.
- Physical insight in the process of heat transfer is marginal. It can be seen what the values of the heat transfer coefficients are but it is unclear what physical phenomena lead to these values.
- The method is fast due to its simplicity. High accuracy was acquired for a complex process in a time efficient way.
- The Schmidt number showed a significant influence on the heat transfer in the developed correlation, so it can be expected that mass transfer is an important parameter for this absorption process and also that the Schmidt number is a reasonable dimensionless quantity to represent this parameter.

The method gives accurate results but there are some issues with the method as well. Some are inherent for the method and some can be solved by improving the correlation. To improve the correlation it is recommended to look at the following aspects:

- More experimental data has to be gathered to make sure a global optimum was found for the curve fit.
- A better understanding of the dominant processes in a two phase mixture condenser has to be obtained to be able to more accurately make a selection of dimensionless quantities.
- Investigating other dimensionless quantities to make the correlation more generally valid. A dimensionless quantity involving surface tension could be interesting.
- For the current fit only data from one heat exchanger was used, which could also add to the optimum being more local. Similar flows should be tested in heat exchangers with different geometries as well.
- In part II of this report a more insightful method is used to describe the heat transfer in the working fluid. From this method the dominant heat transfer mechanisms can be extracted. This knowledge can be used to improve the curve fit of the heat transfer correlation.

II

Advanced two phase heat transfer method

5

Theoretical background

Fernández-Seara et al. [10] developed a combined mass and heat transfer model to describe heat transfer for a two phase flow. The two phase flow is divided into a liquid phase film and a vapor phase. Both phases are described by single phase correlations. The interaction that is present in a two phase fluid between the two phases is described by this model. The model incorporates the heat transferred through mass transfer between the liquid and the vapor phase. Figure 5.1 is a schematic used by Aarts [1] that describes this process and its variables. This chapter elaborates on theories and applications found in literature that should be considered in order to be able to develop a complete model of the heat exchanger with the method developed by Fernández-Seara et al. [10]. The different theories described in this chapter are tested and analysed in Chapter 6.

5.1. Film thickness

To be able to predict the heat transfer inside the heat exchanger the thickness of the liquid film in the channels should be determined. The film thickness can be determined both analytically and empirically. The analytical way comes from the falling film theory developed by Wilhelm Nusselt. It is mostly applied for a vertical film along a flat plate. The assumption is that the film thickness (δ_f) and the flow velocity (u) of the film is 0 at y = 0. Since it is important background knowledge for the rest of this work it will be briefly discussed here. Holman [17] mentions the derivation, this section will be based on his work. Figure 5.2 shows the process of laminar film development along a flat plate. Three forces work on the fluid element. The weight of the fluid element:

$$F_g = \rho_l g(\delta_f - y)dx, \tag{5.1}$$

the weight should be balanced by both the viscous shear force at point y:

$$F_{shear} = \mu \frac{du}{dx} dy \tag{5.2}$$

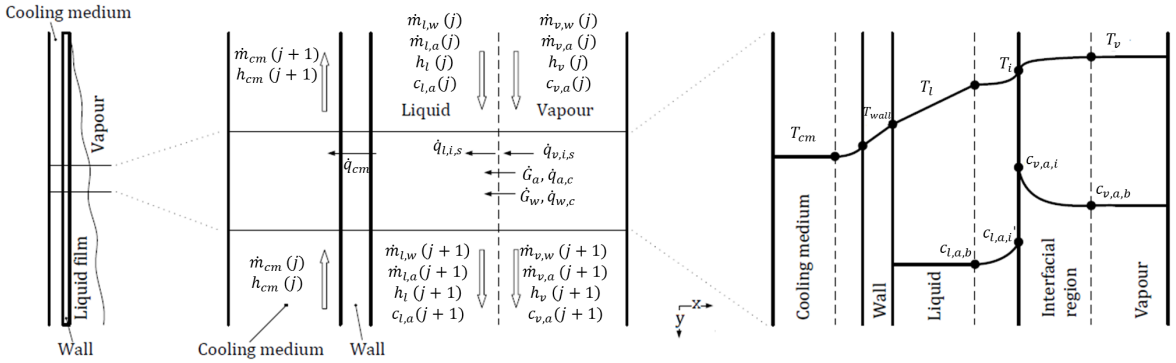

Figure 5.1: Schematic representation of the condensation process (Aarts [1]).

and the buoyance force due to displaced vapor:

$$F_{buoy} = \rho_v g(\delta_f - x)dy. \tag{5.3}$$

Using the force balance the following should apply:

$$F_g = F_{shear} + F_{buoy}. \tag{5.4}$$

Using the assumption that u = 0 at y= 0, equation 5.4 is integrated resulting in:

$$u_l = \frac{(\rho_l - \rho_v)g}{\mu_l}(\delta_f x - \frac{1}{2}x^2), \tag{5.5}$$

therefore the mass flow of the liquid is given by:

$$\dot{m}_l = \int_0^{\delta_f} \rho \left[\frac{(\rho_l - \rho_v)g}{\mu_l}(\delta_f x - \frac{1}{2}x^2) \right] dx = \frac{\rho_l(\rho_l - \rho_v)g{\delta_f}^3}{3\mu_l}. \tag{5.6}$$

A depth of 1 is assumed. The heat flux at the wall in the area dy thus becomes:

$$-\lambda_l dy \left. \frac{\delta T}{\delta_{f\,x}} \right]_{y=0} = \lambda_l dy \frac{T_v - T_{wall}}{\delta_f}. \tag{5.7}$$

A linear temperature profile is assumed. The condensed vapor adds to the liquid film thickness with δ_f from y to y + dy. The amount of condensate added is:

$$\frac{d}{dy}[\dot{m}_l]dx = \frac{d}{dy}\left[\frac{\rho_l(\rho_l - \rho_v)g\delta_f^3}{3\mu_l} \right] dy = \frac{d}{d(\delta_f)}\left[\frac{\rho_l(\rho_l - \rho_v)g\delta_f^3}{3\mu_l} \right] \frac{d(\delta_f)}{dy}dy = \frac{\rho_l(\rho_l - \rho_v)g\delta_f^2 d(\delta_f)}{\mu_l}. \tag{5.8}$$

The heat transferred to the wall must be equal to the mass flow added by the condensate multiplied by the latent heat of condensation:

$$\frac{\rho_l(\rho_l - \rho_v)g{\delta_f}^2 d(\delta_f)}{\mu_l} h_{fg} = \lambda_l dy \frac{T_v - T_{wall}}{\delta_f}. \tag{5.9}$$

Assuming the liquid film thickness to be 0 at y = 0, equation 5.9 can be integrated with the boundary condition $\delta_f = 0$ at $y = 0$ resulting in the film thickness:

$$\delta_f = \left[\frac{4\mu_l\lambda_l y(T_v - T_{wall}}{g h_{fg}\rho_l(\rho_l - \rho_v)} \right]^{\frac{1}{4}}. \tag{5.10}$$

This relation works well for simple laminar condensation on a vertical plate. However, the derivation of this relation becomes a lot more complex when the film cannot be assumed to be laminar or when the shape of the surface is different. Therefore relations have been developed empirically for situations where the analytical solution is not valid or complex. The most common way to determine these relations are with PIV measurements of the film thickness. The data is usually fitted to the following relation:

$$\delta_f = a\left(\frac{\nu_l}{g}\right)^b Re_l^c. \tag{5.11}$$

Where a, b and c are the fitted factors. There is still very little research in this field and most research is limited to turbulent or transition film layers of flat plates. Several variations of this method are analysed in Chapter 6. Alternatively, using the Nusselt condensation film theory, also based on the work by Holman [17], the relation can be written as follows:

$$\delta_f = \left(\frac{3\dot{m}_l\mu_l}{g\rho_l(\rho_l - \rho_v)} \right)^{\frac{1}{3}}. \tag{5.12}$$

A different method is developed by Aarts [1] where the film thickness is assumed to grow exponentially with a fixed profile with the following formula:

$$\delta_f = a\frac{y^{\frac{1}{4}}}{L^{\frac{1}{4}}}, \tag{5.13}$$

this method, however, was never validated.

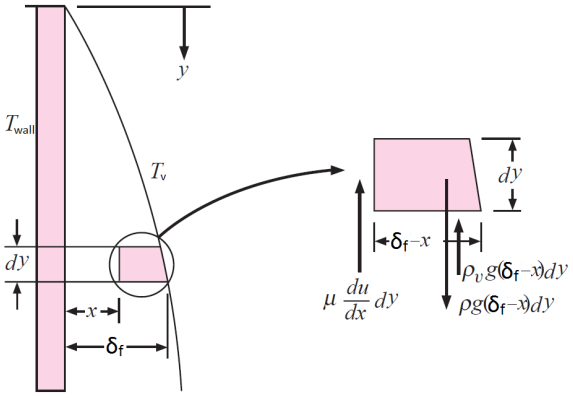

Figure 5.2: Process of laminar film development (Holman [17]).

5.2. Heat transfer coefficients

To describe the amount of heat transferred, the heat transfer coefficients of all the components and phases have to be calculated. Five different regions should be analysed: the cooling medium, the wall and the film, liquid interface and vapor interface of the working fluid.

5.2.1. Liquid film-wall flow

The two factors influencing the film flow heat transfer coefficient are the thickness of the film and the Nusselt number of the flow. Both are not analytically solved for plate heat exchanger applications and therefore correlations available in literature should be tested.

Nusselt number

For the film Nusselt number Aarts [1] and Nuijten [29] assume a unity Nusselt number for plate heat exchanger film flow:

$$Nu_f = 1. \tag{5.14}$$

Nefs [28] and Rijpkema [33] mention a Nusselt number of 2 for low Reynolds numbers (<30) in mini-channels:

$$Nu_f = 2. \tag{5.15}$$

Equation 5.15 assumes that the average Nusselt number of the film flow is the same as the Nusselt number in the middle of the film, which holds true for low Reynolds numbers and could potentially be valid for this case.

Another method of describing the Nusselt number would be to use one of the relations developed for single phase heat transfer in plate heat exchangers. From the relations known in literature, the following format (or a slight variation) is used for all relations specifically developed for plate heat exchangers:

$$Nu = aRe_l^b Pr_l^c. \tag{5.16}$$

Different variations of this relation are tested and analysed in Chapter 6. These relations are developed for single phase heat transfer problems in plate heat exchangers. Therefore the dimensionless quantities have to be redefined. For the Reynolds number the definition used by Winkelmann [45] for film flow in plate heat exchangers is used:

$$Re_f = \frac{4\Gamma}{\mu_l}, \tag{5.17}$$

where:

$$\Gamma = \frac{\dot{m}_l}{P} = \frac{\dot{m}_l}{2W\phi}. \tag{5.18}$$

The regular Prandtl number for liquid is used:

$$Pr_l = \frac{c_{p,l}\mu_l}{\lambda_l}. \tag{5.19}$$

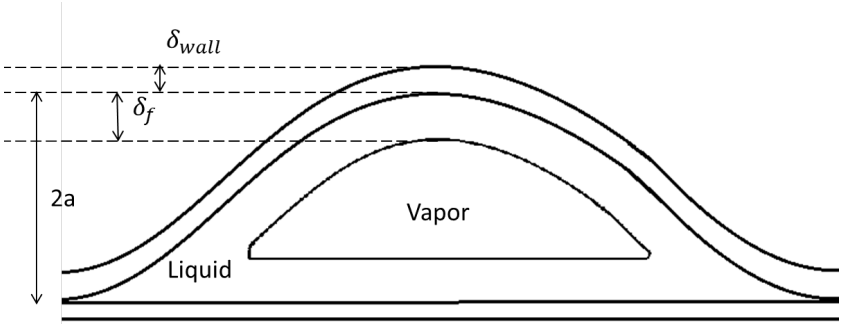

Figure 5.3: Schematic of two phase flow through plate heat exchanger.

Heat transfer coefficient

The heat transfer coefficient developed for film flow then becomes:

$$\alpha_f = \frac{Nu_f \lambda_l}{\delta_f}, \tag{5.20}$$

where the conductivity, λ_l, is the conductivity of the liquid film and is determined by the equations developed by Conde [7].

5.2.2. Liquid interface

The heat transfer coefficient of the liquid interface is determined in a similar way as for the film flow. The Nusselt number is determined using the single phase plate heat exchanger correlations. The definition of the liquid Prandtl number is the same as in equation 5.19. The interface Reynolds number is defined differently, as:

$$Re_l = \frac{u_l d_{h,l}}{\nu_l}, \tag{5.21}$$

where for single phase flow the hydraulic diameter d_h in a plate heat exchanger is defined in VDI [42] as:

$$d_h = \frac{4A}{P} = \frac{4W \cdot 2aL}{2WL\phi} = \frac{4 \cdot a}{\phi}. \tag{5.22}$$

In figure 5.3 the two phase channel flow is shown. From this figure it can be concluded that the liquid is enclosed by both the vapor and the wall. From the definition of the hydraulic diameter and figure 5.3 it can be concluded that the hydraulic diameter for the liquid in a two phase substance is defined as:

$$d_{h,l} = \frac{4A}{P} = \frac{4W \cdot 2\delta_f L}{2WL\phi} = \frac{4 \cdot \delta_f}{\phi}. \tag{5.23}$$

The liquid interface heat transfer coefficient is thus:

$$\alpha_{l,i} = \frac{Nu_{l,i} \lambda_l}{\delta_f}. \tag{5.24}$$

5.2.3. Vapor interface

A few different relations were found that represent the heat transfer correlation of the vapor in a two phase plate heat exchanger flow. As mentioned by Nuijten [29] the vapor phase flow can be modelled as natural convection of laminar flow over a plate by the correlation developed by Mills [27]. This results in the following Nusselt number:

$$Nu_{v,i} = 0.68 + 0.670(Ra_v \psi_v)^{\frac{1}{3}}, \tag{5.25}$$

where:

$$\psi_v = \left[1 + \left(\frac{0.942}{Pr_v}\right)^{\frac{9}{16}}\right]^{\frac{-16}{9}}. \tag{5.26}$$

The Rayleigh number is defined as:

$$Ra_v = \frac{\Psi(T_{v,b} - T_i)y^3(\rho_v)^2 c_{p,v}}{\lambda_v \mu_v}. \tag{5.27}$$

Aarts [1] defines the vapor flow as a turbulent flow over a flat plat and suggests two correlations that fit that definition; Seader and Henley [34]:

$$Nu_{v,i} = 0.037 Re_v^{0.8} Pr_v^{0.33}, \tag{5.28}$$

and Whitaker [44]:

$$Nu_{v,i} = 0.029 Re_v^{0.8} Pr_v^{0.43}. \tag{5.29}$$

Alternatively, the flow can be modelled with one of the single phase heat transfer correlations developed specifically for plate heat exchangers. This is similar to equation 5.16 but with dimensionless quantities related to the vapor:

$$Nu = a Re_v^b Pr_v^c. \tag{5.30}$$

The flow is modelled as shown in 5.3 so the vapor can be modelled as a normal plate heat exchanger flow with a smaller hydraulic diameter. Therefore the hydraulic diameter is defined as in equation 5.31.

$$d_{h,v} = \frac{4A}{P} = \frac{4W \cdot 2(a - \delta_f)L}{2WL\phi} = \frac{4 \cdot (a - \delta_f)}{\phi}, \tag{5.31}$$

the vapor Reynolds number is then defined as:

$$Re_v = \frac{u_v d_{h,v}}{\nu_v}. \tag{5.32}$$

Prandtl's number is defined as:

$$Pr = \frac{c_{p,v}\mu_v}{\lambda_v}. \tag{5.33}$$

The heat transfer coefficient for the vapor interface is:

$$\alpha_{v,i} = \frac{Nu_{v,i}\lambda_v}{d_{h,v}}. \tag{5.34}$$

5.2.4. Cooling medium

The heat transfer coefficient of the cooling medium was developed by Goudriaan [12] and Kuikhoven [23] specifically for water. For the heat exchanger that was used in the experiments conducted, the following Nusselt relation was obtained:

$$Nu_{cm} = 0.291 Re^{0.72} Pr^{0.33}. \tag{5.35}$$

5.3. Mass transfer coefficients

A condensation process involves mass particles transferring through the interface. To be able to calculate this mass transfer and consequently the heat transfer, the mass transfer coefficient has to be determined. The mass transfer coefficient is directly linked to the heat transfer coefficient through the analogy that was developed by Chilton and Colburn in 1934 [6]:

$$\kappa = \frac{\alpha D \rho_{mol}}{\lambda} \left(\frac{Sc}{Pr}\right)^{\frac{1}{3}}. \tag{5.36}$$

This relation applies for both the vapor and the liquid phase.

5.4. Heat transfer

By using the heat and mass transfer coefficients the heat transfer can be calculated. In a two phase condenser heat is transferred between the liquid and the vapor in two ways; by convection and by diffusion of the molecules. On the vapor-liquid interface diffusion occurs by the vapor molecules being absorbed into the liquid film and convection occurs between the bulk liquid and the bulk vapor. Between the cooling medium and the liquid medium heat is assumed to be transferred by convection to and from the wall and by conduction through the wall. The calculation methods of the heat transfer mechanisms are described in this section.

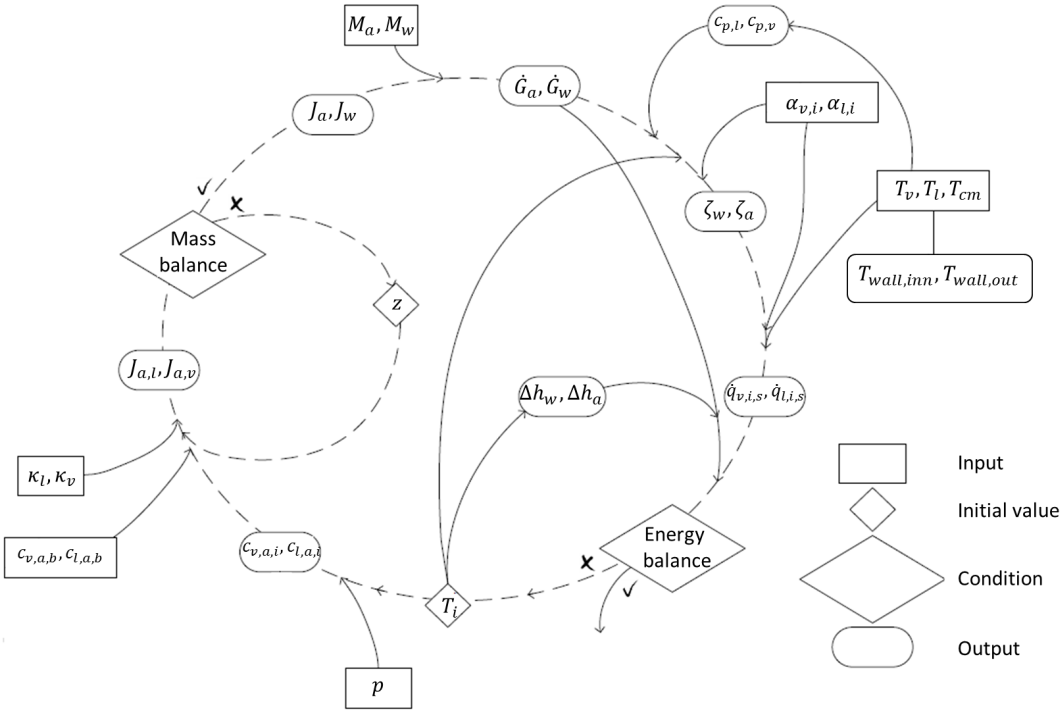

Figure 5.4: Flow diagram of the iterative solver for mass and heat transfer through the interface (Aarts [1]).

5.4.1. Heat flux through the liquid vapor interface

To determine the temperature in the liquid phase film the heat flux between the liquid vapor interface has to be determined. First the heat flux induced by the mass transfer (diffusion) is calculated. To calculate the mass transfer an iterative loop is used as shown in figure 5.4. All the steps of the iteration are explained in the following section. To get the initial values a temperature is guessed for the interface. With this temperature the molar concentrations of the vapor and the liquid are determined using the theory of Lewis and Whitman [25], where equilibrium is assumed at the interface:

$$c_a = c(T_i, p, q), \tag{5.37}$$

where c_a is the concentration of ammonia in either of the two phases. For calculation of the diffusion a parameter z is introduced which is the ratio of ammonia molar flux to the total molar flux. Also equation 5.36 is used for the mass transfer coefficients k_l and k_v. With an assumed value of z the molar fluxes can be determined:

$$j_{a,l} = \kappa_l z ln\left(\frac{z - c_{l,a,b}}{z - c_{l,a,i}}\right) \qquad j_{a,v} = \kappa_v z ln\left(\frac{z - c_{v,a,b}}{z - c_{v,a,i}}\right) \tag{5.38}$$

$$j_{w,l} = \frac{j_{a,l}}{(z - j_{a,l})} \qquad j_{w,v} = \frac{j_{a,v}}{(z - j_{a,v})}. \tag{5.39}$$

Because the mass entering the interface should be equal to the mass leaving the interface, the molar fluxes in the vapor and liquid are equal:

$$j_{a,v} = j_{a,l} = j_a \qquad j_{w,v} = j_{w,l} = j_w. \tag{5.40}$$

z is iterated until the following relation applies:

$$\kappa_L ln\left(\frac{z - c_{l,a,b}}{z - c_{l,a,i}}\right) - \kappa_v ln\left(\frac{z - c_{v,a,b}}{z - c_{v,a,i}}\right) = 0, \tag{5.41}$$

where κ is as defined in equation 5.36. The mass fluxes through the interface of ammonia and water are:

$$\dot{G}_a = j_a M_a \qquad \dot{G}_w = j_w M_w. \tag{5.42}$$

The heat flux due to diffusion by condensation can then be determined by using the mass fluxes and the latent heat:

$$\dot{q}_{a,c} = \dot{G}_a \Delta h_a \qquad \dot{q}_{w,c} = \dot{G}_w \Delta h_w. \tag{5.43}$$

With the mass fluxes known the heat transfer correction factors for the sensible heat (convection) for the vapor and the liquid can be calculated with the following equations:

$$\zeta_l = \frac{(\dot{G}_{a,l} + \dot{G}_{w,l}) c_{p,l}}{\alpha_{i,l}} \qquad \zeta_v = \frac{(\dot{G}_{a,v} + \dot{G}_{w,v}) c_{p,v}}{\alpha_{i,v}}. \tag{5.44}$$

The sensible heat fluxes (convection) are then calculated:

$$\dot{q}_{v,i,s} = \alpha_{v,i} \frac{\zeta_v}{1 - e^{-\zeta_v}} (T_v - T_i) \qquad \dot{q}_{l,i,s} = \alpha_{l,i} \frac{\zeta_l}{1 - e^{-\zeta_l}} (T_i - T_l). \tag{5.45}$$

The energy balance at the interface is thus:

$$\dot{q}_{v,i,s} - \dot{q}_{l,i,s} + \dot{q}_{a,c} + \dot{q}_{w,c} = 0. \tag{5.46}$$

The interface temperature T_i is changed until this energy balance is within the tolerance range of $10^{-6} W$. From the heat transfer balances over the wall the inner and outer wall temperatures can now also be calculated with equations 5.47 and 5.48 [1]:

$$T_{wall,ou} = \frac{\left(\frac{\alpha_{cm}}{\delta_{wall}/\lambda_{wall}} + \frac{\alpha_{cm}}{\alpha_f} \right) T_{cm} + T_l}{\left(\frac{\alpha_{cm}}{\delta_{wall}/\lambda_{wall}} + \frac{\alpha_{cm}}{\alpha_f} \right) + 1} \tag{5.47}$$

$$T_{wall,inn} = \left(\frac{\alpha_{cm}}{\delta_{wall}/\lambda_{wall}} + 1 \right) T_{wall,ou} - \frac{\alpha_{cm}}{\delta_{wall}/\lambda_{wall}} T_{cm}. \tag{5.48}$$

5.4.2. Heat transfer through the wall

The heat flux through the wall depends on the following heat transfer coefficient:

$$U_{wall} = \frac{1}{1/\alpha_{cm} + \delta_{wall}/\lambda_{wall} + 1/\alpha_f} \tag{5.49}$$

The heat flux from the cooling medium to the liquid film is:

$$\dot{q}_{cm} = U_{wall} (T_{cm} - T_f) \tag{5.50}$$

Using the cooling medium heat flux and the previously determined heat transferred in the control volume the effective heat transfer area can be calculated:

$$A_{eff} = \frac{\dot{Q}_{cm}}{\dot{q}_{cm}} \tag{5.51}$$

5.4.3. Total heat transfer per control volume

The total energy balances for working fluid vapor and liquid are then, as illustrated in 5.1:

$$\dot{Q}_l = A_{eff} (\dot{q}_{l,i,s} + \dot{q}_{a,c} + \dot{q}_{w,c} - \dot{q}_{cm}) \tag{5.52}$$

$$\dot{Q}_v = A_{eff} (-\dot{q}_{v,i,s} - \dot{q}_{a,c} - \dot{q}_{w,c}) \tag{5.53}$$

$$\dot{Q}_{cm} = A_{eff} \dot{q}_{cm} \tag{5.54}$$

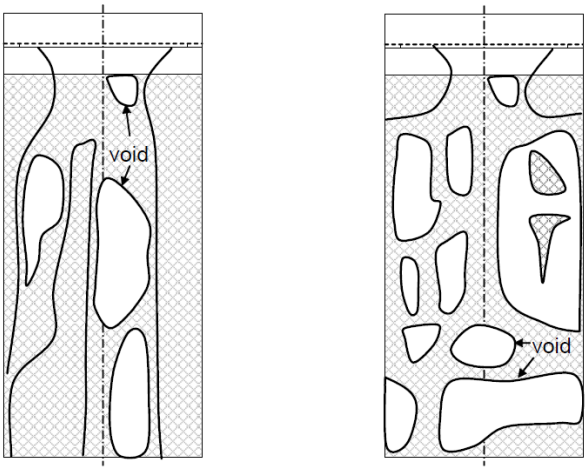

Figure 5.5: Dry surface voids in flow (Kim [21]).

5.5. Condenser pressure

In the configuration of the experimental setup (see Appendix A) there is a buffer tank after the condenser. The gas liquid composition should stay the same in the buffer tank. And since only liquid goes to the pump after the tank only liquid should come in from the condenser. When the vapor doesn't condense properly the liquid could accumulate at the exit of the heat exchanger until enough hydrostatic pressure is build up to push the liquid through. Since there is a constant fluid flow entering the heat exchanger the pressure will rise if this happens. An increase in the pressure inside the condenser is the consequence. A rise of the pressure in the heat exchanger is unwanted since that means that a smaller pressure drop is possible over the turbine, which is proportional to the work output of the turbine. Therefore the pressure is a good indicator of condenser performance.

To determine the working pressure the pressure has to be iterated. From the phenomenon described above, it can be expected that the condenser cools the fluid until it is condensed. Which means that when the condensation is complete the cooling process stops. This is the end statement for the iteration loop.

5.6. Flow pattern

A flow pattern factor could be interesting to take into account in the heat transfer correlation. When a vapor flow is condensing it is vital that the distribution of the droplets is uniform. The method used above as designed by Fernández-Seara et al. [10] assumes that all the condensing liquid becomes a film and skips the droplet phase. This method does not take into account the maldistribution that could occur with the condensing liquid. Kim [21] suggests that this maldistribution is of influence on the heat transfer coefficient. Especially when using low Reynolds numbers a lot of dry surface voids were observed in the flow shown in figure 5.5. This resulted in a clear slope difference in the Nusselt number shown in figure 5.6. As stated by Kim [21], the slope of the Nusselt number for pure water is steep from 0- 150 Reynolds number because the dry void areas are present in the flow. For higher Reynolds number a liquid film was observed. For the water+octanol solution there was never a liquid film observed, therefore the slope of the Nusselt number is much less steep. In this study only 100 ppm octanol was used for the solution which also shows that the flow pattern is very sensitive to changes when the working fluid is altered.

It is important to understand what properties influence this flow pattern. Several studies are done on minimum wetting rate, which is the minimum flow rate that is required to make or maintain a completely wet surface. Researches on this subject mostly focus on the ratio between inertial and surface forces. For void fractions to appear it is assumed that the surface tension force must balance the fluid pressure along the film curvature at the stagnation point. The equations used to characterize this mostly include the surface tension (σ), the contact angle of the surface (Θ), the viscosity (μ) and the density (ρ).

A more insightful way to review this flow pattern is with the use of flow pattern maps. Several attempts to map flow patterns are found in literature. It is important to choose the quantity on the axis in a way that a clear distinction can be made between different flow regimes. The quantity has to take into account working fluid properties and flow properties. Different kinds of flow pattern maps have been developed. The

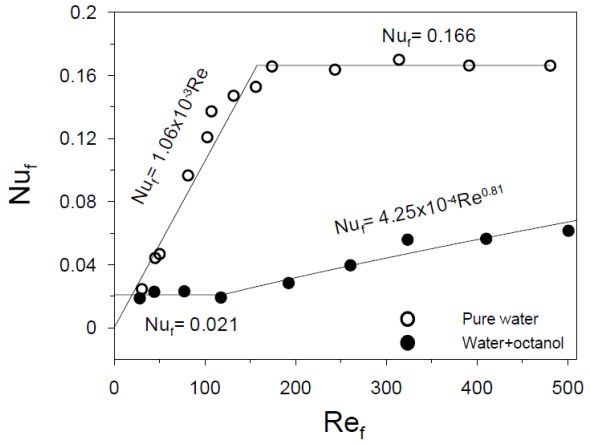

Figure 5.6: Nusselt numbers for water and water+octanol flows at low Reynolds numbers (Kim [21]).

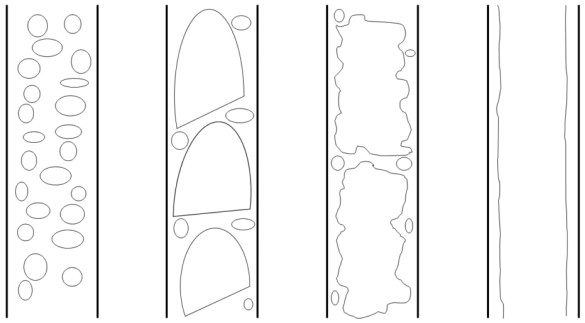

Figure 5.7: Main flow patterns observed for downward two-phase flow in plate heat exchangers. From left to right: bubbly flow, slug flow, churn flow and film flow (Tao et al. [40]).

most common flow pattern regimes that are present in plate heat exchangers were collected by Tao et al. [40]. The results are displayed in figures 5.7. The dimensionless quantities used to determine what regime occurs vary significantly. Velocity dependent quantities are used in all studies in different forms. Early studies simply use mass flux or velocity on one axis and a vapor quality related quantity on the other axis to define the patterns, the differences in these studies are significant. Many recent papers report a map using liquid Reynolds number and a Froude number. The corrugated wave length is included on the y-axis. Examples of these maps are found in figures 5.8a/b/c/d, as can be seen there is a significant difference in the definitions of the flow pattern regimes. The maps in figures 5.8a/b/c/d are used in Chapter 6 to determine the possible flow patterns in the condenser. All of the studies mentioned use water for their experiments and it can thus be inaccurate to predict how ammonia, or even ammonia-water, will behave. Tao et al. [40] included working fluid properties on both axis (figure 5.8c/d) to attempt to generalise the flow pattern map for other working fluids.

Analytical solutions to include the flow pattern behaviour into the heat transfer coefficient were not found in literature. A parameter that determines the flow regime of a developing film was found in the Kapitza number or the film number (Kapitza [19]):

$$K_f = \frac{1}{Ka} = \frac{g\mu_l^4}{\rho_l \sigma_l^3}. \tag{5.55}$$

5.6.1. Correction factor

A correction factor taking into account the influence of the flow pattern on the heat transfer performance was developed by Kim [21] in the following form:

$$\frac{A_{wet}}{A} = bRe^{0.58}, \tag{5.56}$$

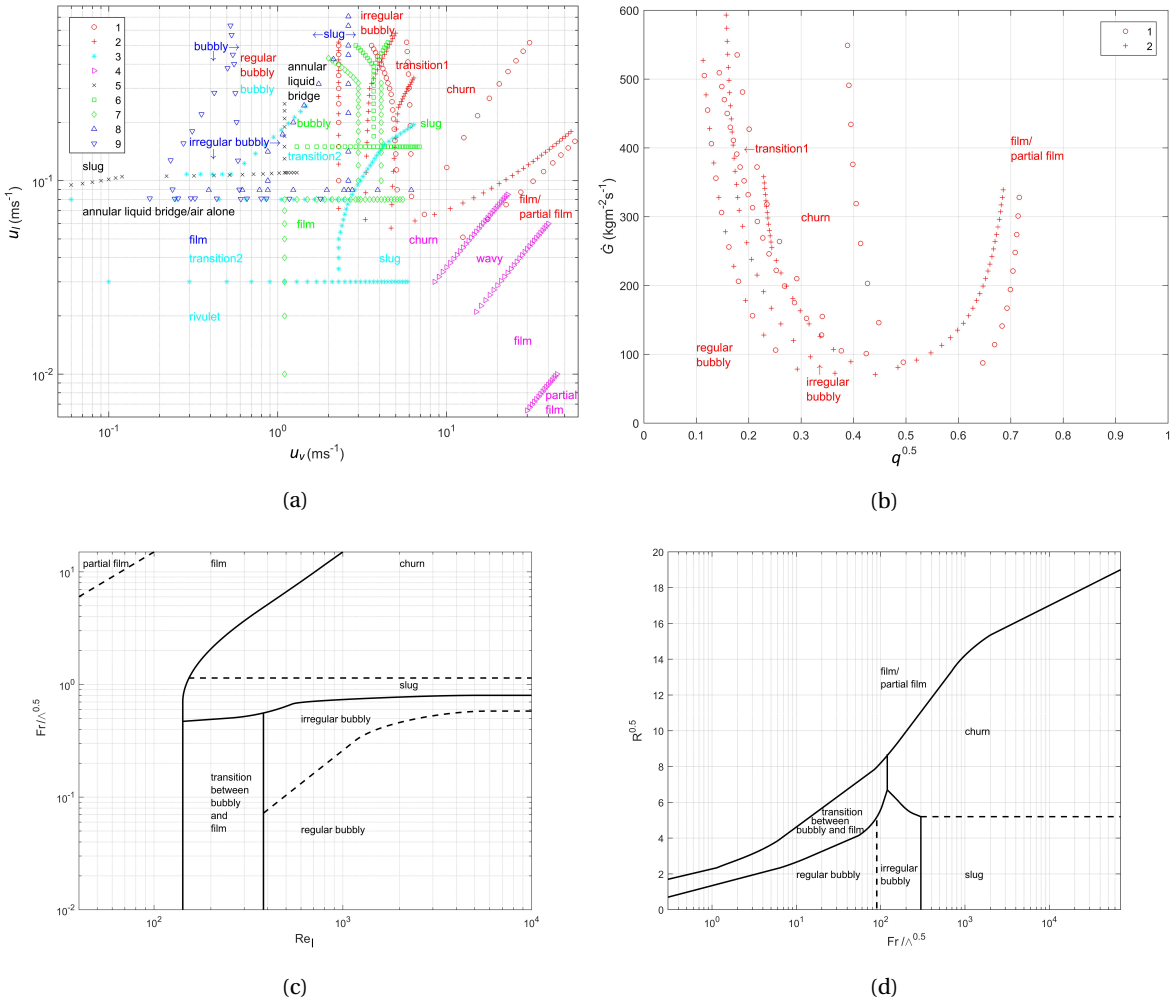

Figure 5.8: Flow pattern maps as described and developed by Tao et al. [40].

where b is the slope angle determined by the working fluid. This correction is solely dependent on the Reynolds number and needs to be refitted for every situation.

5.7. Implementations

As mentioned before the advanced two phase heat transfer method is used in several papers, Fernández-Seara et al. [10], Shi [35], Nuijten [29], Aarts [1], Rijpkema [33] and Nefs [28] are the most prominent ones. Their implementations were all different. Fernández-Seara et al. [10] used it to model an air cooled ammonia-water vertical tubular absorber and developed the model for the first time. Nuijten [29] was the first to model the OTEC system and used a very similar implementation as mentioned above. However, computational time of the model is too high to be practical. Aarts [1] developed a model for a higher temperature ammonia-water resorber plate heat exchanger. In this study more focus was put on computational time and some simplifications were added. Polynomials were fit to the data of REFPROP [24] to speed up the process of looking up enthalpies and specific heat values. Also the temperature profile of the cooling medium was approximated with a polynomial equation. This resulted in a time efficient program, but not much information was found on the validity of the model. Shi [35], Rijpkema [33], Nefs [28] used an ammonia-water mixture in mini-channel heat exchangers. Shi [35] got decent results compared to experiments, the same problems were found with computational time.

5.8. Summary

In this chapter the most important theories for developing a two phase condenser model with the method of Fernández-Seara et al. [10] were described. Film thickness theories are important to model the film flow. The following five heat transfer regions were identified; convective heat transfer by the cooling medium, conduction through the wall, convective heat transfer from the wall to the liquid film and convection and diffusion through the interface. The convective heat fluxes were calculated with heat transfer coefficients. These can be calculated with Nusselt number correlations found in literature. The mass transfer coefficients were derived from these coefficients with the Chilton-Colburn analogy. The iteration method to calculate the diffusion through interface was explained in section 5.4.1 and summarised in figure 5.4. Other relevant phenomena were the pressure mechanism in heat exchangers and flow patterns. Relevant developed models using the method of Fernández-Seara et al. [10] were mentioned in section 5.7.

6

Methods

In chapter 5 the methods and theories that are available in literature were described. In the following chapter these theories and methods are implemented and validated in a model that describes the performance of the condenser used in the OTEC experimental setup. Where needed new methods are introduced. The results are validated with experimental results obtained in previous researches [12][23].

6.1. Solution procedure

In section 5.4 the heat transfer processes in the system were described. In this work the mass transfer through the interface calculations are based on the method of Fernández-Seara et al. [10] and work done by Aarts [1]. These are combined with conventional thermodynamics for the wall and cooling medium regions. To describe the performance of the condenser properly, the pressure must be predicted as mentioned in section 5.5. Combining these theories resulted in the mathematical model developed in this study. A simplified schematic of the model is shown in figure 6.1. The model consists of three main loops.

6.1.1. Liquid-vapor interface loop

The first loop is the liquid-vapor interface loop which iterates the interface temperature T_i until the mass and energy balances through the interface are satisfied. The process is described in section 5.4 and shown in figure 5.4.

6.1.2. Condenser control volume loop

The second loop is the condenser control volume loop. The condenser working fluid side contains a two phase mixture flow. The properties of the fluid are constantly changing because of concentration, vapor quality and film thickness differences. It is therefore necessary to divide the heat exchanger in several control volumes. This is done by guessing the total heat transfer of the cooling medium and dividing this total heat transfer into a finite amount of control volumes. Since the regions at the inlet and at the outlet of the heat exchanger are expected to be most problematic for convergence, a sine function is used to divide the heat exchanger in control volumes. With the inlet conditions known, the area calculated per control volume is calculated with equation 5.51. With the values of the interface heat transfer known, the conditions for the next cell can be calculated. Since it is known what the total heat transfer area of the heat exchanger is, the loop is stopped when that area is reached by the sum of the control volume areas.

6.1.3. Pressure bisection iteration loop

The last loop is the pressure bisection iteration loop. It consists of several IF statements that determine whether the solution is properly converged. As stated in section 5.5 it is expected that the fluid is completely condensed when it reaches the outlet of the condenser. Therefore the vapor quality (q) must be 0 and the liquid should not be subcooled more after reaching 0 vapor quality. The model can get unstable at very low vapor quality, therefore the stopping criteria was taken as $q < 0.01$. If the model is underperforming ($q > 0.01$) the pressure is increased and when the model is overperforming ($T < T_{subc}$) the pressure is decreased. The pressure is iterated until both constraints are met. The iteration method used is the bisection method.

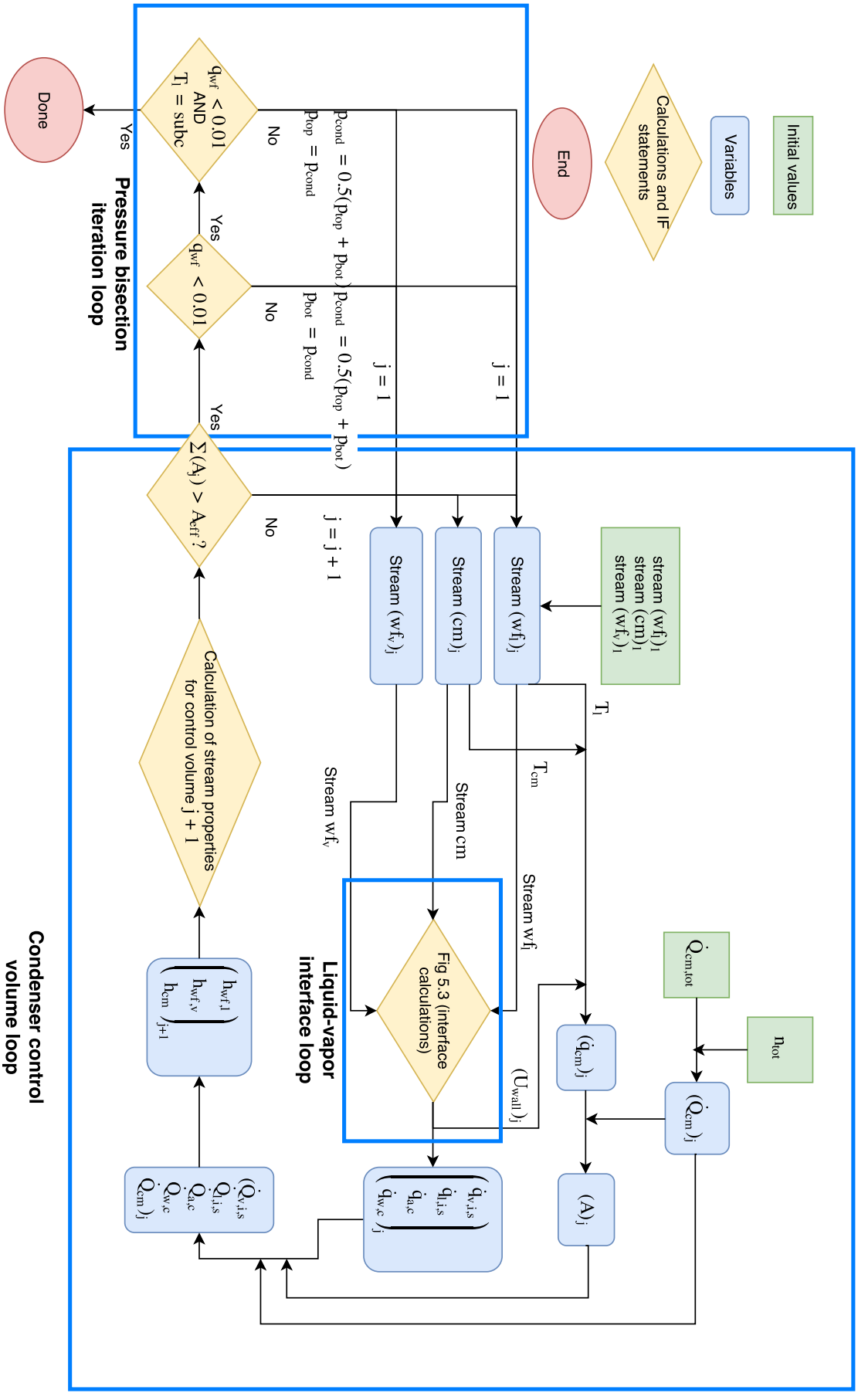

Figure 6.1: Flow chart of mathematical model.

Table 6.1: Single phase correlations evaluated

Correlation	Source
$Nu = 1$	Aarts [1], Nuijten [29]
$Nu = 2$	Nefs [28], Rijpkema [33]
$Nu = 1.615\left(\xi\left(\frac{Re}{64}\right)RePr\frac{d_h}{La}\right)^{\frac{1}{3}}$	Lévèque[42]
$Nu = 0.6Re^{0.51}Pr^{\frac{1}{3}}$	VDI [42]
$Nu = 0.62Re^{0.52}Pr^{\frac{1}{3}}$	Sinnott and Towler [37]
$Nu = 0.2121Re^{0.78}Pr^{\frac{1}{3}}$	Yan et al. [46]
$Nu = 0.2875Re^{0.78}Pr^{\frac{1}{3}}$	Donowski and Kandlikar [9]
$Nu = 0.6Re^{0.51}Pr^{\frac{1}{3}}$	Winkelmann [45]
$Nu = 0.122Pr^{0.33}\left(\frac{\mu_l}{\mu_w}\right)^{\frac{1}{6}}\left(\xi Re^2 sin(2\beta)\right)^{0.374}$	Lévèque Adjusted [42]

6.2. Heat transfer correlations

In the model four distinct contact areas are determined where heat transfer occurs:

- Cooling water to outer wall
- Inner wall to liquid film
- Liquid film to interface
- Vapor to interface

From the correlations mentioned in Chapter 5 a selection of correlation candidates was chosen based on the following statements:

- The fluids in the two phase mixture behave like single phase fluids regarding the convective heat transfer, so only single phase heat transfer correlations were tested.
- The heat exchanger type is a significant factor in the heat transfer, therefore only general heat transfer correlations or correlations specifically developed for plate heat exchangers were tested.
- The Reynolds number in both streams is low (0-250) so only correlations that are valid in this region were considered.

The correlations evaluated can be found in table 6.1.

6.3. Film thickness

The film thickness has an important impact on the solution of the model. However, there are not many film thickness theories available in literature that suit the situation of the OTEC experimental setup. Film flow measurements in plate heat exchangers were also not found in literature. Therefore, theories from other fields were used, mostly flat plate theory, to predict the film thickness.

6.3.1. Film flow regime

To be able to predict the film thickness it is important to know what regime the flow is in. It is expected that there will be a falling film flow from the beginning of the heat exchanger since the Reynolds numbers are low. At some point a transition to some form of bubbly flow is expected. The flow pattern maps of figures 5.8a/b/c/d are used to generate the plots of figures 6.2a/b/c/d. The maps don't provide a unanimous result (table 6.2). There are some similarities however. Figure 6.2a suggests that the flow will stay in the rivulet flow regime. From extrapolating figure 6.2b a bubbly or film flow can be expected. Figure 6.2c and 6.2d both suggest that a falling film will appear at some point. From the flow pattern maps it can be expected that a falling laminar film will be the dominant flow pattern in the channel.

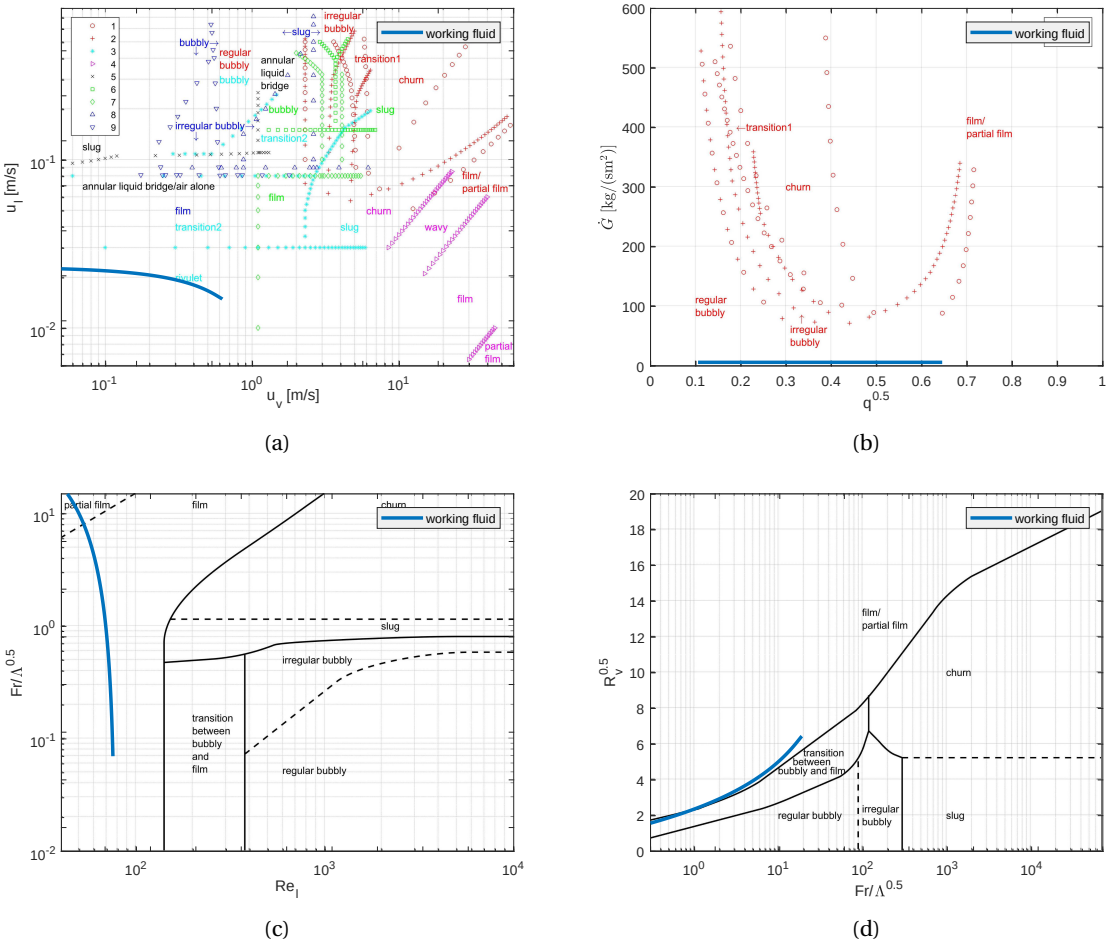

Figure 6.2: flow pattern maps studied and developed by Tao et al. [40] with the working fluid plot of the model at $\dot{m}_{wf} = 0.010$ kg/s and $c_a = 0.954$.

Table 6.2: Overview of different regimes as shown in figure 6.2.

Flow pattern map	Regimes	
a	Rivulet	
b	Film/partial film	Bubbly
c	Partial film	Film
d	Film	Transition

Table 6.3: Different film thickness correlations tested.

Correlation	Regime	Source
$\delta_f = \left(\frac{4\mu_l \lambda_l x(T_{sat,l} - T_{w,inn})}{g h_{fg} \rho_l (\rho_l - \rho_v)}\right)^{\frac{1}{4}}$	General	Holman [17] (Nusselt theory)
$\delta_f = \left(\frac{3{\nu_l}^2}{g}\right)^{\frac{1}{3}} {Re_l}^{\frac{1}{3}}$	Laminar	VDI [42]
$\delta_f = 0.302\left(\frac{{\nu_l}^2}{g}\right)^{\frac{1}{3}} {Re_l}^{\frac{8}{15}}$	Turbulent	VDI [42]
$\delta_f = 0.845\left(\frac{{\nu_l}^2}{g}\right)^{\frac{1}{3}} {Re_l}^{\frac{1}{3}}$	Laminar/wavy	Brauer [5]
$\delta_f = 0.172\left(\frac{{\nu_l}^2}{g}\right)^{\frac{1}{3}} {Re_l}^{0.666}$	Fully turbulent	Brauer [5]
$\delta_f = 0.3035\left(\frac{{\nu_l}^2}{g}\right)^{\frac{1}{3}} {Re_l}^{\frac{1}{3}}$	Laminar/wavy-turbulent	Goedecke [11]
$\delta_f = \left(\frac{3{\nu_l}^2}{8g} Re_l\right)^{\frac{1}{3}}$	Laminar/wavy	Helbig [16]
$\delta_f = 0.473\left(\frac{{\nu_l}^2}{g}\right)^{\frac{1}{3}} {Re_l}^{0.526}$	Turbulent	Takahama and Kato [39]

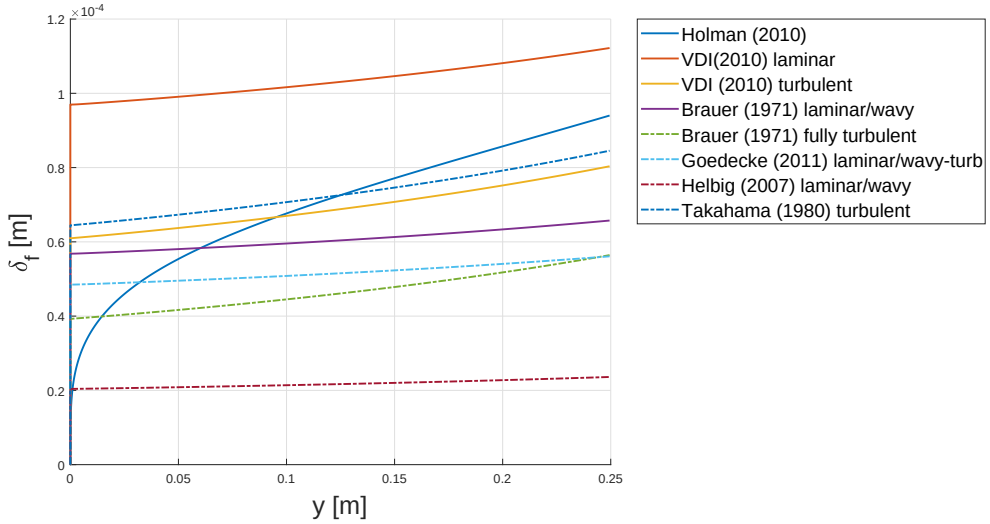

Figure 6.3: Comparison of different film thickness correlations.

6.3.2. Film thickness correlations

The film flow regime maps suggest that a falling film is most likely to occur in the channel. Correlations related to film thickness for falling film flow are thus most interesting. Because of the limited amount of research, most of the film thickness relations that were found were tested. To get a clear overview of the different correlations developed and the differences among them, also correlations based on transition regions and turbulent regimes were investigated. The correlation of equation 5.13 has no real physical background and was therefore not analysed. The tested correlations can be found in table 6.3. As mentioned before, the empirical relations are all based on equation 5.11. The relation of Holman [17] is analytically derived from Nusselt Theory. All of these correlations were developed for flat vertical flow on flat plates. Using the correlations in the present model, the different film thickness values are as shown in figure 6.3.

It is known from the experimental data that with the conditions tested the fluid will condense completely at the outlet of the heat exchanger. Therefore the film thickness predicted by the theories mentioned in table 6.3 is very low, as shown in figure 6.3. The relation from the VDI heat atlas for laminar flow gives the highest film thickness. However, this theory predicts that at the outlet of the heat exchanger the channel is still mostly filled with vapor. Physically this is unlikely since it is expected that the channel will fill with liquid completely. So a relation that predicts a thicker film should be developed.

6.3.3. Adjusted Nusselt falling film correlation

A new correlation can be developed to get a more physically correct correlation for the film thickness. There is no experimental data available to develop a new correlation so it must be analytically derived or corrected. Nusselt theory as derived by Holman [17] assumed a film thickness of $\delta_f = 0$ at $y = 0$. In the case of the OTEC experimental setup the film comes in at a vapor quality of 40%. The film will therefore be thicker. By using equation 5.9 and integrating with boundary conditions $\delta_{f,0}$ at $y = 0$ and δ_f at y this can be taken into account. Rewriting with the wall temperature being $T_{wall,inn}$ and T_{sat} being the saturation temperature the equation becomes:

$$\int_{(\delta_f)_0}^{(\delta_f)} \frac{\rho_l(\rho_l-\rho_v)g(\delta_f)^3 h_{fg}}{\mu_l} d(\delta_f) = \int_{y0}^{y} dy\lambda_l(T_{sat}-T_{wall,inn}) \tag{6.1}$$

$$\frac{\rho_l(\rho_l-\rho_v)gh_{fg}}{\mu_l}\ \frac{1}{4}(\delta_f)^4\Big]_{(\delta_f)_0}^{\delta_f} = y\Big]_{y_0}^{y}\lambda_l(T_{sat}-T_{wall,inn}) \tag{6.2}$$

$$\frac{1}{4}(\delta_f)^4 - \frac{1}{4}(\delta_f)_0^4 = (y-y_0)\frac{\lambda_l(T_{sat}-T_{wall,inn})\mu_l}{\rho_l(\rho_l-\rho_v)gh_{fg}}, \tag{6.3}$$

$x_0 = 0$ and further simplifying yields:

$$\delta_f = \left((\delta_f)_0^4 + \frac{4\lambda_l y(T_{sat}-T_{wall,inn})\mu_l}{\rho_l(\rho_l-\rho_v)gh_{fg}}\right)^{\frac{1}{4}}. \tag{6.4}$$

Equation 6.4 gets a more reasonable value for the film thickness at y = 0. However, the theory only applies for vertical flow over a flat plate. A correction factor should be applied to get a correlation that is valid for plate heat exchangers.

Correction factor

There were no experimental studies on film thickness development on corrugated plates found. However, a paper written by Siebeneck et al. [36] described a study on film thickness of pillow plate heat exchanger plates. The pillow plates work with the same principle as the corrugated plates only the corrugation is less abrupt as it is in a corrugated plate. A factor difference between the experimental film thickness for flat plate and pillow plate was found (see figure 6.4). At a Reynolds number of 50, this factor is as follows:

$$Fact_f = \frac{\delta_{f\,corr}(Re=50)}{\delta_{f\,flat}(Re=50)} \approx \frac{2.5}{1.5} = 1.67. \tag{6.5}$$

The assumption is made that this factor difference is similar to the factor difference between corrugated plate and flat plate. Therefore this factor is added to the Nusselt derived correlation of Holman [17]. This yields the following equation.

$$\delta_{f\,new} = Fact_f\left((\delta_f)_0^4 + \frac{4\lambda_l y(T_{sat}-T_{wall,inn})\mu_l}{\rho_l(\rho_l-\rho_v)gh_{fg}}\right)^{\frac{1}{4}} \tag{6.6}$$

The new film thickness relation compared to the other correlations is shown in figure 6.5.

6.4. Model choices

With the mathematical framework in place it is important to analyse the performance and find the most fitting theories and correlations developed. This is done by using the values obtained from the experimental data, judging its accuracy and comparing them with the numerical values.

6.4.1. Accuracy of the experimental data

In section 1.3.1 the accuracy of the sensors are shown. It was stated that the mass flow and temperature inaccuracies of the experimental data are negligible. The pressure sensors, with 5.37% inaccuracy, have a significant amount of influence on the values obtained. In figure 6.6 the pressure values of the experimental data are shown with the 5.37% accuracy boundaries for a working fluid mass flow of 0.010 kg/s.

The other validation parameters are also influenced by the inaccuracy of the pressure sensors. The pressure has an influence on several different parameters in the model. To investigate the accuracy of the derived variables, the model can be run for both boundary pressures. However, referring back to the flow chart in figure 6.1 it can be seen that the pressure is iterated to a point where the working fluid is exactly condensed. This

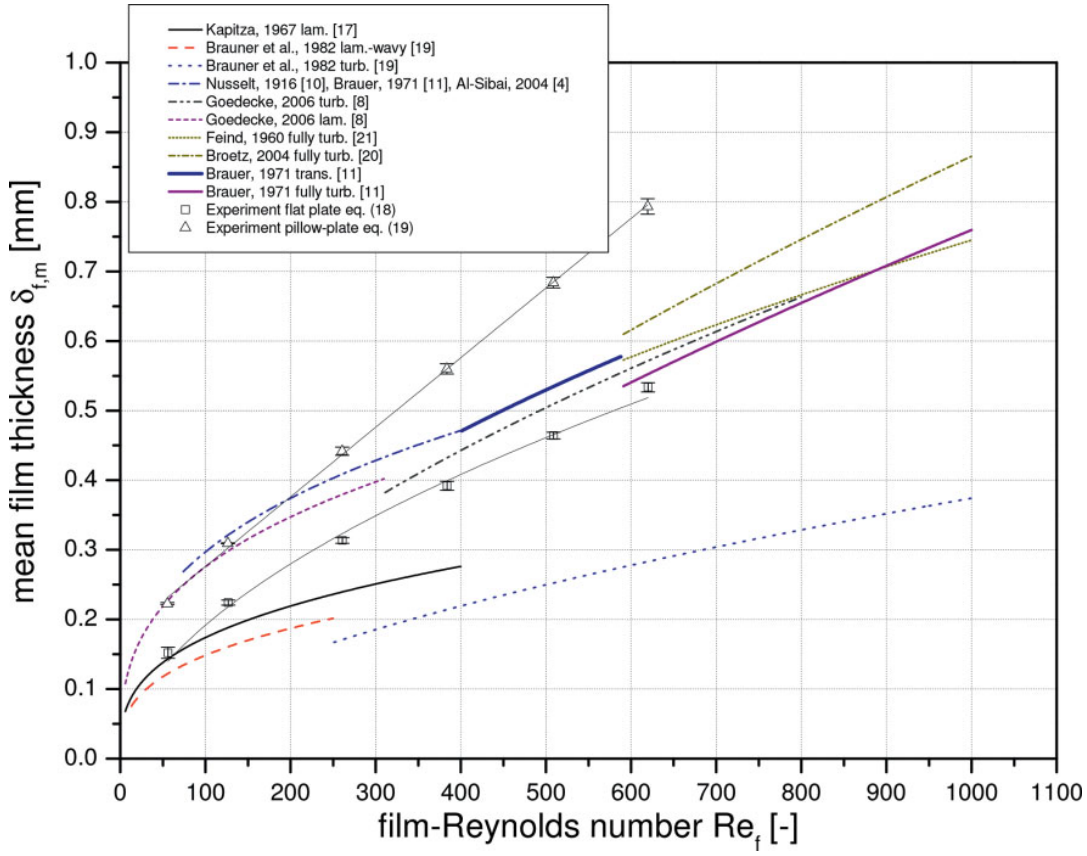

Figure 6.4: Correlations and experimental values for the film thickness over pillow plate and flat plate vs Reynolds number (Siebeneck et al. [36]).

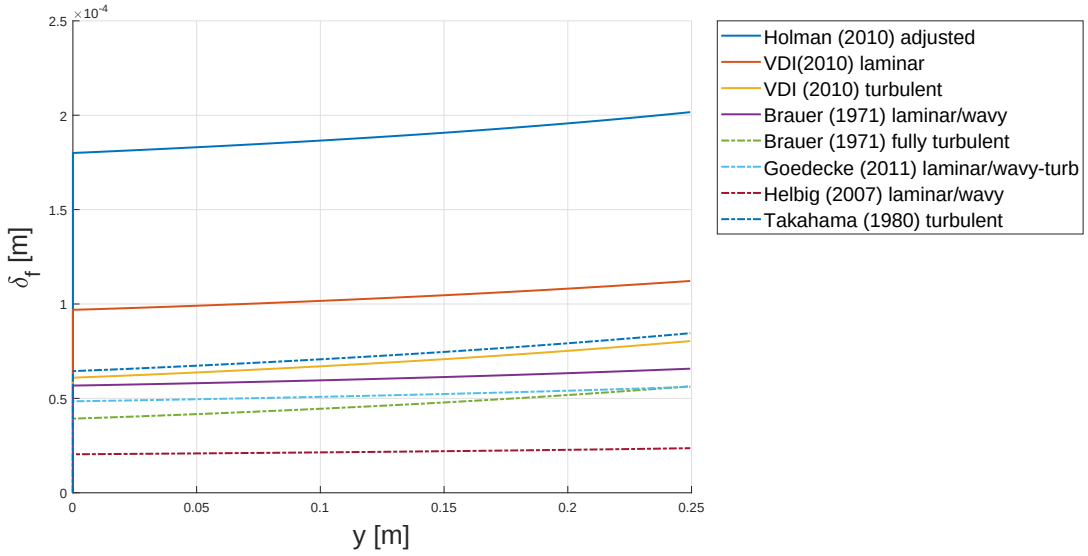

Figure 6.5: New film thickness correlations compared to other correlations developed.

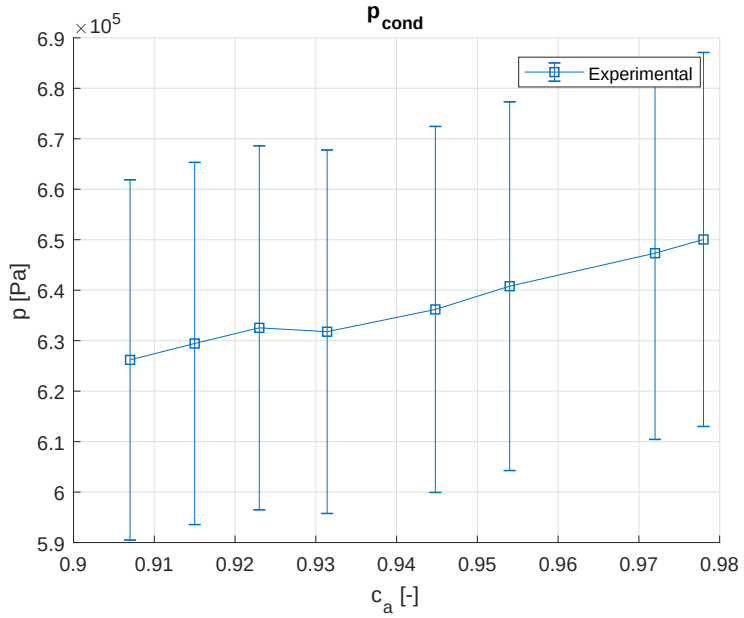

Figure 6.6: Experimental pressure results at $m = 0.010 kg/s$ with accuracy bars.

means that changing the pressure manually to the accuracy boundaries changes the condensation process. When increasing the pressure the performance is enhanced which means that the liquid is subcooled. The process of subcooling a single phase flow has a lower heat transfer coefficient than cooling a two phase flow. As mentioned in section 5.5 this is unlikely to occur. When decreasing the pressure the condensation process is not finished. Therefore the quality of the mixture does not reach 1% vapor quality. Also referring back to section 5.5 this not likely to occur. Changing the pressure manually changes the condensation process in a way that is unrealistic and thus the accuracy of the derived parameters can not be calculated precisely and is therefore not included in the graphs.

6.4.2. Correlation analysis

In literature it was found that several correlations were valid for the regime and conditions of the OTEC experimental setup but that the correlations gave different results. To find out which correlation is the most accurate the results have to be compared to the experimental values. To reduce the amount of variables the following statements were developed:

- The heat transfer coefficients used for the wall to film contact and the liquid to interface contact are expected to be the lowest and therefore the most influential factor [10]. These heat transfer coefficients are proportionally influenced by both the Nusselt number correlations and the film thickness correlation.

- The water side heat transfer coefficient is assumed to be accurate since it was empirically determined for this specific situation by Goudriaan [12] and Kuikhoven [23].

- The vapor side heat transfer coefficient shows little influence on the condensation process relative to the liquid heat transfer so the correlation developed by Sinnott and Towler [37] is used.

- For film thickness, as mentioned in section 6.3.2, there are not many valid relations found in literature. The relation derived by Holman [17] and adjusted in this paper in section 6.3.2 is therefore used. The values resulting from this correlation give physical values that are most likely to be accurate.

This means that two parameters have to be optimized and validated: the wall to film heat transfer coefficient and the liquid to interface heat transfer coefficient.

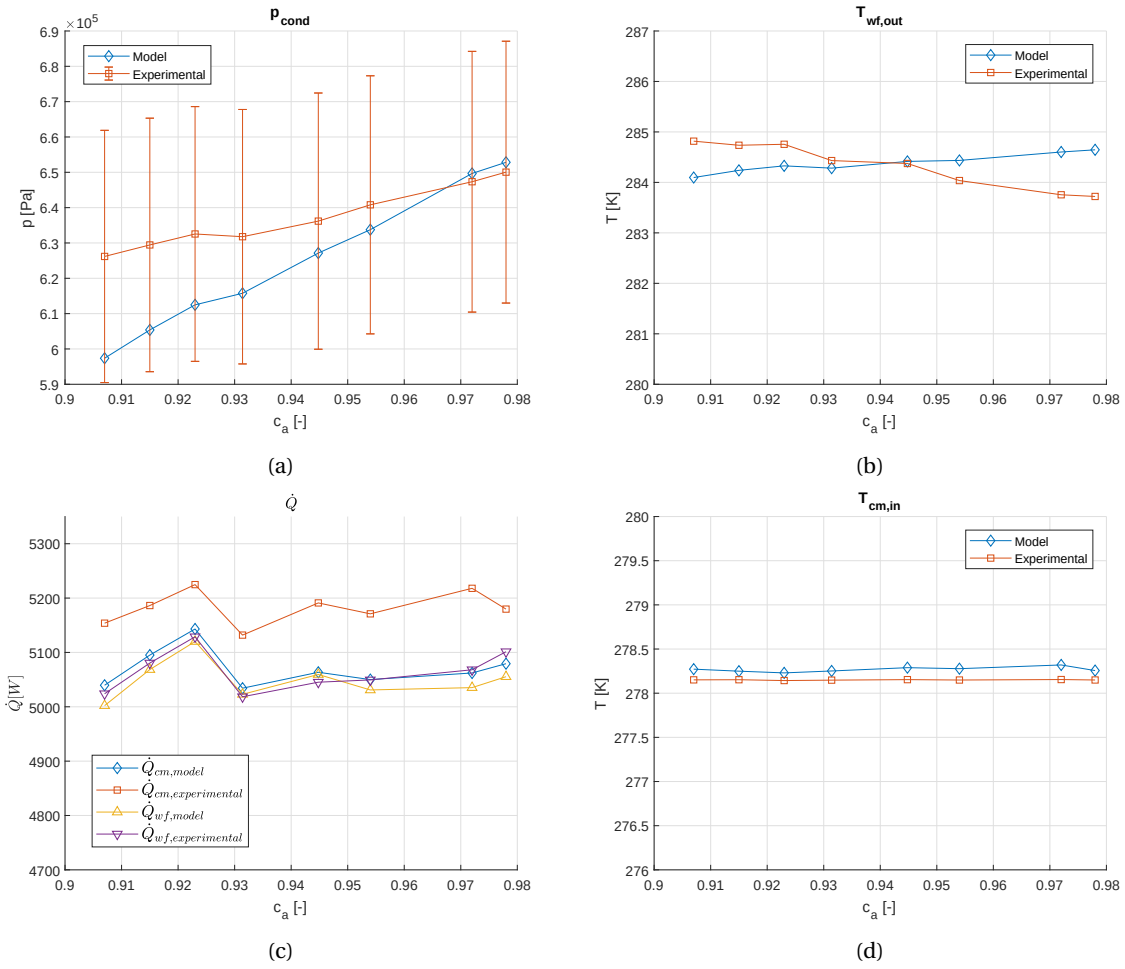

Figure 6.7: Working fluid mass flow of 0.010 kg/s. Difference between experimental and modelled values, without surface tension correction factor, for the (a) pressure in the condenser (b) temperature outlet working fluid condenser (c) heat transferred to cooling medium and working fluid (d) temperature inlet cooling medium.

6.5. Validation

To measure the validity of the different correlation possibilities, characteristic parameters were identified. The pressure and outlet temperature of the working fluid are the main parameters, since these characterise the performance. The heat transferred by the working fluid and the cooling medium were also used for validation. The combination of a film Nusselt number of $Nu = 2$ and the liquid to interface Nusselt number correlation developed by Lévèque [42] had the smallest deviation from the experimental data. The results are shown in figures 6.7a/b/c/d. As can be seen the pressure is within sensor accuracy and the outlet working fluid temperatures are reasonably close. However, the slopes of both the outlet temperature of the working fluid and the condenser pressure deviate from the experimental measurements. Therefore another correction factor was added to fix this problem.

6.5.1. Surface tension correction factor

As can be seen from the results in figure 6.7a/b/c/d the trend of the model temperature and pressure didn't show the same slope as the experimental values. The model showed lower pressure and lower outlet temperature values for lower concentrations, which suggests a better performance. In the experimental data the opposite can be seen. The inconsistency has thus a direct relation with the concentration of the working fluid. In the model the property that has a negative influence on performance for lower concentration is the increasing mass resistance for lower concentrations. However, apparently this effect is not the only concentration induced effect that has a negative influence on the performance.

Another property that could have a significant effect on heat transfer is the surface tension. Ammonia is

known for its good wettability properties due to low values of the surface tension [48]. Water on the other hand is known for its high surface tension and worse wettability properties. It can therefore be expected that adding water to ammonia decreases its wettability [7]. Also from the flow pattern maps in figures 6.2a/c/d it is shown that in this regime less than ideal flow patterns could occur. In Kim [21] experiments were reported where a pure fluid is mixed with an additive in a very low concentration. Flow pattern analysis was reported on this. Results were that the void fractions in the wet surface were significantly larger for the mixture. An increase in dry voids on the wall surface with lower concentrations of ammonia is a possible explanation for the deviation of the model results.

In literature no correction factors were found that quantify this phenomenon so a correction factor was designed for this system. Since the surface tension is the main factor in the occurrence of this effect a correction factor for the wall to liquid heat transfer area was designed based on the ratio of the surface tension of the pure fluid and the surface tension of the mixture (equation 6.7).

$$\epsilon = \left(\frac{\sigma_a}{\sigma_{a,w}} \right)^{\gamma} \tag{6.7}$$

γ is a coefficient fitted to match the results. In the model $\gamma = 2$. The new Nusselt correlation that is used for the heat transfer of the wall to liquid is designed for flow over a flat plate mentioned by Holman [17] (equation 6.8).

$$Nu = 0.453 Re_l^{0.50} Pr_l^{0.33} \tag{6.8}$$

6.5.2. Validation results

As can be seen from figures 6.8a/b/c/d the results with the correction factor showed a more similar trend for the working fluid outlet temperature and condenser pressure than the results without correction factor shown in figures 6.7a/b/c/d. Table 6.4 shows the deviations of all the measured data. The heat transferred to the cooling medium stayed within 3.07% accuracy. The outlet temperature of the working fluid was within 5% accuracy. The cooling medium stayed within 4% accuracy. The pressure stayed within 1.5% accuracy which is within pressure sensor accuracy (5.7%).

6.5.3. Other working fluid mass flows

The model incorporates more physical phenomena than the correlation used in part I, therefore it should be valid for a larger range of conditions. However, numerically the model became unstable for working fluid mass flows of 0.005 kg/s and 0.013 kg/s. The interface iteration loop for mass and heat transfer (see figure 5.4) became unstable or inaccurate at these conditions. This is probably due to the fact that the database of Rattner and Garimella [32] or the way that values are called from the database causes the inaccuracies, this problem will be explained in Chapter 8. However, the results at 0.007 kg/s working fluid mass flow could be assessed. The results are shown in figures 6.9 a/b/c/d.

6.5.4. Discussion validation results

The pressure and the temperature deviations are both indicators of the heat exchanger model performance. The model works in such a way that the pressure is iterated until condensation is achieved exactly at the end of the heat exchanger, as described in section 5.5. A lower pressure necessary for condensation thus indicates that the heat exchanger overperforms in the model compared to the real heat exchanger. Therefore calculated pressure is an indication of total heat transfer performance from the cooling medium to the vapor.

The outlet temperature is the temperature of the liquid working fluid medium at the stage of complete condensation, described in section 5.5. If the pressure necessary for condensation stays constant then the ratio of the heat transfer from the wall to the liquid film and the heat transfer from the interface to the liquid film determines the outlet temperature. In short, a higher model outlet temperature indicates that the model has either a lower wall-film heat transfer or a higher interface heat transfer than the real heat exchanger. That being said the results from figures 6.8a/b/c/d can be interpreted to judge the performance of the model:

- Figure 6.8a shows that the pressure is within the sensor accuracy. The slope of the pressure concentration curve looks very similar which indicates that the concentration dependency is predicted correctly.
- In figure 6.8b the model shows a higher outlet temperature of the working fluid. This means that either the wall-film heat transfer coefficient is too low or that the interface-film heat transfer is too high. The trend is similar indicating a correctly predicted concentration dependency.

Table 6.4: Deviations from the experimental and model (with surface tension correction) values for relevant parameters for $\dot{m}_{wf}$ = 0.010kg/s.

	$T_{wf,out}$	$T_{cm,in}$	p_{cond}	$\dot{Q}_{cm}$	$\dot{Q}_{wf}$
			c = 0.978		
Exp	10.57 °C	5.00 °C	6.51 ± 0.35 bar	5179.7 W	5101.3 W
Mod	10.94 °C	5.04 °C	6.41 bar	5141.1 W	5118.4 W
Deviation	3.48%	0.82%	-1.43%	-0.75%	0.19%
			c = 0.972		
Exp	10.61 °C	5.01 °C	6.48 ± 0.35bar	5218.0 W	5068.1 W
Mod	11.09 °C	5.13 °C	6.39 bar	5095.1 W	5070.4 W
Deviation	4.60%	2.60%	-1.23%	-2.35%	-0.29%
			c = 0.954		
Exp	10.89 °C	5.00 °C	6.42 ± 0.35 bar	5171.0 W	5049.4 W
Mod	11.34 °C	5.12 °C	6.33 bar	5061.6 W	5043.3 W
Deviation	4.12%	2.32%	-1.24%	-2.12%	-0.34%
			c = 0.9448		
Exp	11.23 °C	5.00 °C	6.37 ± 0.34bar	5191.1 W	5048.7 W
Mod	11.47 °C	5.14 °C	6.30 bar	5067.1 W	5059.5 W
Deviation	2.18%	2.63%	-1.03%	-2.39%	-0.21%
			c = 0.9314		
Ep	11.28 °C	5.00 °C	6.33 ± 0.34bar	5131.9 W	5018.4 W
Mod	11.63 °C	5.12	6.248 bar	5020.8 W	5004.3 W
Deviation	3.10%	2.36%	-1.0999%	-2.16%	-0.37%
			c = 0.923		
Exp	11.61 °C	4.99 °C	6.34 ± 0.34 bar	5224.8 W	5128.8 W
Mod	11.94 °C	5.11 °C	6.28 bar	5115.6 W	5099.9 W
Deviation	2.88%	2.32%	-0.80%	-2.09%	-0.39%
			c = 0.915		
Exp	11.59 °C	5.00 °C	6.30 ± 0.34bar	5186.3 W	5080.5 W
Mod	11.99 °C	5.14 °C	6.23 bar	5060.6 W	5043.9 W
Deviation	3.47%	2.67%	-1.04%	-2.42%	-0.49%
			c = 0.907		
Exp	11.67 °C	5.00 °C	6.27 ± 0.34bar	5153.8 W	5024.0 W
Mod	12.05 °C	5.17 °C	6.19 bar	4995.8 W	4977.2 W
Deviation	3.26%	3.35%	-1.21%	-3.07%	-0.50%

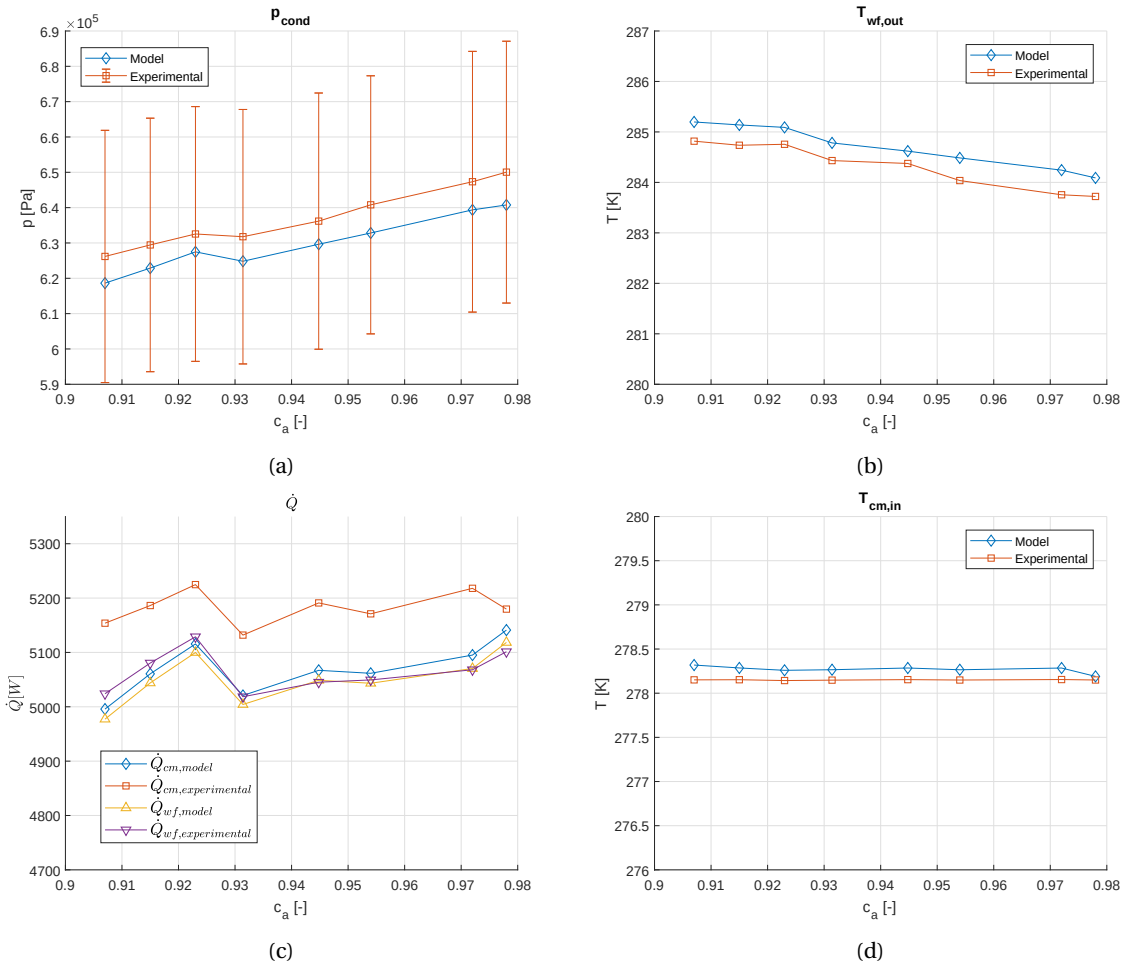

Figure 6.8: Working fluid mass flow of 0.010 kg/s. Difference between experimental and modelled, with surface tension correction factor, values for (a) temperature outlet working fluid condenser (b) pressure condenser (c) heat transferred (d) inlet temperature cooling medium.

- In figure 6.8c the model shows a good agreement with the working fluid heat transfer. The cooling medium heat transferred is predicted to be lower, probably due to losses to the environment. Trends are similar to experiments. The same effect is indicated by figure 6.8d.

The characteristic variables are reasonably accurate (all factors stay within 5% deviation), as is shown more in detail by table 6.4. Also the concentration effects are estimated accurately. One of the main limitations of this validation is the fact that the experimental data available is only for the inlet and the outlet of the heat exchanger. The temperature and pressure profiles generated in this study are expected to approximate the temperatures and pressures inside the heat exchanger. Yet this can only be validated by using local temperature and pressure sensors. Combining this with various co-dependent correlations and coefficients it is difficult to predict where the inaccuracies are in the model. However, knowing the assumptions made in the model, it can be predicted where the most significant deviations are. It is likely that optimising a combination of the following is the key to a more accurate model:

- The film thickness. In the model it is predicted by a correlation based on flat plate theory and a correction factor resulting in a thin film (figure 6.5). A thicker film would lower the heat transfer and thus increase the condensation pressure while also increasing the liquid outlet temperature.
- Mass transfer through the interface. In the model it is predicted by the Chilton-Colburn analogy [6]. Since mass transfer experiments for two phase condensation are rarely quantified in literature it is difficult to validate these values. An increase in mass transfer through the surface would enhance heat transfer and thus lower the condensation pressure while also increasing the working fluid outlet temperature.

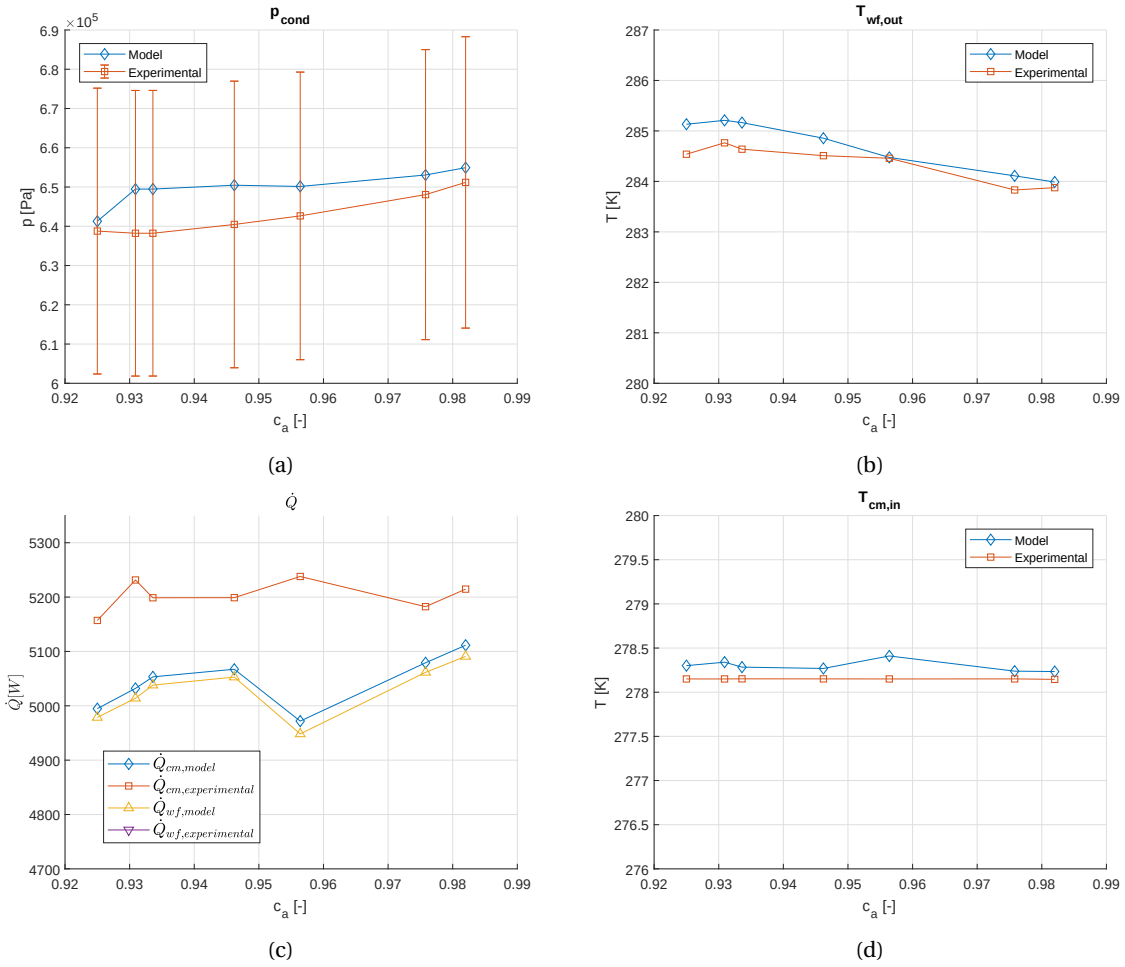

Figure 6.9: Working fluid mass flow of 0.007 kg/s. Difference between experimental and modelled, with surface tension correction factor, values for (a) the pressure of the condenser (b) the working fluid outlet temperature (c) the heat transferred (d) the inlet temperature cooling medium.

Table 6.5: Summary of choices made concerning correlations and coefficients

Model choices		
Nusselt number correlations	Cm to wall	$Nu = 0.291 Re_{cm}^{0.72} Pr_{cm}^{0.33}$ [12][23]
	Wall to wf	$Nu = 0.453 Re_l^{\frac{1}{2}} Pr_l^{\frac{1}{3}}$ [17]
	Liquid to interface	$Nu = 1.615 \left(\xi \frac{Re_f}{64}\right) Re_f Pr_l \frac{d_{h,l}}{d_p}^{\frac{1}{3}}$ [42]
	Vapor to interface	$Nu = 0.62 Re_v^{0.52} Pr_v^{\frac{1}{3}}$ [37]
Mass transfer coefficient	Liquid to interface	$\kappa_l = \frac{\alpha_l D_l \rho_l}{\lambda_l} \left(\frac{Sc_l}{Pr_l}\right)^{\frac{1}{3}}$ [6]
	Vapor to interface	$\kappa_v = \frac{\alpha_v D_v \rho_v}{\lambda_v} \left(\frac{Sc_v}{Pr_v}\right)^{\frac{1}{3}}$ [6]
Film thickness correlation		$\delta_{f\,new} = Fact_f \left((\delta_f)_0^4 + \frac{4\lambda_l y (T_{sat} - T_{wall,inn})\mu_l}{\rho_l(\rho_l - \rho_v) g h_{fg}}\right)^{\frac{1}{4}}$
Properties	wf: c_p and σ cm: all properties	REFPROP [24]
	wf: all properties except for c_p and σ cm: -	Rattner and Garimella [32]

- The surface tension correction factor. One was developed in this research and therefore not validated by any other experimental research apart from the experimental results obtained by Goudriaan [12] and Kuikhoven [23]. The surface tension and flow pattern development are very likely to play a role in the heat transfer however it is likely that a more elaborate coefficient or method should be used to quantify this. Removing this factor decreases heat transfer and thus increases the condensation pressure.
- Heat transfer coefficients. All heat transfer coefficients, apart from the cooling medium heat transfer coefficient [12][23], used for this model were not validated for this kind of application. It is very challenging to isolate the heat transfer coefficients of the two working fluid phases for experimental purposes.
- Cooling medium losses. The model is an ideal model of the condenser, where losses are not taken into account. Therefore heat transferred by the cooling medium and the working fluid are nearly equal. In reality losses to the environment will occur.

At a working fluid mass flow of 0.007 kg/s results were also obtained, as was shown in figure 6.9a/b/c/d. The following can be observed:

- The condenser pressure is within sensor accuracy. From $c_a = 0.93$ to $c_a = 0.982$ the slope of the modelled pressure is similar however a slightly steeper decrease was seen for the experimental values. At a concentration of $c_a = 0.923$ a relatively steep decrease in condenser pressure was shown for the modelled case and a slight increase in pressure was seen for the experimental case, suggesting opposite behaviour.
- The working fluid outlet temperature showed similar behaviour for modelled and experimental values. At lower concentrations the deviation in outlet temperature increased to approximately 0.5 $°C$.
- The working fluid heat transfer behaviour and absolute values were accurate.
- The cooling medium outlet temperature stayed within 0.5 $°C$ deviation with a similar slope.

The previous observations show that the model is also valid for other working fluid mass flows.

6.5.5. Model conditions

All design choices that were made are shown in table 6.5. It contains heat transfer correlations, film thickness correlation, mass transfer coefficients and databases used.

7

Results and Discussion

In the previous chapter the model was validated. With the model validated the performance of the heat exchanger can be analysed. What makes the method so powerful is the ability to see what happens in both the vapor and the liquid phase and to be able to analyse what happens in every section of the heat exchanger. In this chapter general results are shown and discussed in section 7.1 and in section 7.2 the influence of the ammonia concentration on the heat transfer performance is shown and discussed. In plots where results for different concentrations are compared not all available concentrations are plotted to keep the plots clear to view. Important to notice is also that some variables are calculated for the next control volume (j+1) and some are calculated for the current control volume (j), therefore some variables contain a 0 and some contain a normal value for the last vector value.

7.1. General result profiles

In this section the general results and trends of the various characteristic variables throughout the heat exchanger are discussed and analysed. This is done for the case of $c_a = 0.954$. The concentration influence on the system and a more in-depth look into the heat transfer mechanisms are given in section 7.2.

7.1.1. Heat flux profiles

The heat fluxes of the different phase and liquid interfaces are good indicators to identify the main heat transfer mechanisms of the system. The heat fluxes are shown in figure 7.1a/b/c, from the figures the following can be concluded:

- A clear dominance of the liquid bulk sensible heat and ammonia mass transfer heat fluxes is seen. This is to be expected because of the high percentage of ammonia in the vapor and the condensing nature of the process.
- The small amount of water vapor present in the vapor condenses very fast at the inlet of the heat exchanger.
- The overall heat flux increases towards the outlet of the heat exchanger.

7.1.2. Heat and mass transfer coefficient profiles

The sensible heat flux and the molar flux through the interface are largely dependent on the heat transfer and mass transfer coefficients. In figure 7.2 the heat transfer coefficients are plotted against the length in the heat exchanger. The following can be seen:

- The film heat transfer coefficient is lower than the cooling medium heat transfer coefficient. This means that the film heat transfer coefficient is the limiting factor for the heat transfer through the wall. However, it doesn't have to be the limiting factor for the whole system since mass transfer is an important factor at the interface.

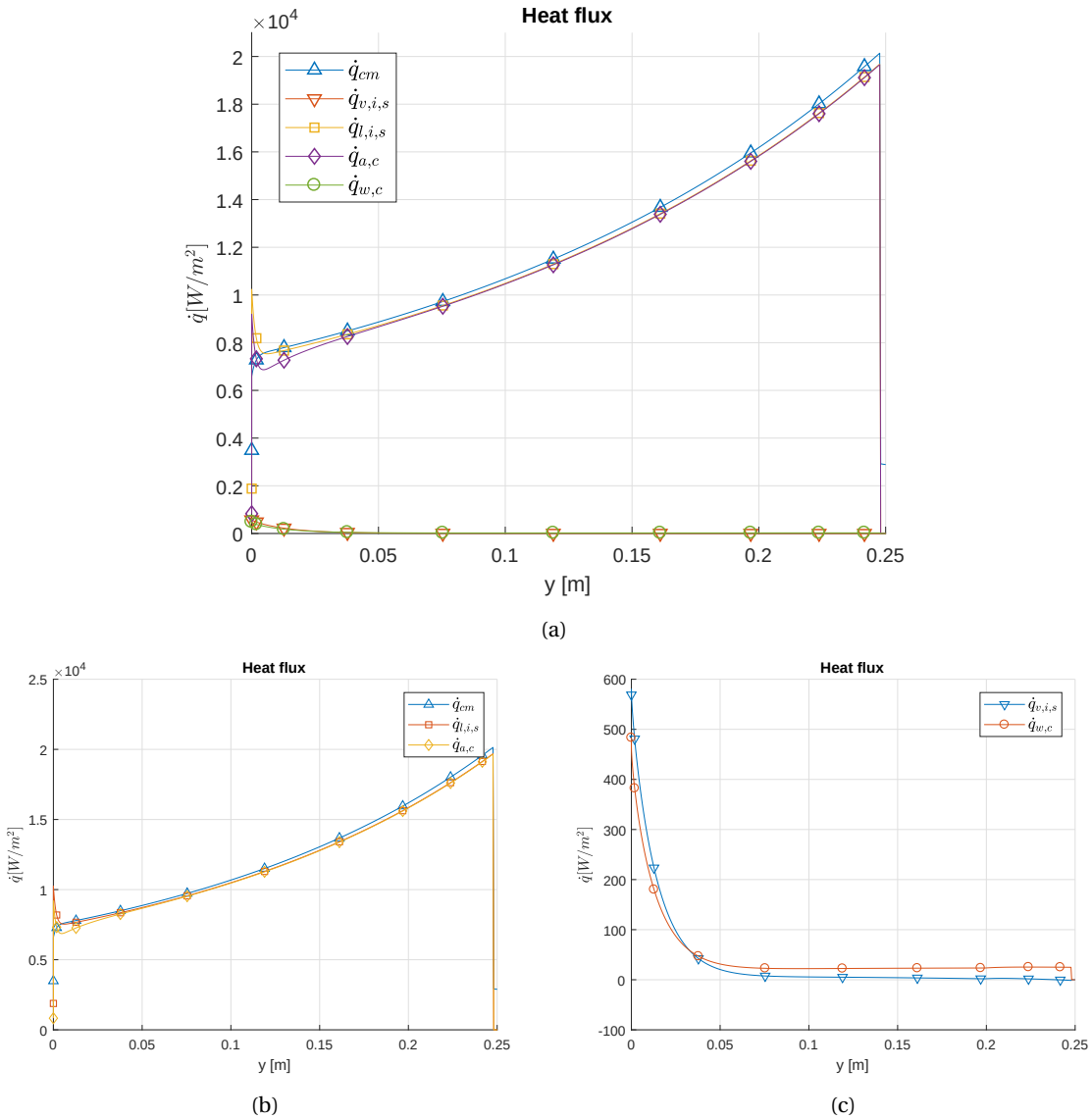

Figure 7.1: (a) Heat fluxes plotted against length in the heat exchanger. (b)(c) Zoomed in to different heat fluxes.

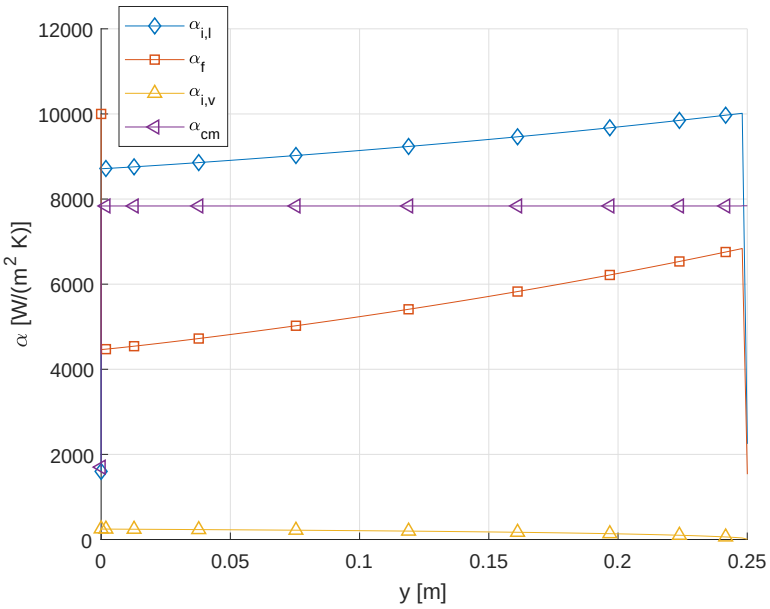

Figure 7.2: Heat transfer coefficients throughout the heat exchanger.

- The heat transfer coefficient at the interface of the liquid side is the highest heat transfer coefficient. Because of the Chilton-Colburn analogy this also has a direct effect on the mass transfer diffusing through the interface.
- As expected, the vapor phase heat transfer coefficient has a small effect. Heat is mostly transferred through mass transfer and the liquid to interface sensible heat.
- The working fluid liquid heat transfer coefficients show an increase in value towards the outlet of the heat exchanger because of an increasing mass flux of the liquid.

A more detailed dissection of the heat transfer coefficients and their behaviour is given in section 7.2. The mass transfer coefficients are shown in figure 7.3. Both the liquid and vapor mass transfer coefficient are analogous to Nusselt's number. It is therefore expected that when the liquid flow increases and the vapor flow decreases, that the mass transfer coefficients show the same trend.

7.1.3. Mass flow profile

The model incorporates mass flux through the interface and thus it is possible to see how that influences the mass flow in the heat exchanger of both the vapor and the liquid. The result is shown in figure 7.4a. A direct result from the mass flows is the vapor quality which is shown in figure 7.4b. The vapor quality plot is cut off at a quality of 1% because the model becomes unstable in that region. Both plots have an exponential character which is explained by the increase in heat flux towards the outlet of the heat exchanger.

7.1.4. Temperature and concentration profiles

The resulting temperature and concentration profiles in the condenser are shown in figure 7.5 and figure 7.6a/b, respectively. The slope of the cooling medium temperature increases towards the outlet of the heat exchanger, this is explained by the increase in heat flux. The difference in temperature between the bulk liquid and the wall increases because of the increasing film thickness.

7.2. Concentration influence on heat transfer

The influence of the concentration of the ammonia water mixture on the performance is most interesting. In theory the temperature glide that occurs when using a mixture can improve the performance of the condenser. However, some negative effects of using a mixture are present as well. When changing the concentration of the fluid the heat flux profiles look as in figures 7.7 a/b. It can be seen that roughly the same trend

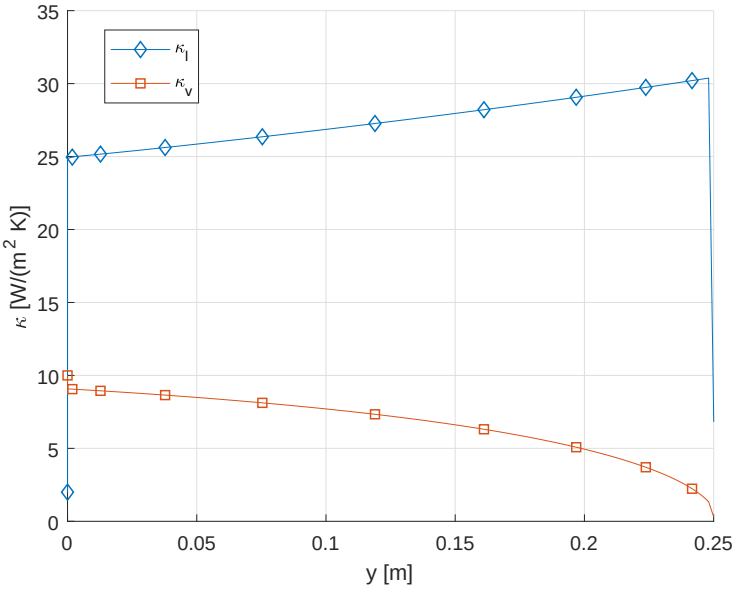

Figure 7.3: Heat transfer coefficients throughout the heat exchanger.

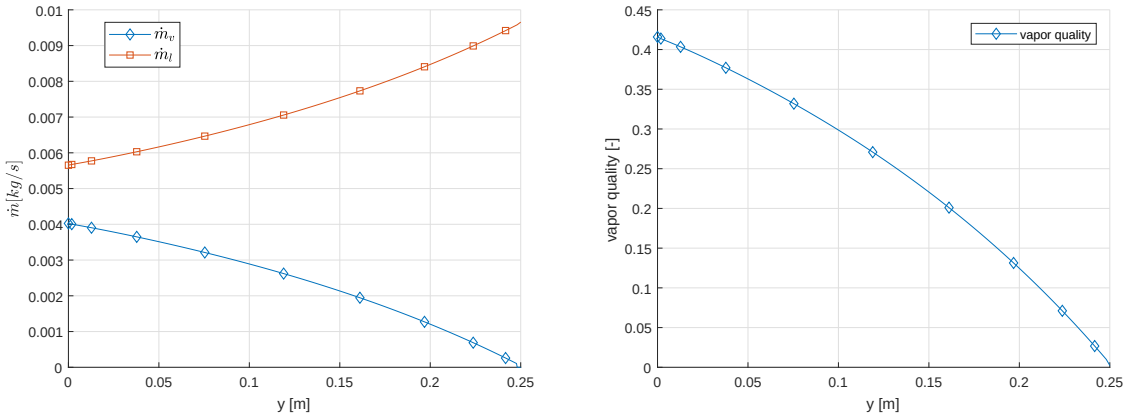

(a) (b)

Figure 7.4: (a) Mass flows of liquid and vapor working fluid throughout heat exchanger (b) Vapor fraction of the working fluid.

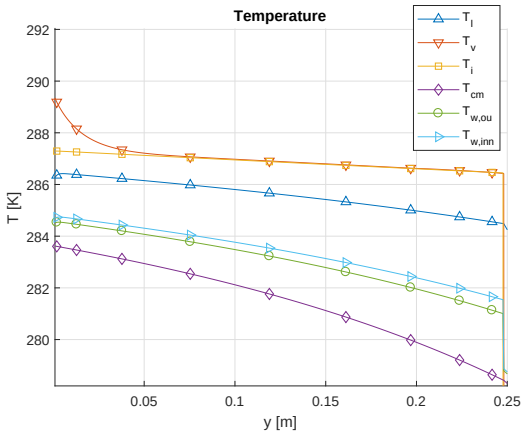

Figure 7.5: Temperature profiles in the condenser.

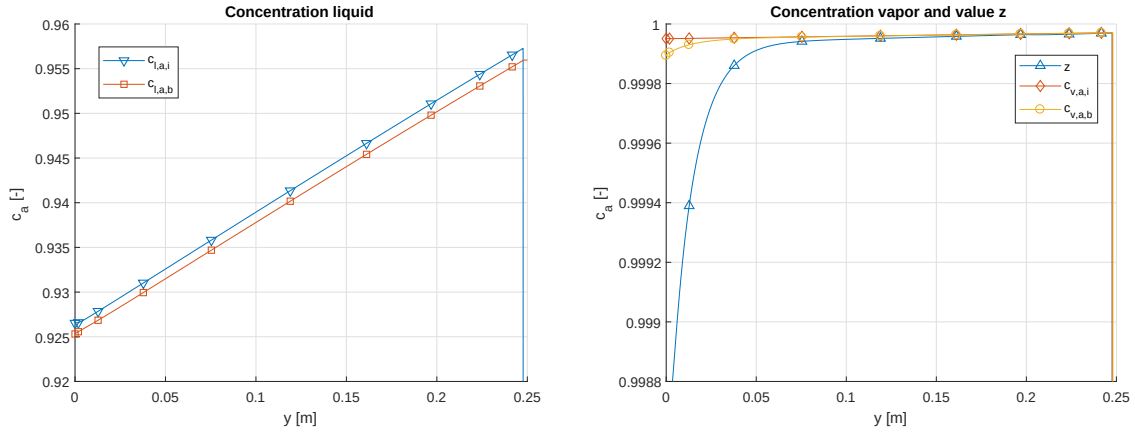

(a) (b)

Figure 7.6: Concentration profiles in the condenser (a) in the liquid phase (b) in the vapor phase (including the value of z).

is seen for both heat fluxes. The lower concentrations have a better performance at the beginning of the heat exchanger and the higher concentrations have a better performance towards the end of the heat exchanger. Both heat fluxes are heavily influenced by one another (equation 5.46). To explain the results in 7.7a/b the factors that influence these heat fluxes have to be analysed. This is done in this section.

7.2.1. Sensible heat transfer coefficient liquid bulk to interface

The sensible heat flux shown in figure 7.7b is described by equation 5.45. The main factors in the heat flux of the interface are the temperature difference $T_i - T_l$, and the interface heat transfer coefficient α_{il}. Figures 7.8a/b/c/d/e show the factors influencing the heat transfer coefficient. The trend of the liquid heat transfer coefficient at the interface, shown in figure 7.8a/b/c/d/e can be explained with the following observations:

- The thermal conductivity increases with decreasing concentrations of ammonia because of the favorable conduction properties of water, however the differences are insignificantly small.
- The liquid Prandtl number increases significantly at lower concentrations of ammonia because of the higher viscosity of water.
- The liquid Reynolds number shows a significantly higher value at higher concentrations. The dominant effect for this is the decrease in viscosity. The relatively steep increase of the Reynolds number during condensation can be explained by the increasing mass flux of the liquid.
- The film thickness has a negative effect on the heat transfer coefficient, a thicker film means more resistance. It is dependent on various variables (see equation 6.6). The difference in viscosity is the dominant factor for the difference in thickness between lower and higher concentrations. The increase in film thickness is physically explained by the increase of liquid mass flow however, mathematically the relation is just dependent on the y coordinate of the flow in the heat exchanger.

The liquid heat transfer coefficient at the interface leads to an optimum at a concentration of c = 0.931, whereas lower concentrations seem to perform better at the inlet of the heat exchanger and higher concentrations seem to perform better at the outlet of the heat exchanger. This can be explained by the decrease of the Prandtl number and the increase in film thickness towards the outlet of the heat exchanger that negatively influence the performance at lower concentrations.

7.2.2. Heat transfer through the wall

The cooling medium heat flux is described by equation 5.50 and is shown in figure 7.7e. Since there is no phase change in the cooling medium and the wall thickness is constant, the term $\delta_{wall}/\lambda_{wall}$ stays constant and α_{cm} is only changing marginally between the inlet and the outlet. α_f is the limiting factor, as seen in figure 7.2. In figures 7.9a/b/c the factors influencing the heat transfer coefficient of the film with varying concentrations are shown. The following can be concluded from the figures:

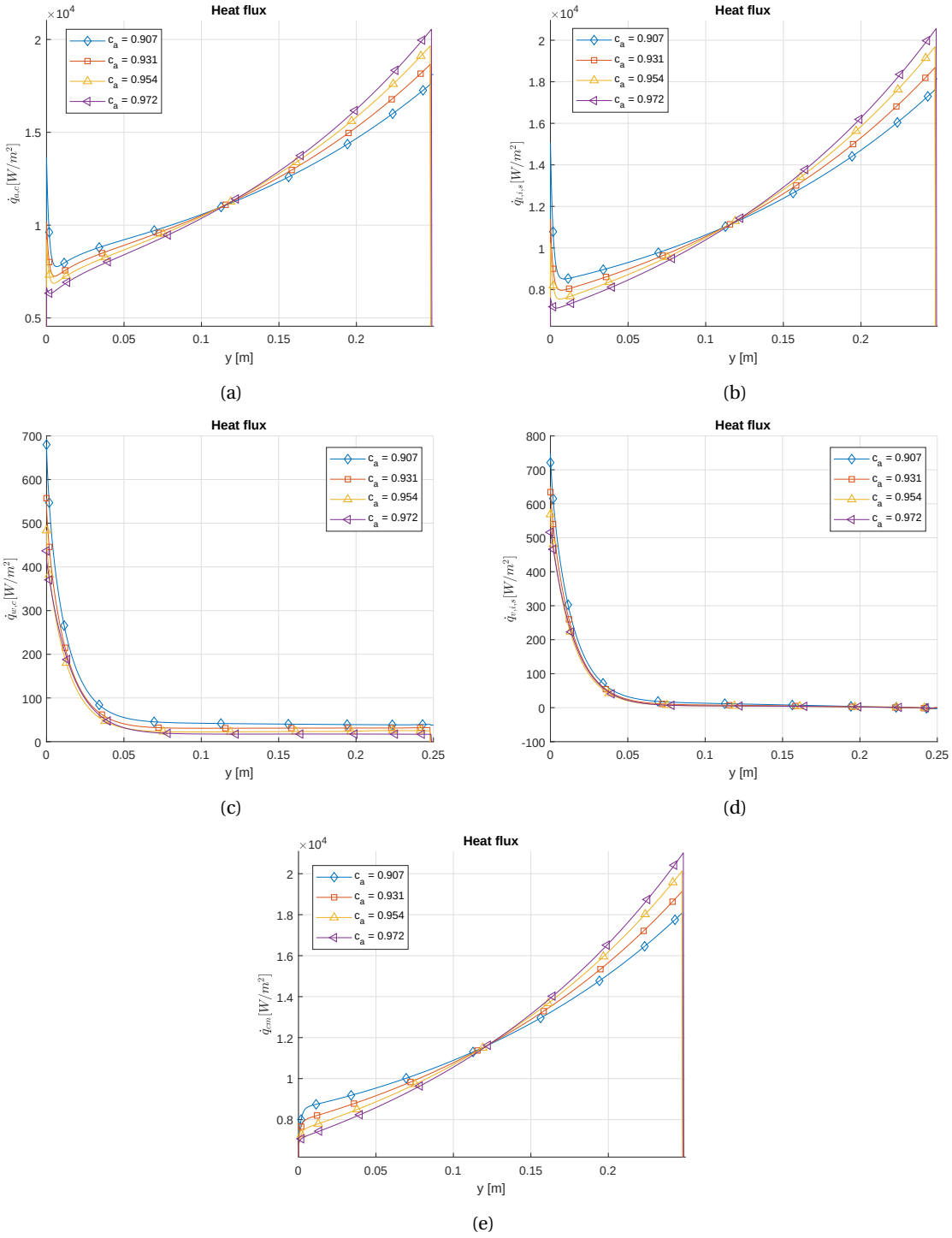

Figure 7.7: (a) Condensation heat flux of ammonia (b) Sensible heat flux liquid-interface (c) Condensation heat flux of water (d) Sensible heat flux vapor-interface (e) Sensible heat flux cooling medium - liquid film.

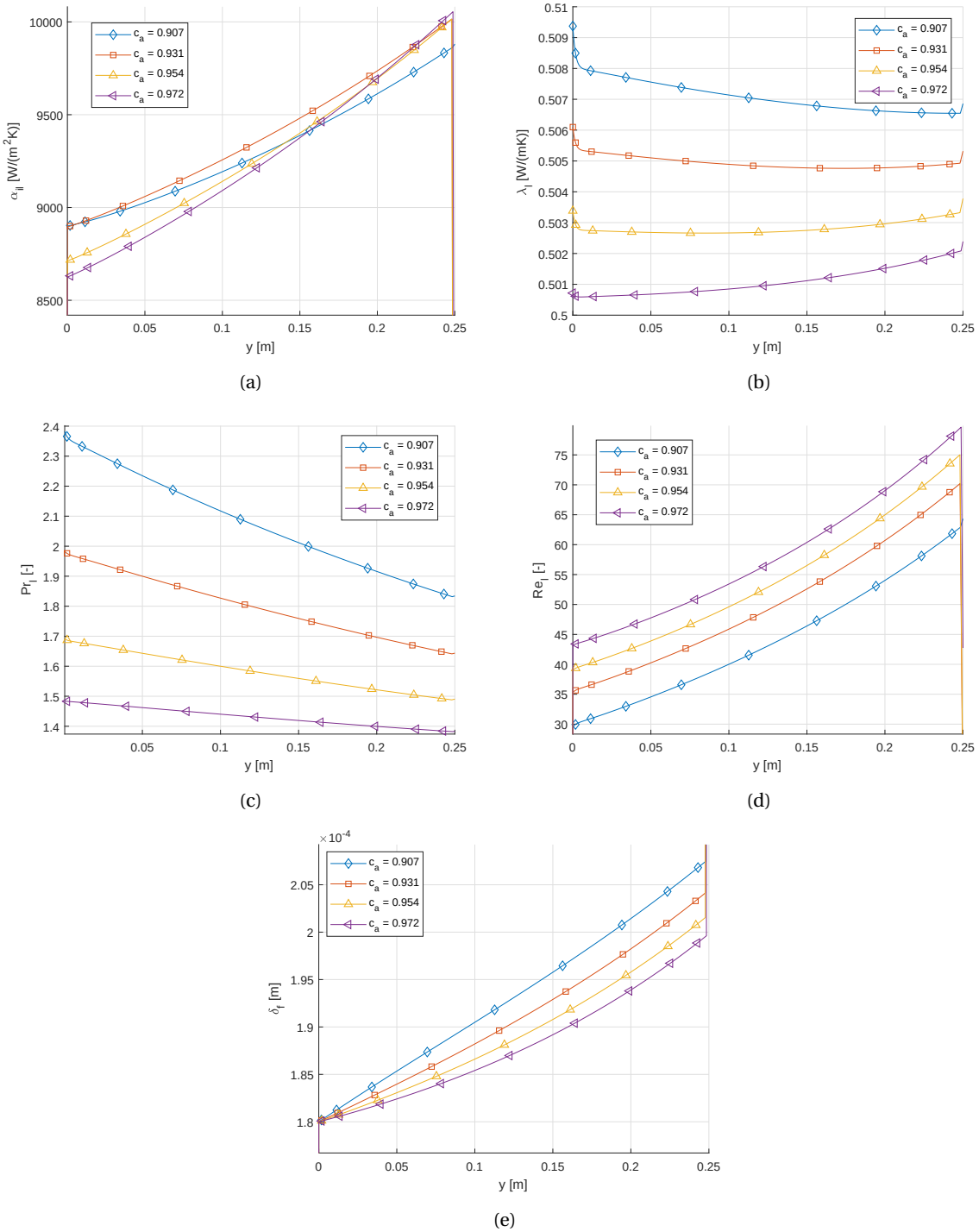

Figure 7.8: Plots of characteristic variables for sensible heat transfer at the interface. (a) Heat transfer coefficient interface (b) Liquid thermal conduction coefficient (c) Liquid Prandtl number (d) Liquid Reynolds number (e) Film thickness.

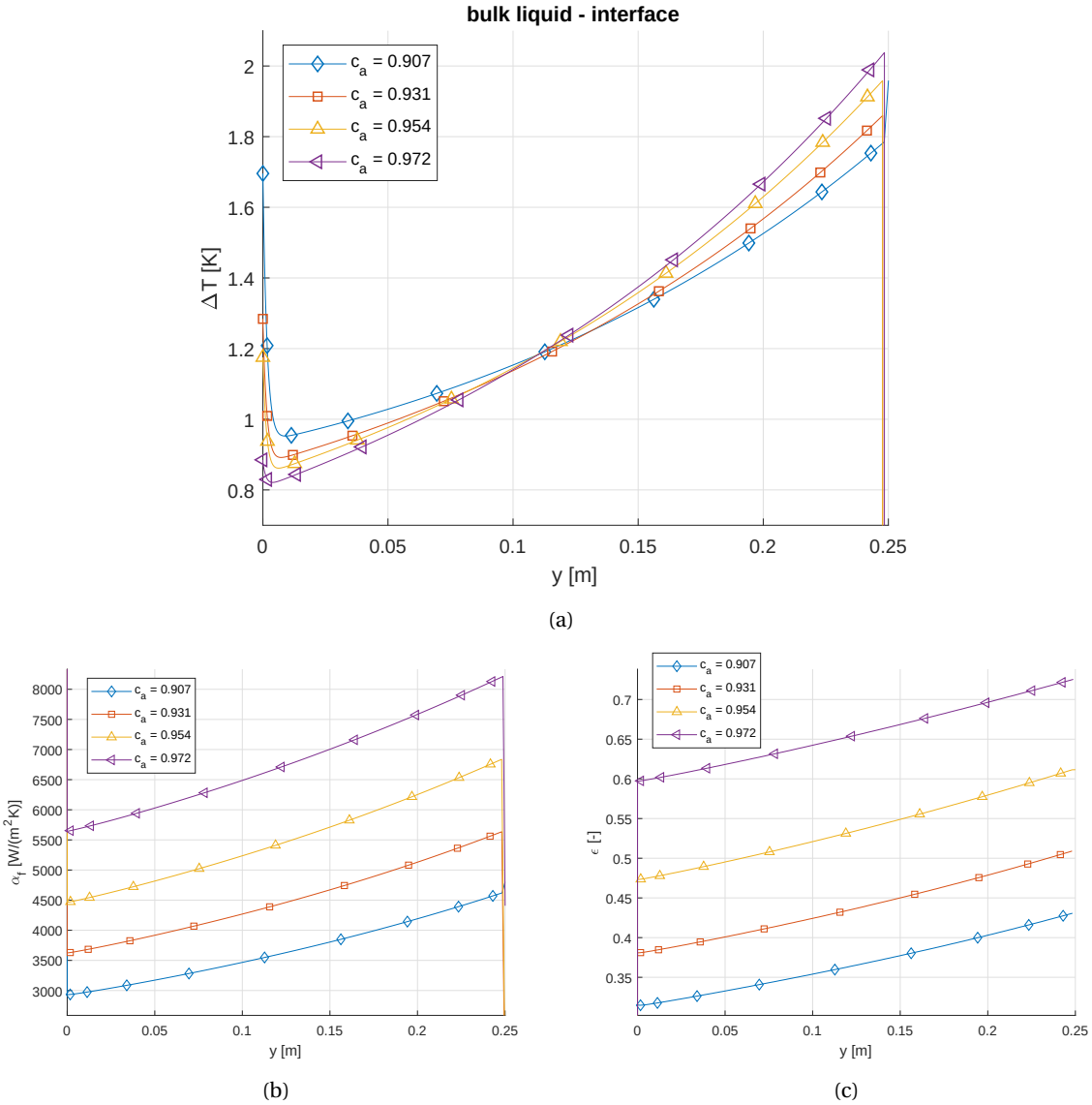

Figure 7.9: Plots of characteristic variables for sensible heat transfer from the cooling medium to the film.(a) Absolute temperature difference between the interface and the liquid bulk (b) Heat transfer coefficient interface (c) Surface tension factor ϵ.

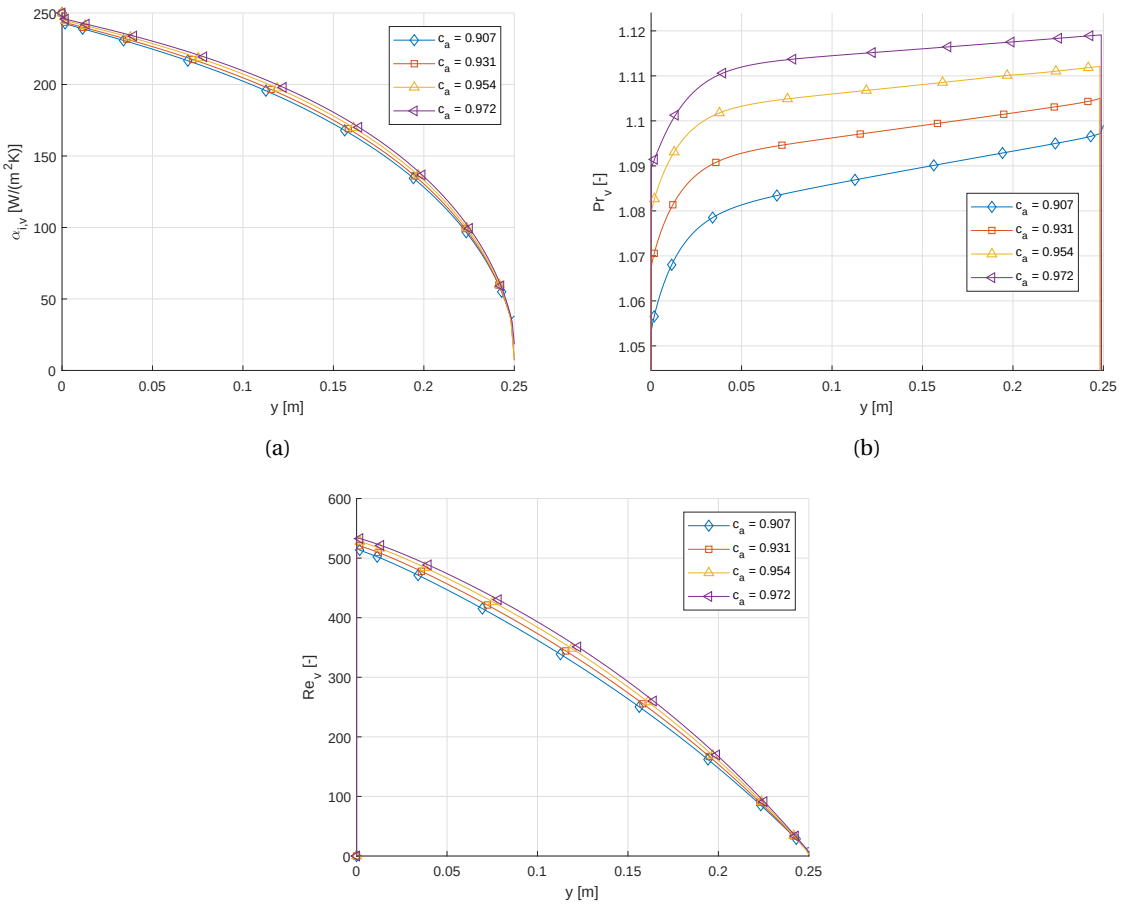

Figure 7.10: Plots of characteristic variables for sensible heat transfer from the vapor to the interface. (a) Heat transfer coefficient (b) Vapor Prandtl number (c) Vapor Reynolds number.

- The heat transfer coefficient of the film is affected by the same variables as the heat transfer coefficient at the interface and the same observations as mentioned for the interface can be made. However, the correlation used for the Nusselt number is different.
- The surface tension correction factor is a dominant factor in determining the heat transfer coefficient. The surface tension correction factor becomes very low for low concentrations. This is one of the major factors contributing to the difference in heat transfer coefficients at different concentrations.
- The increase of the heat transfer coefficient of the film throughout the heat exchanger can be explained by a steeper increase of the Reynolds number compared to the film thickness.
- The heat transfer coefficient of the film is highest at $c_a = 0.972$ throughout the heat exchanger.

7.2.3. Sensible heat transfer coefficient vapor to interface

The influence of the sensible heat transfer coefficient on the total heat transfer behaviour of the system is very small since the heat transfer of the vapor phase is much lower than the heat transfer of the liquid phase, as seen in figure 7.1. The heat transfer coefficient of the vapor and the Prandtl and Reynolds numbers are shown in figures 7.10a/b/c. The behaviour of the heat transfer coefficient of the vapor is as one would expect:

- Towards the end of the heat exchanger the vapor mass flow decreases which results in a lower Reynolds number and lower heat transfer coefficient.
- The vapor ammonia concentration is very high and thus difference in Prandtl number is insignificant compared to the difference in Reynolds number.

- The heat transfer coefficient is much lower compared to the liquid heat transfer coefficients, therefore the influence of the vapor state has little influence on the total heat transfer.

7.2.4. Heat flux through interface induced by mass transfer

The condensation heat flux depends on the molar flux of the ammonia diffusing through the surface which is in turn influenced by the mass transfer coefficient, the concentration of the ammonia and z. The driving force of the molar flux is the difference between the concentration at the interface and the concentration in the bulk (5.38a/b). The mass flux induced heat transfer behaviour from figure 7.7a can be explained with the figures 7.11a/b/c/d by observing the following:

- The ratio $c_{l,a,b}/c_{l,a,i}$, which represents the concentration difference over the interface, slowly decreases over the length of the heat exchanger and thus increases the driving force.
- The ratio z, which represents the ammonia molar flux over the water flux, increases, which has a negative influence on the driving force. At the end of the heat exchanger the z values of different concentrations come closer together and thus decreasing the difference in driving force.
- The mass transfer coefficient increases towards the end of the heat exchanger since it is related to the heat transfer coefficient (see figure 7.8) through the Chilton Colburn analogy (equation 5.36). The difference in coefficient for different concentrations is due to lower mass diffusivity (D) values for lower concentrations.

In short: at the inlet of the heat exchanger the lower values for z and $c_{l,a,b}/c_{l,a,i}$ at lower concentrations make for a better performance. Halfway through the heat exchanger the values for z come closer together and thus the influence of the difference in mass transfer coefficient becomes more apparent and increases the heat flux at the higher concentrations.

7.2.5. Temperature differences

The driving force of the whole system is a combination of temperature difference between the different fluids and the different phase states. The temperatures depend on the mass and heat transfer coefficients described in the subsections above. The temperature differences for different concentrations are shown in figure 7.12 a/b/c/d. What can be seen is that between the bulk liquid and the interface the temperature difference is larger at the inlet of the heat exchanger at lower concentrations. Most significant is the difference observed for the wall to liquid film at varying concentrations (see figure 7.12). This is due to the surface tension correction factor which decreases the heat transfer between the wall and the liquid film and thus increasing its temperature difference.

7.2.6. Overall heat transfer coefficient

More evident conclusions can thus be drawn with respect to the performance using a new performance indicator. In this case the overall heat transfer coefficient is used, for it enables the model to capture all previously mentioned heat transfer phenomena in one factor. As shown in figure 7.13 the overall heat transfer coefficient increases at increasing concentrations and the condenser thus performs better at higher concentrations. Throughout the heat exchanger the overall heat transfer coefficient also shows an increasing trend. This trend can be explained by the increase in working fluid liquid heat transfer coefficient (due to increase in Reynolds number), mass transfer coefficients and mass transfer driving force (see figure 7.11a). However, as was seen in figure 6.5.2, the pressure is also lower at decreasing concentration which is positive for the performance.

7.3. Conclusions and recommendations

The objective of the second part of the study was to develop an advanced heat exchanger model that is able to predict and describe the complex heat transfer phenomena in a two phase mixture condenser. The performance was assessed by predicting the stream properties throughout the heat exchanger and predicting the pressure present inside. The same experimental data as used in Part I was used to judge the validity of the model.

In the model the vapor and liquid phase were separately calculated. Their behaviour could be assessed individually and their interaction could be judged as well. This provided a better understanding of the total process. The highlights of the results can be summarised as follows:

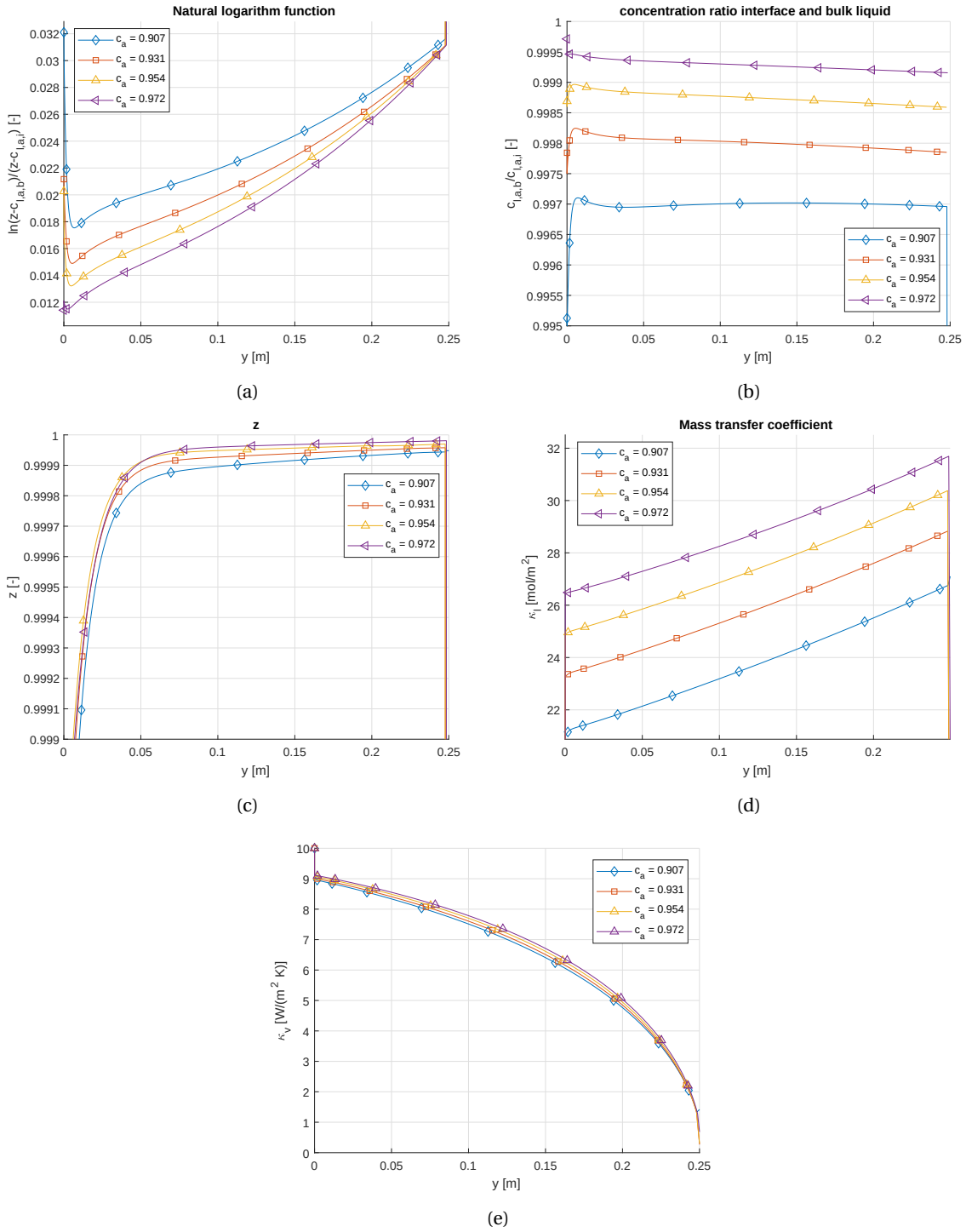

Figure 7.11: Characteristic plots for the heat transfer induced by condensation against the length in the heat exchanger for the liquid. (a) Natural logarithm equation 5.38, mass transfer driving force (b) Ratio of interface concentration and bulk liquid concentration (c) z function (d) Liquid mass transfer coefficient (e) Vapor mass transfer coefficient.

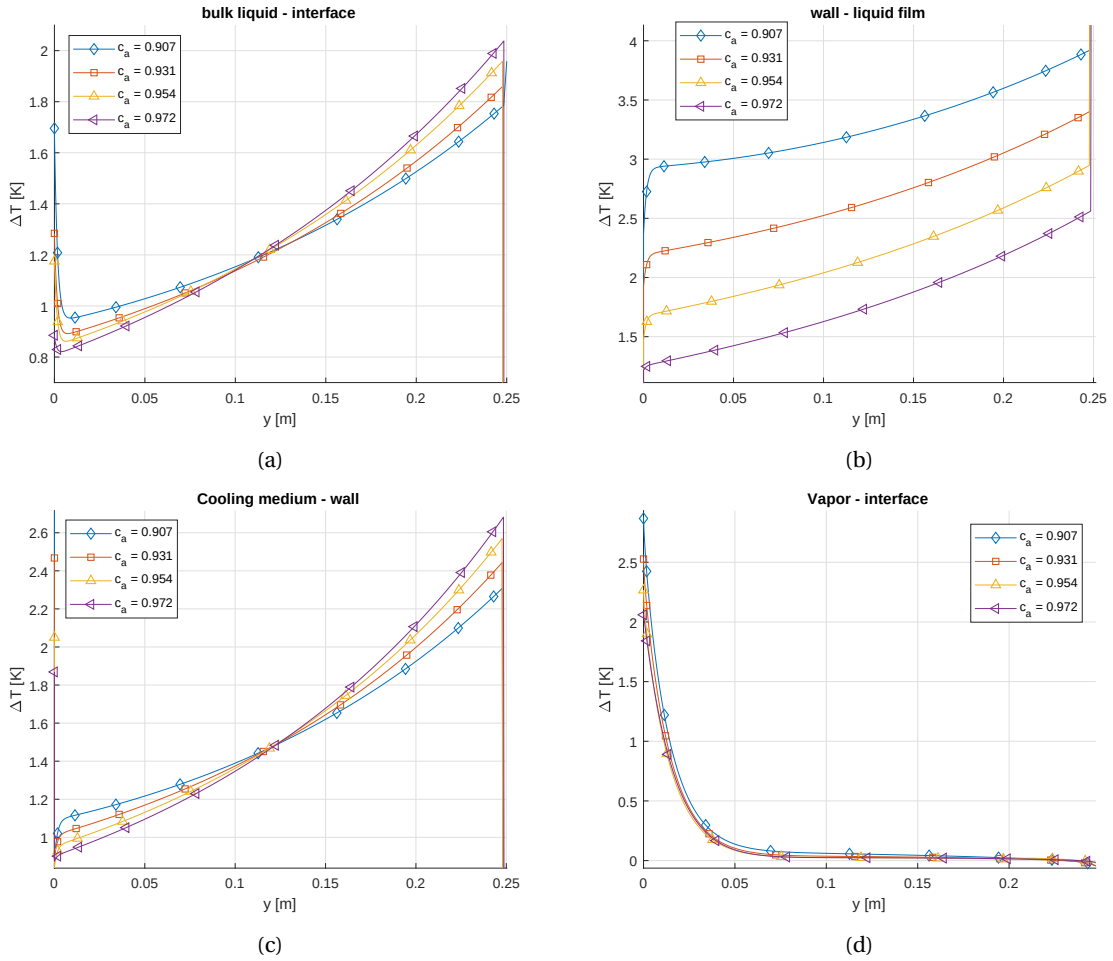

Figure 7.12: Temperature differences of (a) interface and liquid bulk (b) liquid film and wall (c) cooling medium and wall (d) vapor and interface.

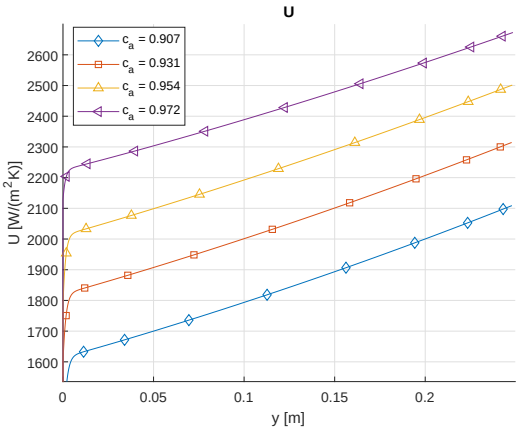

Figure 7.13: Overall heat transfer coefficient.

- For the 0.010 kg/s working fluid mass flow case the following accuracy was seen; the working fluid outlet temperature stayed within 5% accuracy, the cooling medium inlet temperature stayed within 3.4% accuracy, the pressure accuracy stayed within pressure sensor accuracy, the cooling medium heat transfer didn't exceed 3.1% inaccuracy.
- The highest concentration ammonia mixture gave the highest overall heat transfer coefficient.
- Heat transfer became significantly higher towards the outlet of the heat exchanger.
- The working fluid temperature was overestimated by the model with a maximum of 5% inaccuracy and the pressure was predicted lower than the actual pressure.
- Trends of the experimental characteristic variables showed very similar slopes in performance when changing concentrations.

From these results and other observations the following conclusions and statements can be formulated:

- The condenser seems to perform better with increasing concentration of ammonia. Due to non-linear behaviour of the mass diffusivity the mass transfer coefficients are higher at higher concentrations. The smaller film thickness and the higher liquid Reynolds number also contribute to these results. The surface tension correction factor has a strong influence on the decrease in performance at lower concentrations as well, implying that significant areas of dry surface voids appear at the conditions tested.
- Higher concentrations of ammonia seem to perform better overall. When regarding the graph of the overall heat transfer coefficients at different concentrations in figure 7.13 it can be seen that throughout the heat exchanger the difference in overall heat transfer coefficient is fairly constant over all concentrations, indicating that at all different conditions tested an increasing concentration is favourable.
- The ammonia-water mixture has some favourable properties over pure ammonia. At higher vapor quality the driving force for mass transfer is higher (figure 7.11a). This effects compensates for the lower mass transfer coefficient. As seen in figure 7.7a this results in a higher heat flux induced by mass transfer for lower concentration at the inlet of the heat exchanger. If the inlet stream of the condenser is of higher vapor quality than tested in this research this effect could be more dominant. Also the liquid heat transfer coefficient at the interface is higher at lower concentrations. This is due to a higher Prandtl number at the inlet of the condenser, this difference becomes smaller towards the end of the heat exchanger.
- The liquid film behaviour is an important factor in the heat transfer. Voids in the wetted surface are assumed to occur in the condenser due to unfavourable wettability properties at lower concentrations of ammonia. This is an important contributor to the decrease of performance at lower concentrations. However, if the mass fluxes on the working fluid side are increased, a falling film might be achieved more easily, therefore decreasing the effect of surface tension and increasing the performance at lower concentrations.
- A positive effect of using ammonia water with a lower concentration is the lower pressure level necessary of the condenser. A lower pressure induced by the condenser increases the potential power output of the turbine. This was shown in the previous chapter. A lower pressure level also reduces the heat transfer in the heat exchanger. Therefore, when regarding the comparison made in this chapter, it should be taken into account that this has a favourable effect on the heat transfer at higher concentrations.

7.4. Recommendations

With the model developed in this part a lot of insight is gained on dominant heat transfer phenomena occurring when using the ammonia water mixture in a condenser plate heat exchanger. However, further research can be done both experimentally and numerically to improve the model. When regarding experimental research, the following should be investigated:

- Flow pattern research, visual research of the flow patterns can be used to validate the correction factor used in this research. It also gives more insight in whether dry surface voids should be taken into account or not. The influence of using ammonia or ammonia-water on the flow patterns wasn't found in literature.

- More experimental research has to be done on film thickness development in plate heat exchangers for mixture fluids. Most film thickness relations found are for water flow over a flat plate. No researches were found for plate heat exchangers or mixture fluids.
- Experimental research should be performed with different heat exchangers. The heat exchanger used in the OTEC experimental setup could be too large for the low mass fluxes at the working fluid side. Therefore dry surface voids could occur. These voids could have a significant influence on the heat transfer performance.
- Different conditions should be tested. At higher vapor quality the lower concentrated mixture seemed to have some favourable properties, increasing the vapor quality of the inlet stream can be of interest. Different working fluid mass flows should be tested, increasing the mass flows of the working fluid will decrease dry surface voids, thus increasing the performance.
- To properly judge the performance of the condenser, the model should be incorporated in a complete cycle. It can then be judged whether the difference in pressure or the overall heat transfer coefficient at different concentrations have a positive or negative effect on the efficiency of the whole cycle.

Numerically the model should be improved as follows:

- The interface energy balance iteration loop (see figure 5.4) becomes unstable when mass flows are either too high or too low, which occurs at 0.005 kg/s and 0.013 kg/s working fluid mass flows. It should be investigated whether the database of Rattner-Garimella and the way it is called is still accurate for these conditions or if the instability comes from something else.
- The mass transfer coefficients are now analagous to the heat transfer coefficients through the Chilton-Colburn analogy, however it is unsure if this is an accurate estimation for the mass transfer coefficients. With mass transfer being an important part of this research this should be investigated further.

III

General comparison Part I and Part II

8

Comparison

The two calculation methods described in Part I and Part II are completely different, however they are used to predict the same process in the OTEC cycle; condensation of an ammonia water mixture in a plate heat exchanger. Both methods are useful for different purposes. In this chapter the major differences that were found are discussed and from this discussion conclusions are drawn as to which method should be applied for which purpose.

8.1. Heat transfer two phase flow

The two phase heat transfer calculation of the working fluid mixture is the main difference in both methods. For the fitting method a new two phase heat transfer correlation for plate heat exchanger flow was developed. The advanced two phase method uses correlations that are used to describe single phase flow and incorporates a mass transfer model on the interface of the vapor and the liquid. This difference has the following effect on the two phase heat transfer calculations:

- The advanced method allows for a prediction of the heat transfer of the vapor and the liquid as well as the mass transfer induced heat transfer. Through this method different heat transfer mechanisms could be described and bottlenecks of the working fluid heat transfer could more easily be identified.
- The advanced method allows for more physically substantiated theory to be used in the calculations, which potentially makes the model more general. This means that if the model is used for a different situation only the deviant parameters would have to change.
- The downside of the previous property is that the advanced model can not be developed for a situation where the necessary theory isn't available. For instance, for the model developed there wasn't any experimental research found on film thickness in mixture flow in plate heat exchangers.
- The fitting method provides a widely usable concept. If experimental data is available for a flow at certain conditions one can predict the two phase heat transfer within these conditions. The more experimental data is gathered, the more general and accurate the fitted correlation will be. Therefore it is not necessary to describe all the heat transfer mechanisms in the system. This concept was used on the experimental data of the OTEC condenser, and accurate results were found.
- With the fitting method, in a more general way than in the advanced method, quantities can be added that predict specific phenomena that are expected to occur. In the condenser of the OTEC setup it was expected that mass transfer would be an important factor in the heat transfer. By including the Schmidt number this phenomenon was described accurately.

8.2. Pressure prediction

Another important difference is the calculation of the pressure in the condenser. When using the fitting method it is not possible to predict how much the liquid is subcooled when the vapor is completely condensed. To illustrate this difference two typical T-y diagrams are shown in figures 8.1a/b for the fitted method

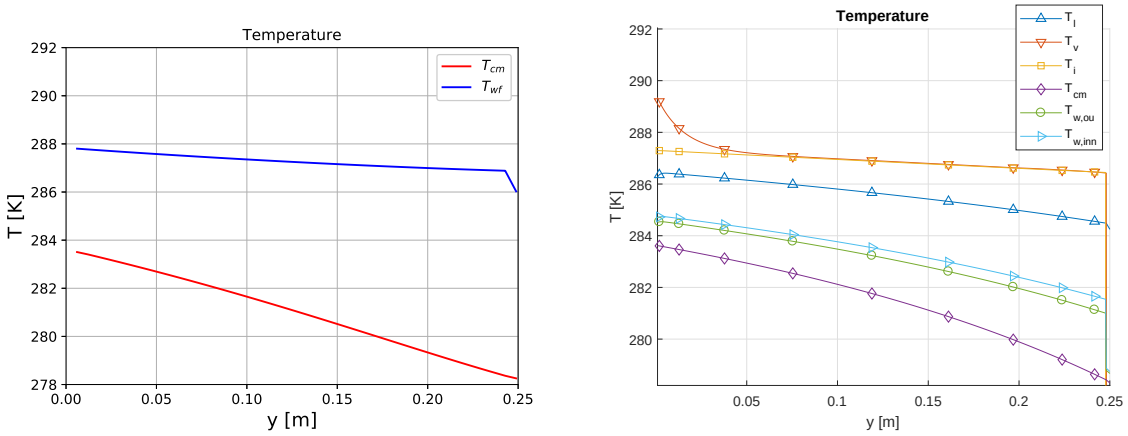

(a) (b)

Figure 8.1: Typical temperature profiles plotted against the y coordinate in the heat exchanger for (a) the fitted model and the (b) advanced model.

and the advanced method, respectively. In the fitted correlation method the two phase flow is represented as one flow with one temperature. Consequently, also because of the condensing nature of the process, the temperature in the model is the saturation temperature. However, if the vapor would be the same temperature as the liquid there would no driving force in between the two flows and thus there would be no condensation. Therefore, as shown in fig 8.1b, in the advanced condenser model, the liquid is always subcooled and the vapor is at saturation temperature, which is correct. To get accurate outlet temperatures of the working fluid for the model using the fitted correlation a subcooled process is incorporated near the outlet of the heat exchanger process, incorrectly assuming that the subcooling happens only after the vapor is completely condensed.

This difference has little influence on the overall heat transferred, but it is important for predicting the pressure of the condenser at the working fluid side. As explained in section 5.5 the pressure is determined by the performance of the condenser. If the working fluid isn't fully condensed at the outlet of the heat exchanger the pressure rises and the performance of the condenser is improved. This effect makes it valid to assume that the working fluid is exactly condensed at the outlet of the heat exchanger. This pressure effect was built in the advanced condenser model as well. The pressure is iterated until complete condensation is reached exactly at the outlet of the heat exchanger. In the fitting method model this iteration can't be applied. In this model the temperature of complete condensation is, as mentioned before, always saturation temperature. Therefore if one would implement the pressure iteration loop in this model an incorrect outlet temperature of the working fluid would be obtained.

8.3. Accuracy

The models showed a decent accuracy compared to the experimental data. Both were in detail compared for a working fluid mass flow of 0.010 kg/s. The differences are shown in table 8.1, the values in red are least accurate. The pressure accuracy is not included because the pressure is not iterated for the fitting method. For part I de deviation of the cooling medium is at the outlet of the heat exchanger and for part II it is at the inlet, therefore the experimental value is not included. From table 8.1 it can be seen that the working fluid and cooling medium temperatures are best described by the fitting method for this mass flow. And also that the accuracy of the heat transfer calculations are similar for both methods. Two other things stand out: the accuracy of the temperature does not agree with the accuracy of the heat transferred calculated by the different methods. This is due to a slight difference in calculation method. For the working fluid this is due to the subcooling part of the fitting method calculation. The temperature of the working fluid outlet becomes much more sensitive towards the outlet of the heat exchanger, as was seen in figure 8.1a. Therefore a slight increase in heat transfer can cause a significant decrease in working fluid outlet temperature.

For the cooling medium the effect can be explained by the calculation method of the advanced model. The advanced model only calculates the two-phase mixture until a quality of 1%. For a quality lower than 1% the medium is assumed to be fully condensed. Thus, there is a discontinuity in the heat transfer at the

Table 8.1: Deviations from the experimental and model values for relevant parameters for a working fluid mass flow of 0.010 kg/s

	$T_{wf,out}$	T_{cm}	$\dot{Q}_{cm}$	$\dot{Q}_{wf}$
c = 0.978				
Experimental value	10.571 °C		5179.7 W	5101.3 W
Advanced method deviation	3.48%	0.82%	-0.75%	0.19%
Fitting method deviation	0.84%	-0.87%	-1.44%	0.07%
c = 0.972				
Experimental value	10.605 °C		5218.0 W	5068.1 W
Advanced method deviation	4.60%	2.6%	-2.35%	-0.29%
Fitting method deviation	0.74%	-1.54%	-2.01%	0.25%
c = 0.954				
Experimental value	10.886 °C		5171.0 W	5049.4 W
Advanced method deviation	4.12%	2.32%	-2.12%	-0.34%
Fitting method deviation	-2.26%	-1.17%	-2.8%	0.35%
c = 0.9448				
Experimental value	11.225 °C		5191.1 W	5045.2 W
Advanced method deviation	2.18%	2.63%	-2.39%	-0.21%
Fitting method deviation	1.48%	-1.63%	-2.37%	0.00%
c = 0.9314				
Experimental value	11.282 °C		5131.9 W	5018.4 W
Advanced method deviation	3.10%	2.36%	-2.16%	-0.21%
Fitting method deviation	0.72%	-1.34%	-2.37%	-0.16%
c = 0.923				
Experimental value	11.605 °C		5224.8 W	5128.8 W
Advanced method deviation	2.88%	2.32%	-2.09%	-0.39%
Fitting method deviation	1.64%	-1.30%	-2.37%	-0.54%
c = 0.915				
Experimental value	11.586 °C		5186.3 W	5080.46 W
Advanced method deviation	3.47%	2.67%	-2.42%	-0.49%
Fitting method deviation	0.14%	-1.45%	-2.50%	-0.47%
c = 0.907				
Experimental value	11.667 °C		5153.8 W	5024.0 W
Advanced method deviation	3.26%	3.35%	-3.07%	-0.50%
Fitting method deviation	-2.31%	-1.66%	-2.94%	-0.43%

Table 8.2: Deviations from the experimental and model values for relevant parameters for a working fluid mass flow of 0.007 kg/s

	$T_{wf,out}$	T_{cm}	$\dot{Q}_{cm}$	$\dot{Q}_{wf}$
	c = 0.982			
Experimental value	10.73 °C		5214.6 W	5104.3 W
Advanced method deviation	1.04%	1.76%	-2.51%	-0.26%
Fitting method deviation	22.71%	-3.65%	-1.44%	-1.57%
	c = 0.956			
Experimental value	11.31 °C		5237.9 W	4963.6 W
Advanced method deviation	0.15%	5.2%	0.43%	-0.31%
Fitting method deviation	-5.88%	-2.45%	-4.82%	0.44%
	c = 0.934			
Experimental value	11.49 °C		5198.8 W	5068.1 W
Advanced method deviation	4.58%	2.65%	-2.78%	-0.59%
Fitting method deviation	1.69%	-1.31%	-2.63%	-0.12%
	c = 0.925			
Experimental value	11.39 °C		5157.1 W	5009.7 W
Advanced method deviation	5.21%	3.01%	-0.13%	-0.62%
Fitting method deviation	-13.29	-0.88%	-1.84%	1.04%

outlet of the heat exchanger in order to go to 0% quality for the working fluid. This has a small effect on the heat transfer, however the differences in accuracies between the methods are in the order of 0.5%, making it significant enough. Another difference is that for part I the cooling medium temperature is iterated differently which results in a difference for both the inlet and the outlet of the cooling medium. This makes the cooling medium heat transfer more inaccurate then the cooling medium outlet temperature.

Also for both models the control volumes are of a different size, therefore inaccuracies occur in different magnitudes. The advanced model wasn't run for other mass flows than the 0.007 kg/s and 0.010 kg/s working fluid mass flows, therefore only these can be evaluated.

For the working fluid mass flow of 0.007 kg/s the results are compared in table 8.2. What is seen in this table is that heat transferred for both methods is calculated within 5% accuracy. What is also shown in the table is the sensitivity of the working fluid outlet temperature for the fitted method. When the working fluid heat transfer is slightly off, the working fluid outlet temperatures shows significant deviations. This is due to the subcooling part in the fitted model, in the subcooling part the temperature decline of the working fluid is much steeper as seen in figure 8.1. In the advanced method there is no subcooling part and therefore the working fluid outlet temperature solutions is less sensitive to inaccuracy.

8.4. Stability

The stability of the model is another important difference between the two models. The iteration loop that calculates the interface conditions (see figure 5.4) that is used in the advanced model can become unstable. In this iteration loop the interface temperature is iterated until the energy balance at the interface is satisfied. However, if the calculated values for the heat and mass fluxes are incorrect this iteration loop can become impossible to solve and the energy balance at the interface becomes non zero. This effect usually increases with every following control volume causing the end solution to be incorrect. The model becomes unstable for working fluid mass flows of 0.005 kg/s and 0.013 kg/s. As mentioned in section 6.5.3 this is probably due to incorrect values from the database developed by Rattner and Garimella [32].

The fitted model uses the same database, however the working conditions are very different in both models. In the fitted model the working fluid is represented as one flow, this means that the concentration, whether vapor or liquid, is always the same. Consequently, the concentration of ammonia is always mod-

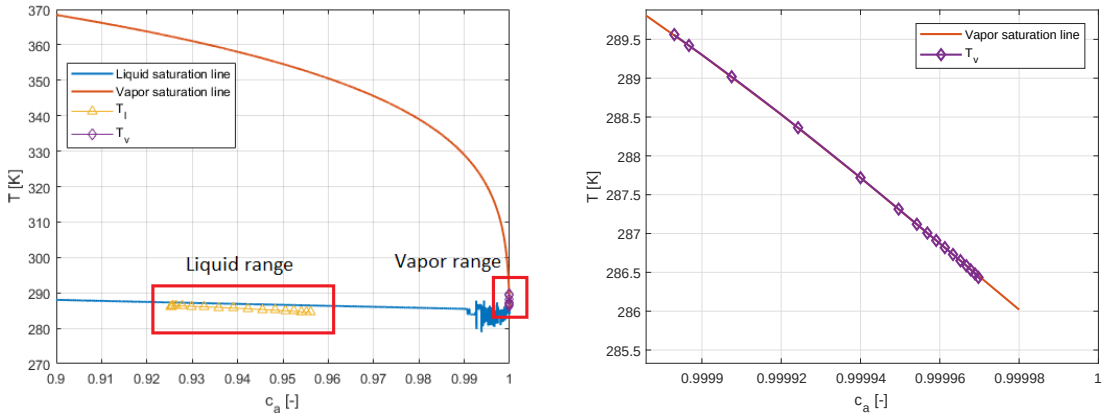

(a) (b)

Figure 8.2: (a) Typical bubble dew curve with temperatures of the liquid and the vapor of the working fluid for the advanced model. (b) Zoomed in on the vapor phase process.

Table 8.3: Calculation time both models at different concentrations of ammonia

	Calculation time	
$c_a[-]$	Fitted model	Advanced model
0.907	20 s	162 s (2.7 min)
0.931	10 s	116 s (1.9 min)
0.954	6 s	188 s (3.1 min)
0.972	10 s	293 s (4.9 min)

elled between 90-98% ammonia, where the values returned are stable and accurate. The bubble-dew curve with the temperature progression is plotted in figure 8.2a. As can be seen for the advanced model the concentration of the vapor and the liquid are different. Since the ammonia has a lower boiling point, most of the vapor will be ammonia causing the ammonia concentration in the vapor to be much higher (see figure 8.2b). Therefore, a slight error in the vapor could cause the model to return values for the concentration that are larger than 1. Since the REFPROP database and the database of Rattner and Garimella are both used in this model the inaccuracy could be accumulated as well.

8.5. Computational time

From a practical point of view, computational time is the most significant difference among the methods. The advanced method is more complex and is thus computationally more expensive. The differences in computational time are huge, therefore it is not necessary to do an in-depth comparison between the two. However, for the order of magnitude difference, the calculation time at four different concentrations for the working mass flow rate of 0.010 kg/s are shown in table 8.3. The calculation time of the advanced model is sensitive to input variables and iteration boundaries, therefore conclusions should not be drawn from the concentration influence on the computational time.

Practically, this means that the advanced model is limited in its applicability. In the model that was developed by Goudriaan [12] and Kuikhoven [23] the fitted correlation was part of an outer iteration loop of the whole cycle. Their model, using the fitted correlation, took 1 hour to converge to a solution for the whole cycle. It can be expected that incorporating the advanced model into their model of the total cycle would lead to a computational time that is practically not usable. Unless significantly faster computers are used or significantly more efficient models are developed, the fitted model remains the best choice for practical cycle calculations and the advanced model can be used for physical insight of one component.

8.6. Summary

A comparison was made between the two parts of this study. It was concluded that the advanced model is physically more substantiated and is therefore more useful for identifying bottlenecks in the heat transfer

process. On the other hand, developing a fitted correlation is generally an easier process which can be applied to many situations with high accuracy. Furthermore, it was seen that the advanced model provides a pressure prediction method which the fitted method does not. When regarding accuracy, it can be said that both models showed decent results, although the working fluid outlet temperature of the fitted method can be inaccurate for other mass flows then 0.010 kg/s. The stability of the model is a problem for the advanced model, whereas the fitted model is more robust, which was seen for the working fluid mass flows of 0.005 kg/s and 0.013 kg/s. Finally, the computational time was compared, the advanced model is more clearly more expensive in computational time, making it practically more difficult to implement than the fitted model.

Appendices

A

OTEC experimental setup

In this Appendix the OTEC experimental setup used by Goudriaan [12] and Kuikhoven [23] to generate experimental data is shown. These results were used for the validation in this study. The labview interface of the experimental setup is shown in figure A.1. The labview interface gives a good overview of the configuration of the experimental setup. It can be seen from this figure where the sensors are placed for measurements of different state values. The values of the sensors are only indicator values.

A.1. Condenser heat exchanger

The heat exchanger used is a brazed plate heat exchanger from AlfaLaval. The dimensions are shown in table A.1. Some dimensions are confidential and not stated here. The plate dimension definitions are shown in figure A.2.

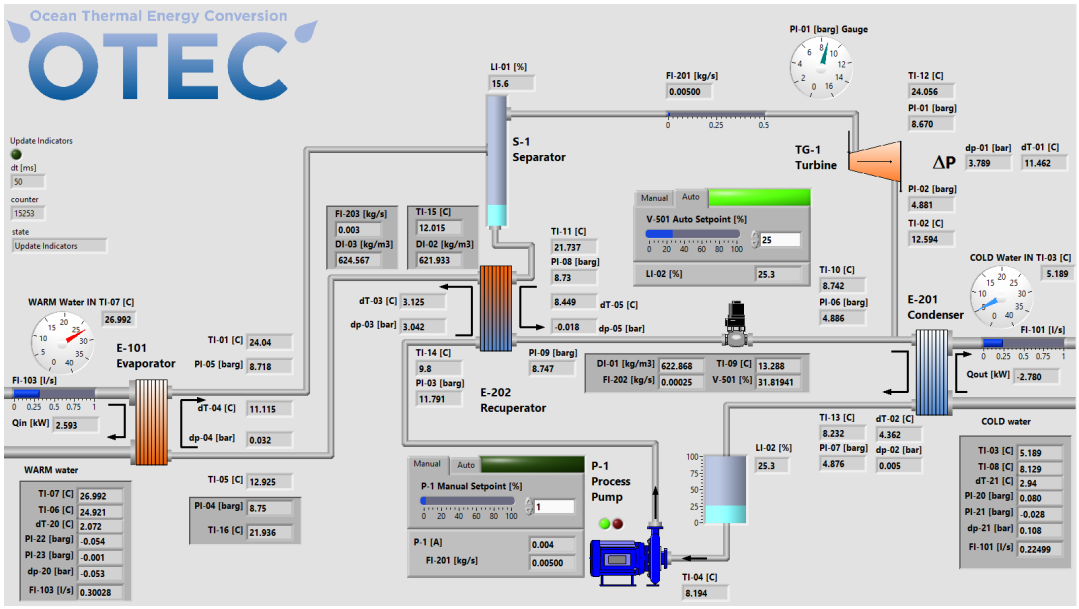

Figure A.1: Labview interface of the experimental setup. TI are temperature sensors, PI are pressure sensors, Fl are mass flow sensors and DI are density sensors.

Table A.1: Dimensions condenser heat exchanger in experimental setup

Heat Exchanger	AlfaNova27-18H
	Condensor
Type	Brazed plate heat exchanger
Number of passes	1
Flow	Counterflow
Total number of channels	17
Number of channels in pass 1 hot	9
Number of channels in pass 1 cold	8
Horizontal port centres distance [mm]	50
Vertical port centres distance [mm]	250
Plate thickness [mm]	0.4
Plate pitch [mm]	2.42
Port diameter [mm]	23/30
Plate width [mm]	100
Area of plate(s) [m^2]	0.025
Total number of plates	18
Total effective area [m^2]	0.4

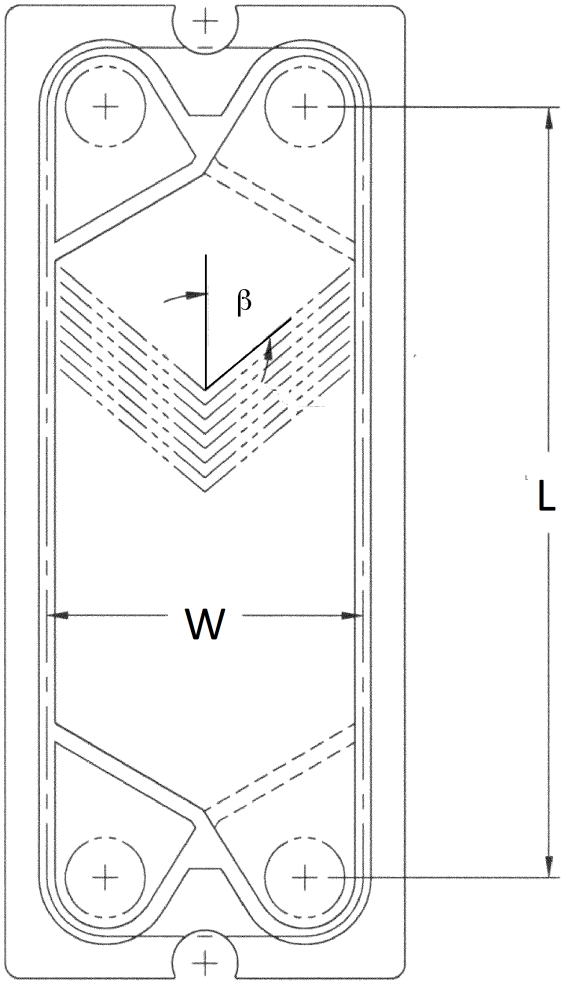

Figure A.2: Definitions heat exchanger dimensions

Bibliography

[1] S.P. Aarts. Entropy production minimisation of a compression-resorption heat pump To save energy and costs in waste heat recovery in industry, Master's thesis Delft University of Technology. 2016.

[2] R.L. Amalfi, F. Vakili-Farahani, and J.R. Thome. Flow boiling and frictional pressure gradients in plate heat exchangers. Part 2: Comparison of literature methods to database and new prediction methods. *International Journal of Refrigeration*, 61:185–203, 2016. ISSN 01407007. doi: 10.1016/j.ijrefrig.2015.07.009. URL `http://dx.doi.org/10.1016/j.ijrefrig.2015.07.009`.

[3] Z.H. Ayub. Literature Survey and New Heat Transfer and Pressure Drop Correlations for Refrigerant Evaporators. *Heat Transfer Engineering*, 24(5):3–16, 2003. ISSN 0145-7632, 01457632, 15210537. doi: 10.1080/01457630390218074.

[4] A. Binger. Potential and Future Prospects for Ocean Thermal Energy Conversion (OTEC) in Small Islands Developing States (SIDS), 2004.

[5] H. Brauer. Grundlagen der Einphasen- und Mehrphasenstromungen. *Verlag Sauerländer, Aarau u. Frankfurt/M*, (8):1972, 1971. doi: 10.1002/cite.330440821.

[6] T. H. Chilton and A. P. Colburn. Mass Transfer (Absorption) Coefficients: Prediction from Data on Heat Transfer and Fluid Friction. *Industrial and Engineering Chemistry*, 26(11):1183–1187, 1934. ISSN 00197866. doi: 10.1021/ie50299a012.

[7] M. Conde. Thermophysical Properties of {NH3 + H2O} Mixtures for the Industrial Design of Absorption Refrigeration Equipment. 2006.

[8] J.F. Davidson. Absorption of gases. *Transaction of the Faraday Society*, 1:656–687, 1956.

[9] V. Donowski and S. Kandlikar. Correlating Evaporation Heat Transfer Coefficient of Refrigerant R-134a in a Plate Heat Exchanger. pages 1–18, 2000.

[10] J. Fernández-Seara, J. Sieres, C. Rodríguez, and M. Vázquez. Ammonia-water absorption in vertical tubular absorbers. *International Journal of Thermal Sciences*, 44(3):277–288, 2004. ISSN 12900729. doi: 10.1016/j.ijthermalsci.2004.09.001.

[11] R. Goedecke. *Fluidverfahrenstechnik: Grundlagen, Methodik, Technik, Praxis*. 2011. ISBN 9783527332700.

[12] R.J. Goudriaan. Performance analysis of ammonia and ammonia-water as working fluids for OTEC power plants, Master's thesis Delft University of Technology. 2016.

[13] V. Gudjonsdottir. *Analysis of external influences on an OTEC cycle*. PhD thesis, 2015.

[14] Z. Guo and N. K. Anand. Condensation of R-410A in a rectangular channel. *ASHRAE Transactions*, 106 (April), 2000. ISSN 00012505. doi: 10.1080/10789669.1999.10391227.

[15] D.H. Han, K.Y. Lee, and Y.H. Kim. The caracteristics of condensation in brazed plate heat exchangers with different chevron angles. *Journal of the Korean Physical Society*, 43(1):66–73, 2003. ISSN 13594311. doi: 10.1016/S1359-4311(03)00061-9.

[16] K. Helbig. Messung zur Hydrodynamik und zum Wärmetransport bei der Filmverdampfung. *PhD Thesis*, (April 2007), 2007.

[17] J.P. Holman. Heat Transfer. *Mc Graw Hill*, page 758, 2010. URL `https://books.google.se/books?isbn=0073529362`.

[18] Y.Y. Hsieh, L.J. Chiang, and Tsing-Fa Lin. Subcooled flow boiling heat transfer of R-134a and the associated bubble characteristics in a vertical plate heat exchanger. *International Journal of Heat and Mass Transfer*, 45(9):1791–1806, 2002. ISSN 00179310. doi: 10.1016/S0017-9310(01)00294-0. URL http://linkinghub.elsevier.com/retrieve/pii/S0017931001002940.

[19] P.L. Kapitza. Wave flow of thin layers of a viscous fluid: I. Free flow. II. Fluid flow in the presence of continuous gas flow and heat transfer. *Zhurnal Eksperimental'noi i Teoreticheskoi Fizik*, 209(18):1–28, 1949.

[20] M.A. Kedzierski and M.S. Kim. Convective Boiling and Condensation Heat Transfer with a Twisted-Tape Insert for R12, R22, R152a, R134a, R290, R32/R134a, R32/R152a, R290/R134a, R134a/R600a, 1997. URL http://fire.nist.gov/bfrlpubs/build97/art030.html.

[21] D.S. Kim. *Solar Absorption Cooling*. PhD thesis, 2007.

[22] J. A. Kirkenier. Techno-economic optimization of Organic Rankine Cycles using working fluid mixtures for 10 to 25 MW OTEC power plants. page 84, 2014. URL http://www.bluerise.nl/.

[23] L.J. Kuikhoven. Influence of the ammonia concentration on the performance of OTEC power cycles, Master's thesis Delft University of Technology. 2016.

[24] E.W. Lemmon, M.L. Huber, and M.O. McLinden. NIST Standard Reference Database 23: Reference Fluid Thermodynamic and Transport Properties-REFPROP, Version 9.1, National Institute of Standards and Technology. 2013. doi: http://dx.doi.org/10.18434/T4JS3C.

[25] W. K. Lewis and W. G. Whitman. Principles of Gas Absorption. *Industrial and Engineering Chemistry*, 16 (12):1215–1220, 1924. ISSN 00197866. doi: 10.1021/ie50180a002.

[26] G.A. Longo, S. Mancin, G. Righetti, and C. Zilio. A new model for refrigerant boiling inside Brazed Plate Heat Exchangers (BPHEs). *International Journal of Heat and Mass Transfer*, 91:144–149, 2015. ISSN 00179310. doi: 10.1016/j.ijheatmasstransfer.2015.07.078. URL http://dx.doi.org/10.1016/j.ijheatmasstransfer.2015.07.078.

[27] A.F. Mills. *Basic heat and mass transfer second edition*. Pearson Education, 1998. ISBN 9781441972637.

[28] C.W.M. Nefs. Experimental Validation of a Ammonia-Water Absorption / Desorption Model, Master's thesis Delft University of Technology. (July), 2013.

[29] M.P. Nuijten. Modelling the absorption of binary mixtures in plate heat exchangers, Master's thesis Delft University of Technology. 2015.

[30] L.A. Nurse, R.F. McLean, A.J. Trinidad, P.L. Briguglio, Vi. Duvat-Magnan, N. Pelesikoti, E. Tompkins, and A. Webb. *Small Islands*. 2014. ISBN 097294382X. doi: 10.2134/jeq2008.0015br.

[31] S.C. Palmer, W.V. Payne, and P.A. Domanski. Evaporation and Condensation Heat Transfer Performance of Flammable Refrigerants in a Brazed Plate Heat Exchanger, 2000.

[32] A.S. Rattner and S. Garimella. Fast, stable computation of thermodynamic properties of ammonia-water mixtures. *International Journal of Refrigeration*, 62:39–59, 2016. ISSN 01407007. doi: 10.1016/j.ijrefrig.2015.09.009. URL http://dx.doi.org/10.1016/j.ijrefrig.2015.09.009.

[33] J. Rijpkema. Experimental Validation of a New Ammonia / Water Absorption Model in a Minichannel Annulus, Master's thesis Delft University of Technology. (November), 2012.

[34] D. Seader and E.J. Henley. Separation Process Principles. *America*, 1:778–871, 2006. ISSN 0009-4978. doi: 10.5860/CHOICE.36-5112.

[35] L. Shi. Absorption of Ammonia–Water and CO2–NH3–H2O Mixture in Mini-Channel Heat Exchangers, Master's thesis Delft University of Technology. 2017.

[36] K. Siebeneck, W. Popov, T. Stefanak, and S. Scholl. Pillow Plate Heat Exchangers - Investigation of Flow Characteristics and Wetting Behavior at Single-Flow Conditions. *Chemie Ingenieur Technik*, 87(3):235–243, 2015. ISSN 0009286X. doi: 10.1002/cite.201400055. URL http://doi.wiley.com/10.1002/cite.201400055.

[37] R. K. Sinnott and G. Towler. Fundamentals of Energy Balances and Energy Utilization. *Chemical Engineering Design*, pages 83–151, 2008.

[38] D. Sterner and B. Sunden. Performance of plate heat exchangers for evaporation of ammonia. *Heat Transfer Engineering*, 27(5):45–55, 2006. ISSN 0145-7632. doi: 10.1080/01457630600559611.

[39] H. Takahama and S. Kato. Longitudinal flow characteristics of vertically falling liquid films without concurrent gas flow. *International Journal of Multiphase Flow*, 6(3):203–215, 1980. ISSN 03019322. doi: 10.1016/0301-9322(80)90011-7.

[40] X. Tao, M.P. Nuijten, and C.A. Infante Ferreira. Two-phase vertical downward flow in plate heat exchangers : flow patterns and condensation mechanisms. pages 1–56, 2017.

[41] B. Thonon and A. Bontemps. Condensation of Pure and Mixture of Hydrocarbons in a Compact Heat Exchanger: Experiments and Modelling. *Heat Transfer Engineering*, 23(January 2015):3–17, 2002. ISSN 0145-7632. doi: 10.1080/01457630290098718.

[42] VDI. *VDI Atlas*. 2010. ISBN 9783540778769.

[43] H.M. Veijer. Analysis for measurements of an OTEC power plant. Technical report, 2016.

[44] S. Whitaker. Forced convection heat transfer correlations for flow in pipes, past flat plates, single cylinders, single spheres, and for flow in packed beds and tube bundles. *AIChE Journal*, 18(2):361–371, 1972. ISSN 15475905. doi: 10.1002/aic.690180219.

[45] D. Winkelmann. Condensation of pure refrigerants and their zeotropic mixtures in plate heat exchangers, Master's thesis Universität Berlin. page 11, 2010.

[46] Yi-Yie Yan, Hsiang-Chao Lio, and Tsing-Fa Lin. Condensation heat transfer and pressure drop of refrigerant R-134a in a plate heat exchanger. *International Journal of Heat and Mass Transfer*, 42(6):993–1006, 1999. ISSN 00179310. doi: 10.1016/S0017-9310(98)00217-8.

[47] T. Yara, S. Koyama, and H. Suzuki. Condensation of binary zeotropic working fluid in a plate heat exchanger. *Proceedings of the 4th JSME-KSME thermal engineering conference*, 3:757–762, 2000. ISSN 01421123. doi: 10.1016/j.ijfatigue.2017.11.009. URL https://doi.org/10.1016/j.ijfatigue.2017.11.009.

[48] J. Zhang, H. Zhang, and J. Zhang. Evaluation of liquid ammonia treatment on surface characteristics of hemp fiber. *Cellulose*, 21(1):569–579, 2014. ISSN 09690239. doi: 10.1007/s10570-013-0097-y.